Czech Technical University in Prague
Faculty of Electrical Engineering
Department of Electromagnetic Field

Analysis and Synthesis of Antenna Arrays with Respect to Mutual Coupling and Beamforming

Doctoral thesis

Ing. Tomáš Lonský

Ph.D. programme: Electrical Engineering and Information Technology, P2612
Branch of study: Radioelectronics, 2601V010
Supervisor: Doc. Ing. Pavel Hazdra, Ph.D.
Supervisor specialist: Ing. Jan Kraček, Ph.D.

Prague, September 2019

Thesis Supervisor:

Doc. Ing. Pavel Hazdra, Ph.D.
Department of Electromagnetic Field
Faculty of Electrical Engineering
Czech Technical University in Prague
Technická 2
160 27 Prague 6
Czech Republic

Declaration

I hereby declare I have written this technical thesis independently and quoted all the sources of information used in accordance with methodological instructions on ethical principles for writing an academic thesis. Moreover, I state that this thesis has neither been submitted nor accepted for any other degree.

In Prague, September 2019

.....

Ing. Tomáš Lonský

Acknowledgement

I'd like to express my thanks to my supervisor Pavel Hazdra for his help with my work and, also to give me invaluable advice in personal life areas. Many thanks also belong to my supervisor specialist Jan Kraček for his great leading of my work and his kind approach and careful reading of my manuscripts.

I am also grateful to Zdeněk Hradecký for sharing his knowledge and showing me the way how to bring ideas into practice. With grateful regards I thank my colleagues from Department of Electromagnetic Field, for influencing my life and helping me become a better person.

Finally, I'm very grateful to my parents, my sister and to my other half Karolina for their patience and support.

Abstrakt

Tato práce se zabývá analýzou a syntézou (zejména liniových) anténních řad umístěných ve volném prostoru nebo nad nekonečnou zemní rovinou. K charakterizaci problému byla odvozena teorie a algoritmus implementován v programu MATLAB. Pro liniové anténní řady se vyvinutá metoda se vyznačuje velkou rychlostí z důvodu použití vhodné aproximace proudového obložení na jednotlivých prvcích řady.

Pro analýzu řad jsou využity modální techniky, tj. řada je charakterizována maticemi o rozměru $N \times N$ (kde N je počet prvků v řadě) popisujícími její impedační a vyzařovací vlastnosti. Tyto matice jsou následně podrobeny modálním rozkladům, jejichž výsledek poskytuje optimální buzení elementů pro dosažení daných vlastností — rezonance řady, činitel jakosti, směrovost.

Kromě semi-analytických metod aplikovaných na liniové řady byl rovněž vyvinut algoritmus využívající simulátor elektromagnetického pole CST MWS, jež je pomocí maker propojen s programem MATLAB. Takto je možné syntetizovat vyzařovací diagram řady s libovolným typem elementů, tj. nikoli jen s dipóly.

Výše zmíněné metody jsou aplikovány a ověřeny na několika příkladech:

- Optimalizace Yagi-Uda antény s různou délkou elementů
- Optimalizace šířky pásma a směrovosti řady nad zemní rovinou
- Řízení směrovosti kruhové řady
- Syntéza supersměrového buzení řady
- Syntéza daného vyzařovacího diagramu řady včetně zahrnutí vzájemných vazeb

V neposlední řadě jsou tyto příklady a techniky inspirací pro návrh a výrobu anténní řady na frekvenci 26 GHz. Tato řada byla vyrobena, změřena a bude implementována spolu s optickým systémem, který bude tvořit napájecí a přenosovou část pro systém 5G.

Klíčová slova

Syntéza a optimalizace anténních řad, vyzařovací diagram, dipólové antény, řízení anténního svazku, modální dekompozice

Abstract

This work deals with the analysis and synthesis of (especially linear) antenna arrays located in free space or above the infinite ground plane. The theory and algorithm implemented in MATLAB were derived to characterize the problem. For linear antenna array the developed method is characterized by a high computational speed due to the use of suitable current distribution approximation on individual elements of the array.

Modal techniques are used to analyze the array, *i.e.*, the array is characterized by matrices of $N \times N$ dimension (where N is the number of elements) describing its impedance and radiation properties. These matrices are then subject to modal decomposition, the result which provides optimal excitation of the elements to achieve given properties – resonance, quality factor, directivity. In addition to semi-analytical methods applied to linear arrays, an algorithm using electromagnetic field simulator CST MWS, which is connected to MATLAB by macros, was also developed. In this way, it is possible to synthesize a radiation pattern of an array with any type of element, *i.e.*, not just dipoles.

The above methods are tested and validated on several examples:

- Optimization of Yagi-Uda antenna with different element lengths
- Optimization of bandwidth and directivity of an array above ground plane
- Directivity control of circular array
- Synthesis of super-directivity excitation of an array
- Synthesis of a given radiation pattern of an array, including the mutual coupling

Last but not least, these examples and techniques are an inspiration for the design and manufacture of the 26 GHz antenna array. This array has been manufactured, measured and will be implemented together with an optical system that will form the power and transmission part to the 5G system.

Keywords

Antenna arrays synthesis and optimization, Antenna radiation patterns, Dipole antennas, Beam steering, Modal decomposition

List of Author's Publications

Unless explicitly noted, the authorship is divided equally among the listed authors.

Papers in journals with impact factor

- **T. Lonsky**, P. Hazdra, J. Kracek, "Characteristic Modes of Dipole Arrays", *IEEE Antennas and Wireless Propagation Letters* (Vol. 17, Issue: 6, June 2018), pp. 998-1001, DOI: 0.1109/LAWP.2018.2828986. IF: 3.51
- P. Hazdra, M. Capek, M. Masek, **T. Lonsky**, "An Introduction to the Source Concept for Antennas", *Radioengineering*, April 2016, Vol. 25, Issue 1, pp 12-17. IF: 0.967
- P. Hazdra, J. Kracek **T. Lonsky**, "On the End-Fire Super Directivity of Arrays of Two Elementary Dipoles and Isotropic Radiators", *IET Microwaves, Antennas and Propagation*, March 2019, DOI: 10.1049/iet-map.2018.6013, IF: 2.036

Conference papers

- P. Hazdra, **T. Lonsky**, M. Capek, "Bandwidth Optimization of Linear Arrays Above Ground", *10th European Conference on Antennas and Propagation (EuCAP)*, April 2016, Davos, Switzerland
- P. Hazdra, **T. Lonsky**, J. Kracek, "Modal Decomposition Theory for Arrays of Dipoles", *11th European Conference on Antennas and Propagation (EuCAP)*, March 2017, Paris, France
- **T. Lonsky**, P. Hazdra, J. Kracek, "Modal Decomposition for Arbitrary Dipole Array", *Conference on Microwave Techniques (COMITE)*, April 2017, Brno, Czech Republic
- **T. Lonsky**, P. Hazdra, J. Kracek, "Design of Closely Spaced Dipole Array Based on Characteristic Modes", *Progress in Electromagnetics Research Symposium - Fall (PIERS - FALL)*, November 2017, Singapore, Singapore
- **T. Lonsky**, P. Hazdra, J. Kracek, "Superdirective Dipole Arrays", *13th European Conference on Antennas and Propagation (EuCAP)*, March 2019, Krakow, Poland

- **T. Lonsky**, P. Hazdra, J. Kracek, "The Directivity of Two Closely Spaced Isotropic Radiators Above PEC Ground", *8th Asia-Pacific Conference on Antennas and Propagation (APCAP)*, August 2019, Incheon, Korea
- **T. Lonsky**, P. Hazdra, J. Kracek, "Fast Yagi-Uda Antenna Optimization", *8th Asia-Pacific Conference on Antennas and Propagation (APCAP)*, August 2019, Incheon, Korea

Papers in journals with impact factor non-related with this work

- A. Pascawati, P. Hazdra, **T. Lonsky**, M. R. K. Aziz, "Excitation of a Conducting Cylinder Using the Theory of Characteristic Modes", *Radioengineering*, December 2018, DOI: 10.13164/re.2018.0956. IF: 0.967

Conference paper non related with this work

- **T. Lonsky**, P. Hazdra, "Design of a Plexiglass Rod Antenna", *Conference on Microwave Techniques (COMITE)*, April 2017, Brno, Czech Republic

Papers being currently reviewed in journals with impact factor

- **T. Lonsky**, P. Hazdra, J. Kracek, "Superdirective Dipole Array with PSO optimization", *IEEE Antennas and Wireless Propagation Letters*

Financial support acknowledgement

The research presented in the listed papers was conducted under partial financial support of these projects:

- GACR 17-00607S - Complex Electromagnetic Structures and Nanostructures
- SGS16/226/OHK3/3T/13 - Research on High-Frequency Electromagnetic Structures
- 19/168/OHK3/3T/13 - Electromagnetic Structures and Waves
- MPO FV30427 - Radio-Optical Transmission Terminal for 5G Networks

Awards

Tomas Lonsky received an award for: The best student paper presented, on COMITE, April 2017.

Contents

List of abbreviations

3G third generation.

3GPP Third Generation Partnership Project.

4G fourth generation.

5G fifth generation.

5GPP Public Private Partnership.

BS base station.

C-RAN cloud-based radio access network.

CM Characteristic Modes.

CMSA Canonical Minimum Scattering Antennas.

CW continuous wave.

DML directly modulated laser.

DWDM dense wavelength division multiplexer.

EB exabyte.

EHF Extremely High Frequency.

EMF Electromagnetic Field.

EML externally modulated laser.

IoT Internet of Things.

ITU International Telecommunication Union.

LOS line-of-sight.

LPDA log-periodic dipole array.

LTE Long Term Evolution.

LTE-A Long Term Evolution Advanced.

M-MIMO massive multiple-input multiple-output.

MCM multi-carrier modulation.

mm-wave millimeter-wave.

MoM Method of Moments.

MZM Mach-Zehnder Modulator.

NVIS near vertical incidence skywave.

PC polarize controller.

PCB Printed Circuit Board.

PD photodetector.

PEC perfect electric conductor.

PSO Particle Swarm Optimization.

RF radio frequency.

RoF radio-over-fiber.

RoFSO radio-over-free-sace optics.

SDN software-defined networking.

SHF Super High Frequency.

SIW substrate integrated waveguide.

SLL side-lobe level.

SMF single mode fiber.

SNR Signal to Noise Ratio.

UHF Ultra High Frequency.

VNA vector network analyzer.

List of Figures

List of Tables

Chapter 1

Introduction

There are many types of software programs that help the engineer to design to create an antenna. Still, the design and development of an antenna and antenna arrays are complex and costly. This work is focused on analysis, synthesis and optimization of electromagnetically coupled radiators with respect to different measures. The aim of this work is to present results and develop tools for such analysis and synthesis. Recently, a novel paradigm, relating to source current distribution with other important measures, in antenna theory appeared [1]–[4]. Except for already known characteristics, as near or far fields, gain, radiated power, antenna impedance, it is also possible to evaluate stored energies and in turn the Q-factor of a radiator, indicating its bandwidth potential [3].

The main goal of the work is to make an extensive study on closely spaced dipole arrays backed by electric ground plane and arbitrary oriented, closely spaced arrays. Antenna geometry, such as spacing between elements, height above ground plane or number of dipoles, should be synthesized. Optimization of excitation coefficients (voltages, currents) concerning driving impedance, bandwidth, gain, field distribution in space and other measures is treated. The directivity of the end-fire arrays will be treated due to superdirective properties.

The effective antenna analysis and design was and still is a very actual topic since the number of applications is ever growing with the increasing popularity of wireless communications. High computational power of today computers makes possible to simulate full-wave behavior of not only separate parts of a wireless device but the system as a whole. However, understanding the fundamental principles by performing such a complex analysis can be very difficult.

The analysis and design of array antennas is complicated due to the fact that array elements are not independent of each other. Instead, the elements interact electromagnetically through what is called mutual coupling. There has been much effort directed toward developing analysis methods that account for the effects of mutual coupling in an array environment. The knowledge of mutual coupling effects is important in the design of array elements, for array geometry selection to reduce mutual coupling among elements, and for compensating the mutual coupling effects with feeding circuits.

But even if the antenna design or array design is complicated, it would be useless if it was not applied in the real world. An antenna is basically a device that allows transferring

data to the user. Currently, we are living in a hurried time with a lot of data coming to us from all sites. The number of videos with 4K resolution is dramatically increasing. Also the videos from the internet are more and more watched on mobile phones or tablets and smart devices. Thus there is great compulsion on the amount of data transmission and that implies the increasing of a transmission rates. The amount of transmitted data is dependent on coding of the data and antenna parameters such as operational frequency, bandwidth or gain.

It is expected that the amount of transmitted data in wireless networks will exceed 500 exabyte (EB) in year 2021, in contrast there was transmitted around 3 EB in year 2010 [5]. To fulfill these requirements, a 4th generation of network named Long Term Evolution (LTE) was launched, reaching speeds of 3 Gb/s for downlink and 1.5 Gb/s for uplink when using technology of Long Term Evolution Advanced (LTE-A) [6]. Next extension to mobile networks will be mobile network of 5th generation named fifth generation (5G) [7].

Due to increasing transmission capacity and limited frequency bandwidth requirements, 5G networks will significantly increase transmission frequencies towards higher unlicensed bands that provide the necessary bandwidth for large data transmissions. While the macro signal is going to be in the Ultra High Frequency (UHF) band (< 3 GHz) due to smaller dissipation losses, it is expected that smaller cells will grow massively with Internet of Things (IoT). These cells will use Super High Frequency (SHF) and Extremely High Frequency (EHF) exceeding 24 GHz [8]. In addition, other transmission technologies and wireless standards are moving to shift to higher bandwidths. Increasing frequency, however, involves higher transmission system costs as well as stricter demands on microwave technology used in the communications link, for example, metallic connecting cables and cable connectors greatly increase attenuation and thus contribute to poor signal quality. Another key factor is the higher non-linearity of such a system in comparison to the optical link. Achieving the necessary Signal to Noise Ratio (SNR) can be very complicated, along with reduced flexibility of the system due to the need to shorten the cables to a minimum. In this case, the radio-over-fiber (RoF) [9] technology is able to effectively disconnect the metallic conductors and, without major problems, to bridge longer distances and, at the same time, lead in the immediate vicinity of, for example, high voltage.

The thesis first introduces techniques of antenna analysis and a developed methods for array description, such as impedance of arbitrary array elements and directivity of array elements. These techniques are described in Chapter 3, the accomplished results with many array examples could be found in Chapter 4. In this chapter the bandwidth of a linear arrays above perfect electric conductor (PEC) is optimized, the use of the Characteristic Modes (CM) is shown on simple three-element dipole antenna array above PEC ground. To present the usefullness of the developed method a Yagi-Uda antenna is synthesized. In Chapter 5 the developed theory is applied to an antenna array with four dipole elements designed for 5G network.

Chapter 2

State of the art in antenna array design

In the past years, the antenna designers are looking for ways on how to increase frequency bandwidth of their systems. This is because of a simple fact that using just one antenna, or antenna array for the whole microwave frequency spectrum, is needed for low-cost manufacturing devices and using very fast miniaturization of the devices. Very large frequency bandwidth is also needed for applications such as radar where the increased bandwidth is required for better spatial resolution and tracking accuracy.

One way how to accomplish this goal is to design and use wide-band elements that often require a very complicated design and manufacturing. Unfortunately, as the antenna design is more complex, there is no close description of how to analyze it. Thus, the use of numerical methods [10], [11] becomes in consideration. These numerical methods have been implemented in commercial electromagnetic simulators, such as FEKO [12], HFSS [13] or CST [14] and others. With the help of these simulators, the time for the antenna design is reduced, however, the designer needs to have some intuition and experience to develop a well-done design of antenna or antenna array.

The second approach how to get a wider bandwidth of the system is to use wide-band elements in arrays. Interesting phenomena was discovered by using narrow-band elements in antenna arrays. The designers found, that the bandwidth of such array is wider than the individual antennas. This phenomenon was first introduced with the use of Vivaldi antennas, which are relatively wide-band elements, but when used in an antenna array, the bandwidth is even wider if properly designed [15]. As previously mentioned in introduction of this work, recently this phenomenon was observed in closely spaced dipole arrays [16] . The advantage of using dipoles instead of Vivaldi antennas is their area when printed like a planar array. This bandwidth increase is attributed to strong mutual coupling between the radiators. Overall the analysis of antenna array is complicated due to the fact that array elements are not independent on each other. Instead, the elements interact with each other through what is called mutual coupling. There has been much effort in reduction of the mutual coupling effects and also for compensating the mutual coupling effects with feeding circuits. But the mutual interaction could be useful in some cases.

Many techniques for the antenna design have been developed in the last 50 years.

Current state of the art allows very precise modeling of all properties of the array such as radiation pattern, input impedance and current distribution on each antenna element. All these parameters are obtained based on solving Maxwell's equations. Depending on the task and the solution technique chosen, either an integral form of differential Maxwell's equation in frequency domain or the time domain is selected to solve the problem. These equation are solved thanks to the many numerical methods now available.

When multiple radiating elements are presented the analysis and design become more and more complex and hard to achieve the proper result. Then the theory of CM [17] becomes handy. The CM is method used for design of the antennas, because the modes depend only on the antenna geometry without any excitation presented. When CM is applied to an object, a set of unique currents is found.

Early antenna engineers historically approached the design of an array on one fundamental concept, the array element pattern [18]. The array factor is the pattern solely stemming from the array shape, amplitude and phase of feeding and phasing between elements. This array element pattern, which is actively used since 1960s, corresponds to the case when, in the transmitting mode, the excitation signal is fed to the input of only one element in an array while all other elements are assumed to be terminated with matching loads. This first-order approach can work only if the influence of one element on another is not essential. This means that the impedance of isolated element does not change when inserted into an array, not even the element pattern such as the far-field radiation pattern of an array element radiating in the presence of the other array elements. When the influence of these effects is meaningful, engineers often lump them together as mutual coupling. Since the electromagnetic interaction always exist in the array elements, the radiation corresponding to excitation of one input is formed by all the rest elements. For this reason, the element pattern is also named as a partial array pattern. For all these reasons engineers often design an array with large distance between each element to mitigate the mutual coupling and side lobes suppression. These effects are much stronger when the distance between elements is $d < 0.5\lambda$, where c is speed of light and f is frequency,when $d = 0.5\lambda$ is assumed to be the minimum spacing at the lowest frequency. However, in this work we will focus on the opposite problem, closely spaced dipole arrays and we will use benefit of this mutual coupling in arrays. Another approach how to describe antenna array and the mutual coupling is the mutual impedance of the element $\mathbf{Z}_{\mathrm{A}mn}$, as a ratio of the current at element generated by a voltage across the feed at element n so that the entire input impedance of the array is represented by the matrix $\mathbf{Z}_{\mathrm{A}}$ [19].

If antenna 1 is driven and antenna 2 is open-circuited, the field generated by the current on antenna 1 will cause an open-circuit voltage, $V_{21,\mathrm{oc}}$, on antenna 2. The mutual impedance of antenna 2 due to antenna 1 is defined to be

$$Z_{21} = \frac{V_{21,\mathrm{oc}}}{I_1} \tag{2.1}$$

where I_1 is the input current on antenna 1 [20].

At the driving points of the several elements in an array, currents and voltages are related by the usual coupled circuit equation. Assume the V_p is the driving voltage across

the terminals of the element p in an array of N element. Let the I_p be the current in the same terminals, then, if a Kirchhoff equation is written for each element, the following set is obtained.

$$\begin{aligned} V_1 &= I_1\mathbf{Z}_{\mathrm{A},11} + I_2\mathbf{Z}_{\mathrm{A},12} + ...I_n\mathbf{Z}_{\mathrm{A},1n} + ...I_N\mathbf{Z}_{\mathrm{A},1N} \\ &\vdots \\ V_m &= I_1\mathbf{Z}_{\mathrm{A},m1} + I_2\mathbf{Z}_{\mathrm{A},m2} + ...I_n\mathbf{Z}_{\mathrm{A},mn} + ...I_N\mathbf{Z}_{\mathrm{A}mN} \\ &\vdots \\ V_N &= I_1\mathbf{Z}_{\mathrm{A},N1} + I_2\mathbf{Z}_{\mathrm{A},N2} + ...I_n\mathbf{Z}_{\mathrm{A}mn} + ...I_N Z_{A,Nn}. \end{aligned} \tag{2.2}$$

The coefficient $\mathbf{Z}_{\mathrm{A},mn}, m \neq n$, is the mutual impedance between element m and n. Also for the array that is in an isotropic medium such as air, $\mathbf{Z}_{\mathrm{A},mn} = \mathbf{Z}_{\mathrm{A},nm}$. The coefficient $\mathbf{Z}_{\mathrm{A},mm}$ is the self-impedance of element m [21]. The input or driving-point impedance of an element is a function of both self and mutual impedances and excitation currents

$$\mathbf{Z}_{d,m} = \frac{I_1}{I_m}\mathbf{Z}_{\mathrm{A},m1} + \cdots \mathbf{Z}_{\mathrm{A},mm} + \cdots \frac{I_n}{I_m}\mathbf{Z}_{\mathrm{A},mn} + \cdots \frac{I_N}{I_m}\mathbf{Z}_{\mathrm{A},mN} \ . \tag{2.3}$$

The driving terminals of an antenna coincide with the line-load junction between it and its feeding transmission line. Thus, determining the mutual impedance of elements in an array requires measurement or knowledge of the open-circuit voltage at each element when one element is driven and the driving-point currents of all other elements in the array are zero, that is, when all other elements are in open-circuit configurations [22]. Further notation of impedances includes isolated impedance, active impedance and embedded impedance. Isolated impedance is that of an array element with all other elements removed and active impedance is that where all elements are in place and excited. Often the active impedance is also named as scan impedance or driving impedance [23],[24]. Embedded impedance is the terminal impedance at one element when all other elements are terminated in a specified impedance.

Self- and mutual impedances or admittances depend upon the geometrical configuration of each element, surroundings, the relative location and orientation of the element in an array and the total number of elements. It must be considered if the array is used in configuration with an infinite ground plane, or not. Once the self- and mutual impedances have been determined, they can be used in equation (2.2) to calculate the driving point impedances (or admittances) for any set of driving voltages or currents that may be applied to the array.

In 1996, Lee and Chu [25] used block components to describe the impedance matrix $\mathbf{Z}_{\mathrm{A}}$. The goal of this work was to create a solution that is very fast in comparison to full-wave solution and not have the limitations of infinite array techniques.

The design of the antenna is more and more complex topic. For example, the antennas in the mobile phones are designed using computationally complex optimization algorithms, where the antennas shape is determined through a set of predefined requirements. Thus, the designer has no insight, only simple understanding of how these antennas truly function. This lack of internal knowledge leads to difficulties with new antenna shape development. Furthermore, many textbooks analyze the antenna by using a set of elec-

tromagnetic equations, providing more information than simple optimization. However, there is one tool, which provides more complex insight, and that is the CM. When CM is applied to an object, a set of currents are found. Each current is unique and if one of these current is excited, it will resonate differently than any other derived currents. The frequency behaviour of the modal eigenvalues has been helpful in clarifying the bandwidth limits for antennas. Antenna array research faces similar issues, as the element weightings in arrays for phasing and decreased side-lobe levels have been shown to impact element impedance matches and array bandwidths. The orthogonal eigenmodes obtained using the CM provide an excellent way to approach these problems.

The CM was firstly developed by Garbacz in 1965 [17]. His original idea utilized a scattering matrix, which give us a prove, that any excitable current on an object can be decomposed into an infinite set of radiating currents. This theory was further developed by Garbacz in [26] and reworked to the current known formulation by Harrington and Mautz in 1971 [27]. This known formulation since then remained with only one minor change that CM is no longer associated with only PEC. In [28] the computational method for determining both the characteristic currents and eigenvalues is based on the Sturm-Liouville theory for weighted eigenvalue problems [29]. The Sturm-Liouville theory is also the basis for solving Greens' function using a direct approach [30]. In 1972, Harrington and Mautz evaluated the modal Q-factor directly from the eigenvalue of the respective mode [31]. From then, only a few electromagnetic researchers investigated a potential of CM and this theory was almost abandoned. The reason is that a lot of computational time was required for the excitation of modes.

The first antenna design concept based on the CM was the vehicular antenna design for near vertical incidence skywave (NVIS) propagation in [32],[33]. In this work many of the main formulation will be derived, such as Q-factor, CM-based current synthesis to obtain desired gain and gain over quality factor (G/Q), pattern synthesis of arbitrary oriented array. Early work in this area includes [34]–[38]. Since the characteristic modes are computed in the absence of any kind of excitation or incident field, they only depend on the shape, material and size of the conducting object. In our case of arrays, only on number of elements, orientation in space and relative location of each element. Thus, antenna array design using characteristic modes can follow steps like: computation of characteristic modes and the corresponding eigenvalues, optimization of the shape of the array, orientation of antennas and the number of elements and finally choosing the optimum feeding of each element, so that desired mode or combination of modes may be excited.

One of the example in this work is the Yagi-Uda antenna optimization. A Yagi-Uda antenna [39], having two main parts, single driven element and additional "parasitic elements", is worldwide used due to high gain capability, low cost and simple construction. The Yagi-Uda antenna is actually antenna array usually consisting of parallel dipoles. The optimization of even an four element array is not simple, because all of the geometric parameters are affecting the output characteristics, such as gain, bandwidth, reflection coefficient and more. An antenna with N elements with constant radius requires $2N - 1$ parameters, *i.e.*, N wire lengths and $N - 1$ spacing, that are to be determined.

Many efforts have been put in optimizing the Yagi-Uda antenna [40], [41], even using Artificial Intelligence techniques [42], [43].

The developed concept of source currents of a radiating source can be employed to express its directivity in some particular cases analytically. These approaches from previous chapters will be applied to examples of the array of two elementary dipoles and the array of two isotropic radiators. It is well known that an end-fire antenna array of closely-spaced elements is able to show a significant increase in its directivity (termed superdirectivity) compared to a sole element [44], [45]. Uzkov derived the end-fire directivity limit for the case of N isotropic radiators, when the directivity approaches N^2 as the spacing between them reaches zero [46].

Recently, the design of arrays with closely spaced elements (when their spacing is less than $\lambda/4$, where λ is the wavelength) attracted both theoretical and practical interest [47]–[52]. The first realization of such an array, the Kraus W8JK antenna, should be also mentioned [53]. Optimizing a current distribution of an antenna to find its superdirective radiation is also a popular subject, see, e.g., [54]–[56]. A theory of highly directive current distributions is given in [57]. However, this theory is presented using formalism not very familiar to the antenna community. It provides an optimal current distribution for a circular loop in two and three dimensions, but no closed-form expression for its (super)directivity is given. It can be concluded that most of the recent approaches when formulating the (super)directivity problem rely finally on numerical techniques without revealing a closed-form solution. Note that this approach is nowadays also valid due to high computational ability of computers and efficiency of numerical solvers.

It is well known that the array can show an increase in directivity [44], [45], [58] when the feeding currents are not uniform but are designed to be optimal in this respect. Since the directivity may be expressed as a ratio of two quadratic Hermitian forms, the optimization is performed by solving the associated eigenvalue problem [59]–[62]. Equivalent solution may be obtained by involving the inverse of array power matrix [58], [59], [63].

The problem of finding the superdirective excitation of a dipole/monopole array has been treated by many authors both theoretically [63], [64] and practically [47]–[51]. Most of the previous theoretical evaluation consider the dipole radiation pattern to evaluate the quantities for directivity expression. In this paper the approach is different. We treat arrays of thin-wire dipoles of arbitrary length and assume a current distribution to be of a given form (particularly three-term King approximation [20]). Therefore, the matrices of interest have dimension $N \times N$ where N is number of elements in the array. The results of the decomposition are then just the excitation currents or voltages to be applied to the center of dipoles, see [65]. Consequently, the proposed approach (coded in MATLAB [66]) is very fast.

Several interesting properties are found. It is known [53] that one horizontal dipole above ground show maximum directivity when its height goes to zero. However, for more horizontal dipoles, it is shown that the directivity reaches its maxima (with optimal superdirective currents provided) for quite unexpected height around 0.7λ regardless the number of radiators. This observation is also supported by analysis of two isotropic radiators above the ground plane.

It is also noted that for case of a dipoles above the ground, the superdirective currents are purely real.

Also in this thesis it is considered feeding synthesis of an arbitrary N-port antenna array connected to independent voltage/current sources or reactive loads. Such configuration is attractive for developing wireless communication systems requiring variable radiation patterns [36], [67], [68].

Further application of the proposed method is the possibility to generate extraordinary directivity [44], [49], particularly when the array elements are closely-spaced (separation $< \lambda/4$). For example, best [51] achieved directivity of 10.2 dBi with a two element array spaced by $0.1\,\lambda$. To avoid multiple excitation, Haskou [48] proposed technique when only one element is excited while the others are parasitic with proper reactive load. Another approach, based on spherical wave expansion, was used by Clemente [52] to design four element parasitic superdirective array.

Since the superdirective operation is very sensitive, precise knowledge of the feeding amplitudes/phases or reactive load values is needed.

Several semi-analytic methods for array feeding synthesis were already developed. In [69] Harrington expresses the gain as a quadratic form involving array excitation and impedance matrix. Mautz and Harrington in [70] extends the CM theory [28] towards the network CM, *i.e.*, N-port loaded scatterers. Based on this framework, iterative pattern synthesis is presented in [35]. Tzanidis in [71] use CM to find the array excitation current such that the active impedances at all the ports are equalized.

The properties of each antenna array depend on the characteristics of the individual radiating elements. The most widely used radiating elements in arrays are dipoles and patch antennas. The dipole is very easy to simulate in commercial simulators, also is mathematically easy to describe, simple manufacturing and analytical circuit representation helps to expand dipole arrays techniques.

It is important to mention that the elementary dipole/loop and isotropic radiator belong to a class of so-called Canonical Minimum Scattering Antennas (CMSA), *i.e.*, single-mode antennas [72], [73]. They have the important property that the far field of a standalone antenna is identical with the far field of the same antenna embedded as an element of an array and influenced by its other open-circuited elements.

There are techniques that lead to current description of the finite length dipole from the elementary dipole. These techniques could be found in [74]. In short, the fundamental building block of a finite length dipole is the ideal Hertzian dipole. This ideal dipole is infinitesimal element with a current of uniform magnitude and phase distribution. Then the radiation field from the dipole of finite length will be the sum (integration) of the contributions from all ideal dipoles weighted by the current distribution.

To reduce mathematical complexity, it will be assumed, that the dipole has a negligible diameter in comparison with wavelength. First order approximation, that gives reasonable impedance and radiation pattern around first resonance. This distribution assumes that the current on the antenna is maximum at the center and then vanishes at the end points of the antenna [74]. For a half-wave dipole, the current is in phase and its amplitude can be approximated by a sinusoid. The infinitely thin $\lambda/2$ dipole in free space has a center

fed radiation port resistance of 73.1Ω. For the real dipole with no infinitesimal radius, the impedance will be slightly inductive.

The dipole impedance will change because the current distribution is different due to other near objects. As the impedance changes, the current on the dipole may become redistributed and thus alter the dipole's radiation pattern.

The image theory, which is the simplest equivalence principle, can be used when the dipole in placed above infinite PEC ground [17], [75], [76].

Uniqueness theorem then says that the field above the plane must be the same in both cases. This image theory can be applied for case with perfect electric ground or with the perfect magnetic ground. The case with the electric ground of a current-carrying dipole is shown in Figure 2.1.

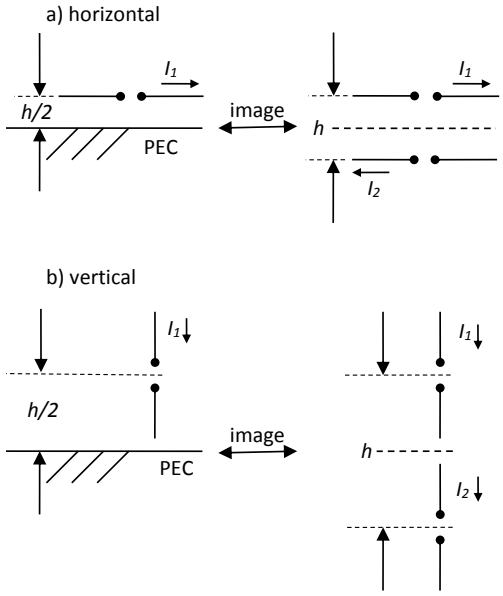

Figure 2.1: Image theory for horizontal and vertical electric dipole

By reciprocity theorem, the mutual impedance of the image dipole is equal to that of source dipole itself, so $Z_{21} = Z_{12}$.

The radio frequency (RF) spectrum is a limited public resource. Due to this and the demand for higher data rate, higher frequencies have been suggested as candidates for future 5G mobile phone applications. The higher frequencies have considerably larger bandwidth and thus we can increase the capacity of the link and enable to transmit several gigabits-per-second data rates [5], [77]. Moreover, mm-Wave frequencies lead to miniaturization of RF front end including antennas. But shifting the frequencies towards mm-Wave band introduces some new problems that needs to be considered. The antenna is the most crucial component of a wireless systems as it highly affects the total receiver sensitivity, thus transceiver designs and choices of digital modulation schemes and the link budget [78]. It is not sufficient to scale down currently used antennas and antenna arrays. One problem is increase in free-space loss. This problem can be evaded by beamforming, to synthesize high gain narrow beam radiation pattern. Link budget analysis is required to

obtain antenna gain for 28 GHz communication. The low equivalent isotropically radiated power, 78 dBm for downlink and 43 dBm for uplink and big free-space loss demands the directional antennas for high data rate [79]. Also 5G communication will be mostly to line-of-sight (LOS). To achieve full coverage of the user we need to steer the beam towards the user or smart device. It is also god to mention, that the usage of 5G networks will be mostly to the smartphones and smart devices when the older generation networks will be used to IoT.

The 5G wireless communication systems need to be designed to support high data rates with maximum coverage for different application. One of the most essential requirements of such systems is high gain antenna which is desirable as it will balance high path loss at mmWave frequency and decrease the system cost. The other desirable properties for such antenna design are high-efficiency and stable radiation patterns over the entire desired band, compact size and low profile with simplicity of integration with other elements. The designed system capacity can be increased by using multiplexing techniques based on baseband signal processing [78].

The spectrum available for 5G, allocated by the Third Generation Partnership Project (3GPP) in partnership with International Telecommunication Union (ITU) and Public Private Partnership (5GPP) [7] is subdivided into band below 6 GHz and above 6 GHz, in this case in mm-Waves at 28 GHz and 39 GHz [80]. In the 3GPP Release-16 was introduced the plan for "5G phase 2", that should be completed in December 2019 [80]. The 5G network is expected to be able to accomplish certain requirements such as 1000-fold system capacity, 100-fold energy efficiency, milliseconds end-to-end latency, 10 Gbps maximal throughput and connectivity for numerous devices compared to the counterpart 4G network [81], [82]. Furthermore the infrastructure of the current wireless communications will not be able to to meet the requirements of 5G, so, a set of novel radio access technologies will be required.

There are various innovative technologies such as massive multiple-input multiple-output (M-MIMO), millimeter-wave (mm-wave), multi-carrier modulation (MCM), software-defined networking (SDN), flexible spectrum management, small cells, HetNets, energy harvesting, and cloud-based radio access that have been envisaged as s potential enablers of 5G [83]–[86]. In the third generation (3G) cellular networks, the density of macrocell base station (BS)s is comparatively lower than that of the microcell BSs of the fourth generation (4G) cellular networks, such as LTE-A mobile communication systems. Generally, the motivation for further cellular densification through more BS deployment is the required capacity that has to be provided to the subscribers. Furthermore, in the 5G cellular networks, in which mm-wave and M-MIMO technologies are envisaged to be integrated into the BSs, small cell networks with higher density are expected to be deployed so as to offer relatively higher throughput to the subscribers. Consequently, the 5G cellular network is anticipated to be an ultra-dense cellular network [86]. Moreover in the 5G networks, to deliver high data rate, there should be dense deployment of small-cell BSs with much smaller coverage over the traditional macro-cell. This bring the better frequency reuse and significantly improves energy efficiency due to the reduction in the path loss by the cell densification.Significant attention is given on the cloud-based radio

access network (C-RAN) [87].

In 2016, SK Telecom and Ericsson completed first multi-vehicular 5G trials with BMW demonstrating a Ka-band 5G system [88]. The trend in the 5G band is to make antenna array with 4 elements (channels) on a chip unit cells that will allow spatial filtering, direct its radiation beam (beamforming), as well as a greater coverage [89] [90]. Antenna arrays with 1×8 and 4×4 elements are also in interest. The 4×4 Yagi antenna in [91] can achieve a maximum gain of 18 dBi. But these antennas structures are either multi-layered or complex structures, which perhaps fetch difficulties in fabrication. For the simplicity of fabrication, printed log-periodic dipole array (LPDA) and patch antennas are designed in the mmWave frequency, which provides enormous bandwidth with stable gain over the entire frequency range, as well as simple geometrical design [78], [92]. A mesh type patch antenna array with dual feed and 2×16 elements for 28 GHz was designed in [93]. The peak array gain was 24 dBi, but the maximum bandwidth was too narrow. Another grid array of 4×4 patch antennas in [94] showed peak gain 16.5 dBi and fractional bandwidth 5.4 %. In [95] a notch array 1×4 elements based on microstrip feeding and aperture coupled slot antennas with gain 9.9 dBi was designed nd acomplished compact structure, but still with low bandwidth. Simple waveguide structure dealing with wider bandwidth 2 GHz was designed in [96]. With a peak gain 11 dBi this 1×4 array was able to coverage quarter of entire space. More 1×4 element arrays was in [97] using dipole elements achieving gain 7.5 dBi and 12 GHz bandwidth, SIW structure in [98] with bandwidth 3.9 GHz but achieved a low gain, monopoles in [99] with peak gain 10 dBi and $\pm 90^\circ$ steerable beam, and in [100] the tapered slot structure with peak gain 9.6 dBi, 8 GHz bandwidth and $\pm 35^\circ$ scanning angle. Dipoles were also used in [101] but in configuration 1×8 with peak gain 11 dBi and 2 GHz bandwidth.

The mentioned 20-30 GHz pioneer spectrum is the first to be used in mobile networks above 6 GHz. This will bring number of challenges including a significantly high attenuation (*i.e.*, 3 dB/m) when the RF signal is transmitted over a metalic cables, which limits the transmission span. To overcome this phenomena, the RoF technology was proposed [81], *e.g.*, to use between a central officeand the pico- or femto-cell BSs. The RoF technology offers many benefits including high transmission bandwidth (THz and beyond), low attenuation, low cost and immunity to electromagnetic interference. Moreover the RoF technology [102] which refers to an analog transmission over fiber infrastructures, has been adopted between a central station and a set of BSs and to support small-cell-based scenarios while using the C-RAN [81].

In the RoF technology a data-carrying RF signal at a high frequency is used for modulating the optical signal before being transmitted over the optical link. In doing so, RF signals are optically distributed to BSs, where the signals are then converted back to the electrical domain prior to amplification and transmission via an antenna or the antenna array. Therefore, there is no need for frequency up/down conversion at various BSs. In addition, the centralization of RF signal processing functions enables dynamic allocation of resources, equipment sharing, simplified system operation, lower power usage and reduced maintenance cost. Also, the RoF technology is protocol and bit-rate transparent, therefore, it can be used to employ in any current and future technologies [103]. Commonly utilized

RoF modulation techniques such as an externally modulated laser (EML), using Mach-Zehnder modulator, and directly modulated laser (DML) have been investigated in [104]. The DML solution, compared to EML, represents a more compact solution with higher transmit power, higher energy efficiency and linear modulation characteristics, which plays a key role in RoF systems [105]. On the other hand, DML typically operates at lower frequencies. However, in [106] a DML 1550 nm buried-heterostructure passive feedback laser with a bandwidth up to 34 GHz at low distributed feedback driving currents, being highly suitable for RoF applications, was investigated. The most detailed survey of RoF operating within the frequency band of 24-28 GHz was reported in [107].

The deployment of the DML-based radio-over-free-sace optics (RoFSO), RoF, and their combination in the emerging 24–26 GHz band as part of the future 5G mobile networks for connection of micro-, pico-, and femto-cells, is shown in Figure 2.2.

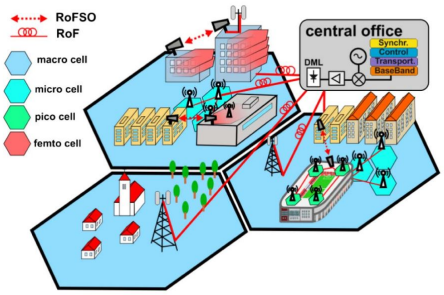

Figure 2.2: RoF and RoFSO deployment for connection of micro-, pico-, and femto-cells in 5G architecture [107].

2.1 Goals of the thesis

This work deals with closely spaced antenna arrays located in free space or above the infinite electric ground plane. The theory and algorithms were derived to characterize the problem. Modal techniques are applied to find optimal excitation of arrays. The electromagnetic field simulator CST MWS was also connected with MATLAB to synthesize far field of other antenna types.

The main goals of the thesis are:

- Developing of theory and algorithms for dipole antenna arrays.
- Analysis, synthesis and optimization of coupled elements with respect to far field, gain, quality factor, efficiency and other measures.
- Study and design of closely spaced array elements using optimization tools.
- Development of MATLAB code for evaluating self/mutual/driving impedances for arbitrarily oriented radiators in space and including infinite ground plane.
- Optimization of excitation coefficients (voltages/currents) based on required farfield pattern. Analysis of closely-spaced arrays with respect to superdirectivity properties.

- Design of antenna array with given radiation pattern.

Chapter 3

Theory

The most important and basic computation in antenna array theory is impedance matrix. This matrix is often computed by Method of Moments (MoM). Our case purely relies on the antenna impedance matrix consisting only from self- and mutual impedances. Each element in the array is described by one impedance parameter so the computation is very fast. The disadvantage of this method is that it is dependent on knowledge of the current distribution on dipoles, however in case of dipoles, the current distribution can be quite accurately modeled. In the code the antenna array is defined just by few parameters (antenna diameter, antenna length, element orientation and center of the element). Thus, the optimization of such array is very fast. Some examples of the array geometries are in Figure 3.1.

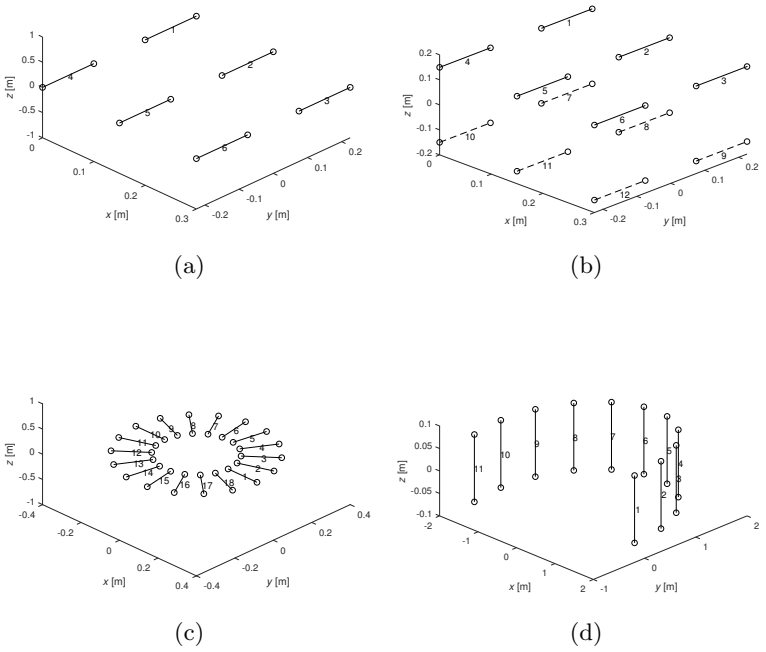

(a) (b)

(c) (d)

Figure 3.1: Selected possible geometries of the dipole arrays.

3.1 Derivations of necessary equations

If we introduce arbitrary array, the basic relations for the m-th antenna in the array can be written. These equations include: Green's function, magnetic vector potential, electric scalar potential, continuity equation and electric field intensity. A Green's function is the field due to a point source described by a delta function. Once it is known, the field due to an arbitrary source can be calculated by a convolution integral involving the source distribution and the Green's function [108]

$$G\left(\mathbf{r},\mathbf{r}_m\right)=\frac{\mathrm{e}^{-\mathrm{j}kR(\mathbf{r},\mathbf{r}_m)}}{R\left(\mathbf{r},\mathbf{r}_m\right)}, \tag{3.1}$$

where $k=2\pi/\lambda$ and in an unbounded isotropic medium

$$R\left(\mathbf{r},\mathbf{r}_m\right)=\left|\mathbf{r}-\mathbf{r}_m\right|=\sqrt{\left(x-x_m\right)^2+\left(y-y_m\right)^2+\left(z-z_m\right)^2}\,, \tag{3.2}$$

where the position vector are $\mathbf{r}$, $\mathbf{r}_m$ as shown in Figure 3.2.

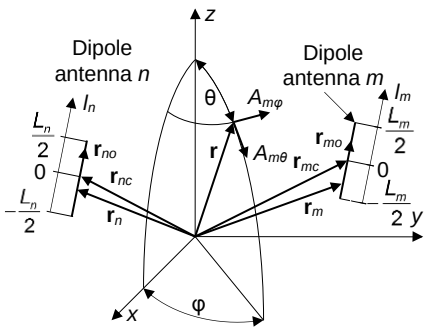

Figure 3.2: Array geometry and coordinate system.

From the Maxwell's equation, we can derive the magnetic vector potential and electric scalar potential

$$\mathbf{A}\left(\mathbf{r},\mathbf{r}_m\right)=\frac{\mu_0}{4\pi}\int\limits_{V_m}\mathbf{J}_m\left(\mathbf{r}_m\right)G\left(\mathbf{r},\mathbf{r}_m\right)\mathrm{d}V_m \tag{3.3}$$

$$\varphi\left(\mathbf{r},\mathbf{r}_m\right)=\frac{1}{4\pi\varepsilon_0}\int\limits_{V_m}\rho_m\left(\mathbf{r}_m\right)G\left(\mathbf{r},\mathbf{r}_m\right)\mathrm{d}V_m\,. \tag{3.4}$$

Notice that for better understanding, the factor $1/4\pi$ is now before the integral and not in the Green's function. The continuity equation

$$\nabla\cdot\mathbf{J}_m\left(\mathbf{r}_m\right)=-\mathrm{j}\omega\rho_m\left(\mathbf{r}_m\right)\,, \tag{3.5}$$

and then the electric field strength is

$$\mathbf{E}\left(\mathbf{r},\mathbf{r}_m\right)=-\mathrm{j}\omega\mathbf{A}\left(\mathbf{r},\mathbf{r}_m\right)-\nabla\varphi\left(\mathbf{r},\mathbf{r}_m\right)\,. \tag{3.6}$$

If we insert equation (3.3), (3.4) and (3.5) into equation (3.6) we can derive

$$\begin{aligned}\mathbf{E}(\mathbf{r},\mathbf{r}_m) &= -\tfrac{\mathrm{j}\omega\mu_0}{4\pi}\int\limits_{V_m}\mathbf{J}_m(\mathbf{r}_m)\,G(\mathbf{r},\mathbf{r}_m)\,\mathrm{d}V_m - \nabla\left(\tfrac{1}{4\pi\varepsilon_0}\int\limits_{V_m}\rho_m(\mathbf{r}_m)\,G(\mathbf{r},\mathbf{r}_m)\,\mathrm{d}V_m\right)\\ &= -\tfrac{\mathrm{j}\omega\mu_0}{4\pi}\int\limits_{V_m}\mathbf{J}_m(\mathbf{r}_m)\,G(\mathbf{r},\mathbf{r}_m)\,\mathrm{d}V_m - \nabla\left(\tfrac{\mathrm{j}}{4\pi\omega\varepsilon_0}\int\limits_{V_m}\nabla_m\cdot\mathbf{J}_m(\mathbf{r}_m)\,G(\mathbf{r},\mathbf{r}_m)\,\mathrm{d}V_m\right).\end{aligned} \tag{3.7}$$

3.1.1 Far-field approximation for m-th antenna

Because the convention in antenna design is to derive a field in spherical coordinates, the magnetic vector potential is then

$$\mathbf{A}_m(r,\theta,\varphi) = L(\mathbf{J}_m(\mathbf{r}_m)) = \frac{\mu_0}{4\pi}\frac{\mathrm{e}^{-\mathrm{j}kr}}{r}\int\limits_{V_m}\mathbf{J}_m(\mathbf{r}_m)\,\mathrm{e}^{\mathrm{j}k\mathbf{r}_0\cdot\mathbf{r}_m}\mathrm{d}V_m\ , \tag{3.8}$$

where

$$L(\cdot) = \frac{\mu_0}{4\pi}\frac{\mathrm{e}^{-\mathrm{j}kr}}{r}\int\limits_{V_m}(\cdot)\,\mathrm{e}^{\mathrm{j}k\mathbf{r}_0\cdot\mathbf{r}_m}\mathrm{d}V_m\ . \tag{3.9}$$

Electric field strength is

$$\mathbf{E}_m(r,\theta,\varphi) = -\mathrm{j}\omega\mathbf{A}_m(r,\theta,\varphi) = -\frac{\mathrm{j}\omega\mu_0}{4\pi}\frac{\mathrm{e}^{-\mathrm{j}kr}}{r}\int\limits_{V_m}\mathbf{J}_m(\mathbf{r}_m)\,\mathrm{e}^{\mathrm{j}k\mathbf{r}_0\cdot\mathbf{r}_m}\mathrm{d}V_m \tag{3.10}$$

and magnetic field strength

$$\mathbf{H}_m(r,\theta,\varphi) = -\frac{\mathrm{j}\omega}{Z_0}\mathbf{r}_0\times\mathbf{A}_m(r,\theta,\varphi) = \frac{\mathbf{r}_0}{Z_0}\times\mathbf{E}_m(r,\theta,\varphi)\ . \tag{3.11}$$

In previous equations, the position vector is the same as in (3.13) and unit vector in spherical coordinates is

$$\mathbf{r}_0 = \frac{\mathbf{r}}{r} = (\sin(\theta)\cos(\varphi),\sin(\theta)\sin(\varphi),\cos(\theta)) \tag{3.12}$$

and

$$\mathbf{r} = (r\sin(\theta)\cos(\varphi),r\sin(\theta)\sin(\varphi),r\cos(\theta)),\ |\mathbf{r}| = r\ . \tag{3.13}$$

The magnetic vector potential $\mathbf{A}_m$ and current density $\mathbf{J}_m$ can be decomposed in arbitrary coordinate system. In this case, for description of magnetic vector potential $\mathbf{A}_m$ and current density $\mathbf{J}_m$, spherical and Cartesian coordinates are suitable, respectively. They are related [74]

$$\begin{aligned}\mathbf{A}_m(r,\theta,\varphi) &= (A_{mr}(r,\theta,\varphi),A_{m\theta}(r,\theta,\varphi),A_{m\varphi}(r,\theta,\varphi))\\ &= (L(J_{mr}(\mathbf{r}_m)),L(J_{m\theta}(\mathbf{r}_m)),L(J_{m\varphi}(\mathbf{r}_m)))\,,\end{aligned} \tag{3.14}$$

where

$$\begin{aligned} J_{mr}\left(\mathbf{r}_m\right) &= J_{mx}\left(\mathbf{r}_m\right)\sin\left(\theta\right)\cos\left(\varphi\right) + J_{my}\left(\mathbf{r}_m\right)\sin\left(\theta\right)\sin\left(\varphi\right) + J_{mz}\left(\mathbf{r}_m\right)\cos\left(\theta\right) \\ J_{m\theta}\left(\mathbf{r}_m\right) &= J_{mx}\left(\mathbf{r}_m\right)\cos\left(\theta\right)\cos\left(\varphi\right) + J_{my}\left(\mathbf{r}_m\right)\cos\left(\theta\right)\sin\left(\varphi\right) - J_{mz}\left(\mathbf{r}_m\right)\sin\left(\theta\right) \\ J_{m\varphi}\left(\mathbf{r}_m\right) &= -J_{mx}\left(\mathbf{r}_m\right)\sin\left(\varphi\right) + J_{my}\left(\mathbf{r}_m\right)\cos\left(\varphi\right). \end{aligned} \tag{3.15}$$

3.1.2 Generalized impedance for arbitrary oriented array elements

The mutual impedance of m-th and n-th antennas is

$$Z_{\mathrm{A},mn} = \frac{2P_{mn}}{I^*_{m0}I_{n0}}\,, \tag{3.16}$$

where I_{m0}, I_{n0} are current amplitudes on the antenna elements. If we assume that the current distribution on antenna is known, for calculation of the generalized impedance we need to derive just the mutual power of the elements. Complex mutual power radiated by the array element is obtained integrating along the whole dipole m and n.

$$P_{mn} = -\frac{1}{2}\int\limits_{V_m} \mathbf{J}^*_m\left(\mathbf{r}_m\right)\cdot\mathbf{E}_n\left(\mathbf{r}_m,\mathbf{r}_n\right)\mathrm{d}V_m \tag{3.17}$$

If we use the previous equations, specifically equation (3.6) we can write

$$\begin{aligned} P_{mn} =& -\frac{1}{2}\int\limits_{V_m} \mathbf{J}^*_m\left(\mathbf{r}_m\right)\cdot\left(-\mathrm{j}\omega\mathbf{A}_n\left(\mathbf{r}_m,\mathbf{r}_n\right) - \nabla_m\varphi_n\left(\mathbf{r}_m,\mathbf{r}_n\right)\right)\mathrm{d}V_m \\ =& \frac{1}{2}\mathrm{j}\omega\int\limits_{V_m} \mathbf{J}^*_m\left(\mathbf{r}_m\right)\cdot\mathbf{A}_n\left(\mathbf{r}_m,\mathbf{r}_n\right)\mathrm{d}V_m + \\ & \frac{1}{2}\int\limits_{V_m} \nabla_m\cdot\left(\mathbf{J}^*_m\left(\mathbf{r}_m\right)\varphi_n\left(\mathbf{r}_m,\mathbf{r}_n\right)\right) \\ & - \nabla_m\cdot\mathbf{J}^*_m\left(\mathbf{r}_m\right)\varphi_n\left(\mathbf{r}_m,\mathbf{r}_n\right)\mathrm{d}V_m \\ =& \frac{1}{2}\mathrm{j}\omega\int\limits_{V_m} \mathbf{J}^*_m\left(\mathbf{r}_m\right)\cdot\mathbf{A}_n\left(\mathbf{r}_m,\mathbf{r}_n\right)\mathrm{d}V_m - \\ & \frac{1}{2}\int\limits_{V_m} \nabla_m\cdot\mathbf{J}^*_m\left(\mathbf{r}_m\right)\varphi_n\left(\mathbf{r}_m,\mathbf{r}_n\right)\mathrm{d}V_m. \end{aligned} \tag{3.18}$$

Including (3.3) and (3.4) we get the final result

$$\begin{aligned} P_{mn} =& \underbrace{\frac{1}{2}\frac{\mathrm{j}Z_0}{4\pi k}\int\limits_{V_m}\int\limits_{V_n} k^2\mathbf{J}^*_m\left(\mathbf{r}_m\right)\cdot\mathbf{J}_n\left(\mathbf{r}_n\right)G\left(\mathbf{r}_m,\mathbf{r}_n\right)\mathrm{d}V_n\mathrm{d}V_m}_{P^{(\mathbf{J})}_{mn}} \\ & \underbrace{-\frac{1}{2}\frac{\mathrm{j}Z_0}{4\pi k}\int\limits_{V_m}\int\limits_{V_n} \nabla_m\cdot\mathbf{J}^*_m\left(\mathbf{r}_m\right)\nabla_n\cdot\mathbf{J}_n\left(\mathbf{r}_n\right)G\left(\mathbf{r}_m,\mathbf{r}_n\right)\mathrm{d}V_n\mathrm{d}V_m.}_{P^{(\rho)}_{mn}} \end{aligned} \tag{3.19}$$

The above equation when substituted into (3.16) gives the self- and mutual impedance for arbitrary oriented array elements. The entries of $\mathbf{Z}_{\mathrm{A}}$ corresponding to self- and mutual impedances of m-th and n-th dipoles are

$$Z_{\mathrm{A},mn} = \frac{\mathrm{j}30}{k} \int\limits_{-\frac{L_m}{2}}^{\frac{L_m}{2}} \int\limits_{-\frac{L_n}{2}}^{\frac{L_n}{2}} (\Psi - \Upsilon) \frac{e^{-\mathrm{jkR}}}{R} \mathrm{d}l_m \mathrm{d}l_n \ , \tag{3.20}$$

where $\Psi = k^2 \mathbf{j_m}(l_m)\mathbf{j}_n^*(l_n)$, $\Upsilon = \nabla_m \cdot \mathbf{j}_m(l_m) \nabla_n \cdot \mathbf{j}_n^*(l_n)$ and $R = |r_m(l_m) - r_n(l_n)|$ where the thin-wire kernel [109] is used to treat the radii of dipoles and the position vector $\mathbf{r}_m$ and $\mathbf{r}_n$ determine the position of m-th and n-th dipole respectively.

3.1.3 Generalized directivity and radiation intensity for arbitrary oriented array elements

The directivity of an antenna is defined as the ratio of the radiation intensity in a given direction from the antenna to the radiation intensity averaged over all directions. The average radiation intensity is equal to the total power radiated by the antenna divided by 4π. Stated more simply, the directivity of a non isotropic source is equal to the ratio of its radiation intensity in a given direction over that of an isotropic source. The directivity of a radiating source in an angular direction (θ, ϕ) in the spherical coordinates is defined as [20]

$$D(\theta, \phi) = \frac{U(\theta, \phi)}{U_0} = 4\pi \frac{U(\theta, \phi)}{P_{\mathrm{r}}}, \tag{3.21}$$

where U is a radiation intensity in the direction (θ, ϕ), $U_0 = P_{\mathrm{r}}/4\pi$ is an average radiation intensity and P_{r} is a radiated power of the source. If we apply this equation to the array, the mutual directivity of m and n antennas is

$$D_{mn}(\theta, \varphi) = \frac{4\pi U_{mn}(\theta, \varphi)}{P_{mn}} \ . \tag{3.22}$$

Radiation intensity in a given direction is defined as "the power radiated from an antenna per unit solid angle." The radiation intensity is a far-field parameter, and it can be obtained by simply multiplying the power density by the square of the distance [74]. For the array of antennas one can write

$$U_{mn}(\theta, \varphi) = r^2 \mathbf{S}_{mn} \cdot \mathbf{r}_0 = \frac{r^2}{2} \left(\mathbf{E}_m(r, \theta, \varphi) \times \mathbf{H}_n^*(r, \theta, \varphi) \right) \cdot \mathbf{r}_0 \ , \tag{3.23}$$

where r is a distance from the origin of the coordinates, $\mathbf{S}_{mn} \cdot \mathbf{r}_0$ is a radial power density

$$\mathbf{H}_n^*(r, \theta, \varphi) = \left(H_{nr}^*(r, \theta, \varphi), H_{n\theta}^*(r, \theta, \varphi), H_{n\varphi}^*(r, \theta, \varphi) \right) \ , \tag{3.24}$$

$$\mathbf{E}_m(r, \theta, \varphi) = \left(E_{mr}(r, \theta, \varphi), E_{m\theta}(r, \theta, \varphi), E_{m\varphi}(r, \theta, \varphi) \right) \ . \tag{3.25}$$

So the generalized radiation intensity equation is now

$$\begin{aligned} U_{mn}(\theta,\varphi) &= \underbrace{\frac{r^2}{2}E_{m\theta}(r,\theta,\varphi)\,H^*_{n\varphi}(r,\theta,\varphi)}_{U^{(\theta)}_{mn}(\theta,\varphi)} \underbrace{-\frac{r^2}{2}E_{m\varphi}(r,\theta,\varphi)\,H^*_{n\theta}(r,\theta,\varphi)}_{U^{(\varphi)}_{mn}(\theta,\varphi)} \\ &= \frac{r^2}{2}\left(-\mathrm{j}\omega\mathbf{A}_m(r,\theta,\varphi)\times\left(-\frac{\mathrm{j}\omega}{Z_0}\mathbf{r}_0\times\mathbf{A}_n(r,\theta,\varphi)\right)^*\right)\cdot\mathbf{r}_0 \\ &= \underbrace{\frac{r^2\omega^2}{2Z_0}A_{m\theta}(r,\theta,\varphi)\,A^*_{n\theta}(r,\theta,\varphi)}_{U^{(\theta)}_{mn}(\theta,\varphi)} + \underbrace{\frac{r^2\omega^2}{2Z_0}A_{m\varphi}(r,\theta,\varphi)\,A^*_{n\varphi}(r,\theta,\varphi)}_{U^{(\varphi)}_{mn}(\theta,\varphi)} \\ &= \underbrace{\frac{\omega^2\mu_0^2}{32\pi^2Z_0}\int_{V_m}\int_{V_n}J_{m\theta}(\mathbf{r}_m)\,J^*_{n\theta}(\mathbf{r}_n)\,\mathrm{e}^{\mathrm{j}k\mathbf{r}_0\cdot(\mathbf{r}_m-\mathbf{r}_n)}\mathrm{d}V_n\mathrm{d}V_m}_{U^{(\theta)}_{mn}(\theta,\varphi)} \\ &\quad + \underbrace{\frac{\omega^2\mu_0^2}{32\pi^2Z_0}\int_{V_m}\int_{V_n}J_{m\varphi}(\mathbf{r}_m)\,J^*_{n\varphi}(\mathbf{r}_n)\,\mathrm{e}^{\mathrm{j}k\mathbf{r}_0\cdot(\mathbf{r}_m-\mathbf{r}_n)}\mathrm{d}V_n\mathrm{d}V_m}_{U^{(\varphi)}_{mn}(\theta,\varphi)}, \end{aligned} \tag{3.26}$$

where $U^{(\theta)}_{mn}(\theta,\varphi)$ and $U^{(\varphi)}_{mn}(\theta,\varphi)$ are contributions to θ and ϕ polarizations and

$$\begin{aligned} \mathbf{r}_0\cdot(\mathbf{r}_m-\mathbf{r}_n) = {} & (x_m-x_n)\sin(\theta)\cos(\varphi) + \\ & (y_m-y_n)\sin(\theta)\sin(\varphi) + \\ & (z_m-z_n)\cos(\theta)\,. \end{aligned} \tag{3.27}$$

Normalized mutual radiation intensity of m-th and n-th antennas is

$$u_{mn}(\theta,\varphi) = \frac{U_{mn}(\theta,\varphi)}{I_{m0}I^*_{n0}} = \frac{U^{(\theta)}_{mn}(\theta,\varphi)}{I_{m0}I^*_{n0}} + \frac{U^{(\varphi)}_{mn}(\theta,\varphi)}{I_{m0}I^*_{n0}} = u^{(\theta)}_{mn}(\theta,\varphi) + u^{(\varphi)}_{mn}(\theta,\varphi)\ . \tag{3.28}$$

The radiated power P_r required for calculating the directivity D (3.22) can be obtained through the Electromagnetic Field (EMF) method [110], or by integrating the intensity U over the complete solid angle

$$P_\mathrm{r} = \int_0^{2\pi}\int_0^{\pi}U(\theta,\phi)\sin\theta\,\mathrm{d}\theta\,\mathrm{d}\phi = \sum_{m=1}^{N}\sum_{n=1}^{N}P_{mn} \tag{3.29}$$

where

$$P_{mn} = I^*_m I_n\int_0^{2\pi}\int_0^{\pi}u_{mn}(\theta,\phi)\sin\theta\,\mathrm{d}\theta\,\mathrm{d}\phi = I^*_m I_n p_{mn} \tag{3.30}$$

is a mutual radiated power of the m-th and n-th elements and p_{mn} is its normalization to the currents I_m and I_n.

Consequently, the directivity D (3.21) takes a compact matrix form using (3.26), (3.29),

(3.30) [58], [63], [60], [65]

$$D(\theta,\phi) = 4\pi \frac{\mathbf{I}^{\mathrm{H}} \begin{bmatrix} u_{11}(\theta,\phi) & \cdots & u_{1N}(\theta,\phi) \\ \vdots & \ddots & \vdots \\ u_{N1}(\theta,\phi) & \cdots & u_{NN}(\theta,\phi) \end{bmatrix} \mathbf{I}}{\mathbf{I}^{\mathrm{H}} \begin{bmatrix} p_{11} & \cdots & p_{1N} \\ \vdots & \ddots & \vdots \\ p_{N1} & \cdots & p_{NN} \end{bmatrix} \mathbf{I}} = 4\pi \frac{\mathbf{I}^{\mathrm{H}} \mathbf{u}(\theta,\phi) \mathbf{I}}{\mathbf{I}^{\mathrm{H}} \mathbf{p} \mathbf{I}} \tag{3.31}$$

where H stands for Hermitian transpose, $\mathbf{I} = [I_1, \cdots, I_N]^{\mathrm{T}}$ is a vector of the excitation currents and $\mathbf{u}$ and $\mathbf{p}$ are matrices of the normalized mutual intensities u_{mn} and powers p_{mn} respectively. The mutual intensity u_{mn} and power p_{mn} represent influence of interaction of the m-th and n-th elements on the directivity D.

3.2 Matrix treatment of dipole arrays

To increase calculation speed in our approach, while keeping reasonable accuracy around fundamental half-wavelength resonance of the dipoles, we assume simple sinusoidal current distribution with central feeding at the m-th dipole

$$I_m(l_m) = I_{0m} \sin\left(k\left(\frac{L_m}{2} - |l_m|\right)\right) = I_{0m} f_m(l_m), l_m \in \left\langle -\frac{L_m}{2}, \frac{L_m}{2} \right\rangle , \tag{3.32}$$

where k is wavenumber, L_m is length of the dipole, l_m is coordinate along m-th dipole and I_{m0} is amplitude of a feeding current of a m-th dipole.

Now if we assume linear current, it can be writet

$$\mathbf{J}_m(\mathbf{r}_m) = (J_x(\mathbf{r}_m), J_y(\mathbf{r}_m), J_z(\mathbf{r}_m)) = I_m(l_m)\mathbf{r}_m, \tag{3.33}$$

where $\mathbf{r}_m$ is position vector along dipole element and then the divergence of this current is

$$\nabla_m \mathbf{J}_m(\mathbf{r}_m) = \frac{\partial I_m(l_m)}{\partial l_m} = -I_{m0}\mathrm{sgn}(l_m)\, k \cos\left(k\left(\frac{L_m}{2} - |l_m|\right)\right) . \tag{3.34}$$

From the equation (3.16) and (3.19) we can write

$$
\begin{aligned}
Z_{\mathrm{A},mn} = & \underbrace{\frac{1}{I^*_{m0} I_{n0}} \frac{\mathrm{j} Z_0}{4\pi k} \int_{-\frac{L_m}{2}}^{\frac{L_m}{2}} \int_{-\frac{L_n}{2}}^{\frac{L_n}{2}} k^2 \mathbf{J}^*_m(\mathbf{r}_m) \cdot \mathbf{J}_n(\mathbf{r}_n) G(\mathbf{r}_m, \mathbf{r}_n) \, \mathrm{d}l_n \mathrm{d}l_m}_{Z^{(\mathbf{J})}_{mn}} \\
& \underbrace{-\frac{1}{I^*_{m0} I_{n0}} \frac{\mathrm{j} Z_0}{4\pi k} \int_{-\frac{L_m}{2}}^{\frac{L_m}{2}} \int_{-\frac{L_n}{2}}^{\frac{L_n}{2}} \nabla_m \cdot \mathbf{J}^*_m(\mathbf{r}_m) \nabla_n \cdot \mathbf{J}_n(\mathbf{r}_n) G(\mathbf{r}_m, \mathbf{r}_n) \, \mathrm{d}l_n \mathrm{d}l_m}_{Z^{(\rho)}_{mn}} \\
& \underbrace{= \frac{\mathrm{j} Z_0 k}{4\pi} \mathbf{r}_{mo} \cdot \mathbf{r}_{no} \int_{-\frac{L_m}{2}}^{\frac{L_m}{2}} \int_{-\frac{L_n}{2}}^{\frac{L_n}{2}} \sin(\xi_m) \sin(\xi_n) G(\mathbf{r}_m, \mathbf{r}_n) \, \mathrm{d}l_n \mathrm{d}l_m}_{Z^{(\mathbf{J})}_{mn}} \\
& \underbrace{-\frac{\mathrm{j} Z_0 k}{4\pi} \int_{-\frac{L_m}{2}}^{\frac{L_m}{2}} \int_{-\frac{L_n}{2}}^{\frac{L_n}{2}} \mathrm{sgn}(l_m) \cos(\xi_m) \mathrm{sgn}(l_n) \cos(\xi_n) G(\mathbf{r}_m, \mathbf{r}_n) \, \mathrm{d}l_n \mathrm{d}l_m,}_{Z^{(\rho)}_{mn}}
\end{aligned}
\tag{3.35}
$$

where

$$
\xi_m = k \left(\frac{L_m}{2} - |l_m| \right), \tag{3.36}
$$

and

$$
\xi_n = k \left(\frac{L_n}{2} - |l_n| \right). \tag{3.37}
$$

The evaluation of mutual intensity of the dipole array is very similar to radiation intensity for arbitrary oriented antenna array. We are going to use equation (3.26) and

equation (3.32), where the volume integral will become line integral, so

$$\begin{aligned}
U_{mn}(\theta,\varphi) &= \underbrace{\frac{\omega^2\mu_0^2}{32\pi^2 Z_0}\int_{-\frac{L_m}{2}}^{\frac{L_m}{2}}\int_{-\frac{L_n}{2}}^{\frac{L_n}{2}} j_{m\theta}(\mathbf{r}_m)\, j^*_{n\theta}(\mathbf{r}_n)\, \mathrm{e}^{\mathrm{j}k\mathbf{r}_0\cdot(\mathbf{r}_m-\mathbf{r}_n)}\mathrm{d}l_n\mathrm{d}l_m}_{U^{(\theta)}_{mn}(\theta,\varphi)} \\
&\quad + \underbrace{\frac{\omega^2\mu_0^2}{32\pi^2 Z_0}\int_{-\frac{L_m}{2}}^{\frac{L_m}{2}}\int_{-\frac{L_n}{2}}^{\frac{L_n}{2}} j_{m\varphi}(\mathbf{r}_m)\, j^*_{n\varphi}(\mathbf{r}_n)\, \mathrm{e}^{\mathrm{j}k\mathbf{r}_0\cdot(\mathbf{r}_m-\mathbf{r}_n)}\mathrm{d}l_n\mathrm{d}l_m}_{U^{(\varphi)}_{mn}(\theta,\varphi)} \\
&= \underbrace{\frac{\omega^2\mu_0^2}{32\pi^2 Z_0} I_{m0}I^*_{n0}q^{(\theta)}_{mn}\mathrm{e}^{\mathrm{j}k\mathbf{r}_0\cdot(\mathbf{r}_{mc}-\mathbf{r}_{nc})}\int_{-\frac{L_m}{2}}^{\frac{L_m}{2}}\int_{-\frac{L_n}{2}}^{\frac{L_n}{2}} j'_m j'_n \mathrm{e}^{\mathrm{j}k\mathbf{r}_0\cdot(\mathbf{r}_{mo}l_m-\mathbf{r}_{no}l_n)}\mathrm{d}l_n\mathrm{d}l_m}_{U^{(\theta)}_{mn}(\theta,\varphi)} \\
&\quad + \underbrace{\frac{\omega^2\mu_0^2}{32\pi^2 Z_0} I_{m0}I^*_{n0}q^{(\varphi)}_{mn}\mathrm{e}^{\mathrm{j}k\mathbf{r}_0\cdot(\mathbf{r}_{mc}-\mathbf{r}_{nc})}\int_{-\frac{L_m}{2}}^{\frac{L_m}{2}}\int_{-\frac{L_n}{2}}^{\frac{L_n}{2}} j'_m j'_n \mathrm{e}^{\mathrm{j}k\mathbf{r}_0\cdot(\mathbf{r}_{mo}l_m-\mathbf{r}_{no}l_n)}\mathrm{d}l_n\mathrm{d}l_m}_{U^{(\varphi)}_{mn}(\theta,\varphi)},
\end{aligned} \tag{3.38}$$

where $q^{(\theta)}_{mn}$ and $q^{(\phi)}_{mn}$ is contribution to θ and ϕ polarization, $j'_m = \sin\left(k\left(\frac{L_m}{2}-|l_m|\right)\right)$ and $j'_n = \sin\left(k\left(\frac{L_n}{2}-|l_n|\right)\right)$ are normalized current density. Thus, the absolute directivity will be

$$D = D_\theta + D_\varphi = \frac{4\pi U_\theta}{P_r} + \frac{4\pi U_\varphi}{P_r}\,. \tag{3.39}$$

For a better performance we can use King's three term current approximation [20], but will lose some computational time. An antenna, whether transmitting or receiving, is always driven by an external source field. In transmitting mode, the antenna is driven by a generator voltage or current applied to its input terminals, and in receiving mode, by an incident electric field (typically, a uniform plane wave if it is arriving from far distances.) The incident field E_{in} induces a current on the antenna. In turn, the current generates its own field E, which is radiated away. Assuming a perfectly conducting antenna, the boundary conditions are that the tangential components of the total electric field vanish on the antenna surface. These boundary conditions are enough to determine the current distribution induced on the antenna [20]. Then the current on the antenna element would be approximated

$$\begin{aligned}
I_m(l_m) =& A_1\left(\sin k|l_m| - \sin k\frac{L_m}{2}\right) \\
&+ A_2\left(\cos kl_m - \cos k\frac{L_m}{2}\right) \\
&+ A_3\left(\cos k\frac{l_m}{2} - \cos k\frac{L_m}{4}\right),
\end{aligned} \tag{3.40}$$

To determine the expansion coefficients A_1, A_2, A_3 one need to insert it into the Hallen's equation. A comparison of the current along the dipole is depicted in Figure 3.3, which shows current distributions according to the numerical solution of Hallen's equation and King's three-term approximation with sinusoidal approximation given by (3.32) for the two cases of $L_m = 0.5\lambda$ and $L_m = \lambda$. As it is apparent that sinusoidal current distribution given by (3.32) is acceptable approximation for a half-wavelength dipole. The numerical

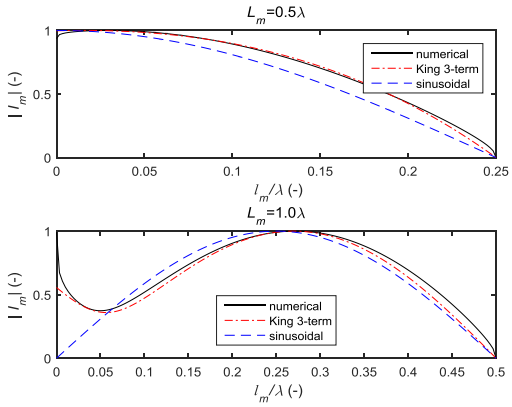

Figure 3.3: Comparison of current distributions for half- and one-wavelength dipoles obtained by different approaches.

integration are done with a 32-point Gauss-Legendre quadrature integration routine implemented with the function quadr, which provides the appropriate weights and evaluation points for the integration. As is evident from the above example, King's three-term approximation does not work particularly well for larger antenna lengths (about $l > 1.25\lambda$). This can be attributed to the crude approximation of computing the coefficients A_i by matching the defining currents only at one point along the antenna (at the current maxima). It turns out, however, that the three-term approximation is very accurate if fitted to the "exact" current as computed by solving Hallen's equation numerically, with a range of applicability of up to about $l = 2\lambda$. With a 4-term fit, the range increases to $l = 3\lambda$. The developed method is a framework of self- and mutual radiation intensities and self- and mutual radiated powers of array elements which is similar to the approach developed by Hansen who used mutual radiation resistances in his derivation of the array directivity [111].

3.3 Modal decomposition

The concept of characteristic mode analysis is conventionally used to find basis for a single structure (antenna) that simultaneously minimize the net reactive power and maximize radiated power [2]. Characteristic current modes $\mathbf{J}$ can be obtained as the eigenfunctions of the following particular weighted eigenvalue equation

$$\mathbf{XJ} = \lambda \mathbf{RJ} \,, \tag{3.41}$$

here $\mathbf{R}$ and $\mathbf{X}$ are the real and imaginary part of the complex impedance matrix $\mathbf{Z}$ given by for instance MoM, λ are the eigenvalues and $\mathbf{J}$ is the eigen function or eigen current. The impedance matrix $\mathbf{Z}$ is symmetric.

Next it is known from reciprocity theorem that if $\mathbf{Z}$ is a linear symmetric operator, then, its Hermitian parts $\mathbf{R}$ and $\mathbf{X}$ will be real and symmetric operators, λ are real and all the eigen currents $\mathbf{J}$ can be chosen equiphase over the antenna. Additionally, the eigenmodes are all orthogonal and can be made orthonormal using normalization and scaled to unit radiated power [27]

$$\frac{1}{2}\langle \mathbf{J}, \mathbf{RJ} \rangle = 1 \ , \tag{3.42}$$

where $\langle\rangle$ is inner product. From the basic equation that describes the orthogonality of the modes [112] one can write these equations

$$\langle \mathbf{J}_\mathbf{m}^*, \mathbf{R}(\mathbf{J_n}) \rangle = \delta_{mn} \ , \tag{3.43}$$

$$\langle \mathbf{J}_\mathbf{m}^*, \mathbf{X}(\mathbf{J_n}) \rangle = \lambda\delta_{mn} \ , \tag{3.44}$$

where δ_{mn} is the Kronecker delta. Furthermore, (3.43) is equal to the active power of the antenna and (3.44) reactive power respectively [27]. The characteristic eigenvalue can be found, when proper currents are known, using

$$F(J) = \frac{\langle \mathbf{J}^*, \mathbf{XJ} \rangle}{\langle \mathbf{J}^*, \mathbf{RJ} \rangle} = \frac{2\omega((W_\mathrm{m} - W_\mathrm{e})}{P_r} \ . \tag{3.45}$$

In general, the eigenvalues λ_p ranges from $-\infty$ to $+\infty$. When the eigenvalue is zero, the antenna is at resonance. Additionally, the sign of the eigenvalue determines whether the mode contributes to store magnetic energy ($\lambda > 0$) or electric energy ($\lambda < 0$). As mentioned before, eigenvalues are handy for finding the resonant frequency of the modes. Nevertheless, in practice is preferred other alternative representation called as characteristic angles [113]. The characteristic angle is defined as [114]

$$\delta = 180^\circ - \arctan(\lambda) \ . \tag{3.46}$$

From a physical point of view, a characteristic angle models the phase angle between a characteristic current $\mathbf{J}$ and the associated characteristic field [115], or as mentioned in [116]. At a resonant frequency f_0, characteristic number satisfies the condition $\lambda(f_0) = 0$, that is the characteristic angle $\delta(f_0) = 180^\circ$, as follows from (3.46). Therefore, when the characteristic angle is close to 180°, the mode is a good radiator. Thus, the bandwidth of a mode can be deduced from the slope of the curve with frequency described by the characteristic angles. From the modal significance [32] one can deduce the values of characteristic angle, which correspond to one-half the power radiated at resonance. These eigenvalues generate characteristic angles of 135° and 225°.

3.3.1 Modal decomposition in antenna arrays - "Discrete modes"

The theory of characteristic modes could be extended to antenna array. When we rework the equation (3.41) for the antenna array, with prescribed current distribution and only the feeding currents $\mathbf{I}_p$ are unknown, where p is index of the element, in that case we obtain only eigenvectors of each element from the array

$$\mathbf{X}\mathbf{I}_p = \lambda_p \mathbf{R}\mathbf{I}_p \ . \tag{3.47}$$

In the case of antenna array, the characteristic mode problem is analogical and the result from (3.47) is a set of eigenvectors $\mathbf{I}_p$ and eigenvalues λ_p that minimize the following power functional

$$F(I_p) = \frac{\mathbf{I}_p^{\mathrm{H}} \mathbf{X} \mathbf{I}_p}{\mathbf{I}_p^{\mathrm{H}} \mathbf{R} \mathbf{I}_p} = \frac{\text{array reactive power}}{\text{array radiated power}} = \lambda_p \ , \tag{3.48}$$

where H stands for Hermitian transpose. By the definition, the eigenvectors $\mathbf{I}_p$ are real and are used to expand the sinusoidal function (3.32). From the eigenvalue, one can derive valuable information. If the mode with eigenvalue close to zero is excited by characteristic current amplitudes, the array as a whole will be in resonance resulting to simultaneous match of all ports driving (active) impedances [117] when proper impedance on port is provided.

The driving impedance for an elements above PEC ground $\mathbf{Z}_d$ seen at m-th dipole for a p-th CM is evaluated as

$$\mathbf{Z}_{d,mp} = \sum_{n=1}^{N} \frac{I_{np}}{I_{mp}} \mathbf{Z}_{A,mn} \ , \tag{3.49}$$

where $\mathbf{Z}_{A,mn}$ is the mutual impedance between the m-th dipole and n-th dipole minus the mutual impedance between the m-th dipole and the image of the n-th dipole. Similarly, $\mathbf{Z}_{A,mm}$ is the self-impedance of the m-th dipole minus the mutual impedance with its image [118].

As an example let us consider a three parallel thin-wire dipoles placed horizontally above an infinite electric ground plane, equally spaced, each with the same length of $L_1 = L_2 = L_3 = L = \lambda/2$, where $\lambda = 0.3$ m is a wavelength at the frequency 1 GHz. A spacing between each two dipoles is $s_{12} = s_{23} = s = 0.25\lambda$ and a height above the ground plane is $h = 0.25\lambda$, see Figure 3.4. The calculated impedance, when the elements are fed by modal currents (or voltages) for outer and inner dipole and first three modes of the array is in Figure 3.5 and Figure 3.6 respectively.

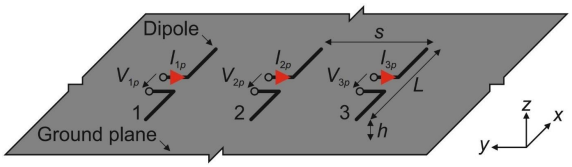

Figure 3.4: Geometry of array of three horizontal dipoles above infinite electric ground plane

.

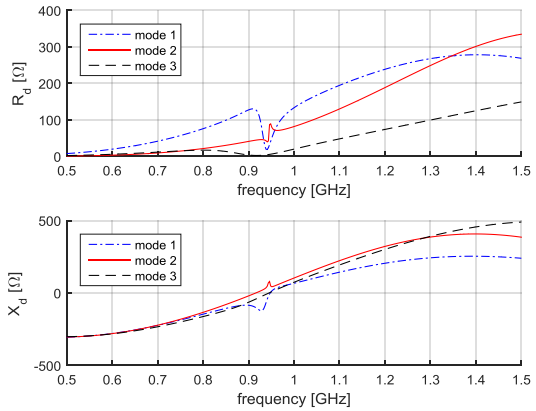

Figure 3.5: Real and imaginary part of the driving impedance for outer dipole when fed by modal currents.

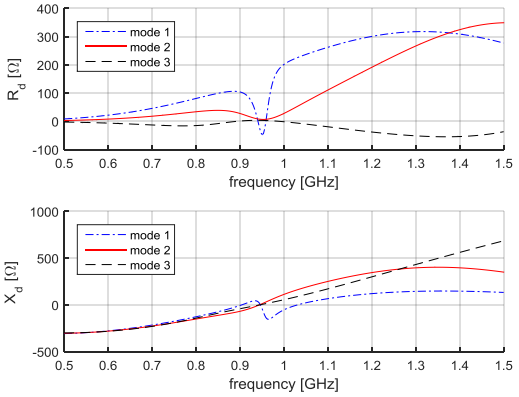

Figure 3.6: Real and imaginary part of the driving impedance for inner dipole when fed by modal currents.

Also, a modal quality factor can be defined from the fractional bandwidth as [31]

$$Q_{\mathrm{rad},p} \approx \frac{1}{BW_p} \,. \tag{3.50}$$

The quality factor measures how sharp the resonant response frequency is, thus, the higher Q, the narrower radiating bandwidth. Several different definitions of Q factor can be found:

$$\widetilde{Q} = \frac{\omega(\widetilde{W}_{\mathrm{m}} + \widetilde{W}_{\mathrm{e}})}{P_r} \,, \tag{3.51}$$

$$Q_{\mathrm{z}} = \frac{\omega}{2R_{\mathrm{in}}} \left| \frac{\partial Z_{\mathrm{in}}}{\partial \omega} \right| \,, \tag{3.52}$$

$$Q_{\mathrm{h}} = \frac{\omega}{2} \frac{\mathbf{I}_p^{\mathrm{H}} \frac{\partial \mathbf{X}}{\partial \omega} \mathbf{I}_p}{\mathbf{I}_p^{\mathrm{H}} \mathbf{R} \mathbf{I}_p} \,, \tag{3.53}$$

where the first definition is conventional definition and $\widetilde{W}_{\mathrm{m}}$, $\widetilde{W}_{\mathrm{e}}$ are magnetic and electric energy modified as in [3] to be finite. The Q_{z} is the impedance definition [116], where Z_{in} is input impedance and Q_{h} is definition done by Harrington and Mautz [31]. Finally, in [31] an interpretation of a modal Q made in terms of the frequency variation of the eigenvalues is also proposed

$$Q_{p,\mathrm{Harrington}} \approx \frac{\omega}{2}\frac{\partial \lambda_p}{\partial \omega} \,. \tag{3.54}$$

A good measure of impedance bandwidth is the impedance quality factor expressed in (3.52). This equation may be understood and obtained from (3.52) as a power ratio

$$Q_{\mathrm{z}} = \frac{P_{\mathrm{app}}}{P_{\mathrm{lost}}} \,, \tag{3.55}$$

where $P_{\mathrm{app}} = \frac{\partial}{\partial \omega}\sqrt{P_{\mathrm{lost}}^2 + \mathrm{jP}_{\mathrm{reactive}}^2}$ is frequency derivative of the apparent power (the change of reactive power is usually dominant) and P_{lost} is sum of radiated power and power lost in conductors. However, it should be noted that there is no exact relation between Q_z and bandwidth and there are cases of $Q_{\mathrm{z}} = 0$ and finite bandwidth [119]. Indeed, the change of impedance with frequency can be made flat at some point $\frac{\partial Z_{\mathrm{in}}}{d\omega} = 0$. In case of antenna arrays this is accomplished by mutual impedances.

As a second example, we consider an antenna array consisting of ten parallel thin-wire dipoles with the same length L, spacing s and height h above the ground plane as in the first example. The characteristic angles δ_p of all CM are in Figure 3.7. For simplicity,

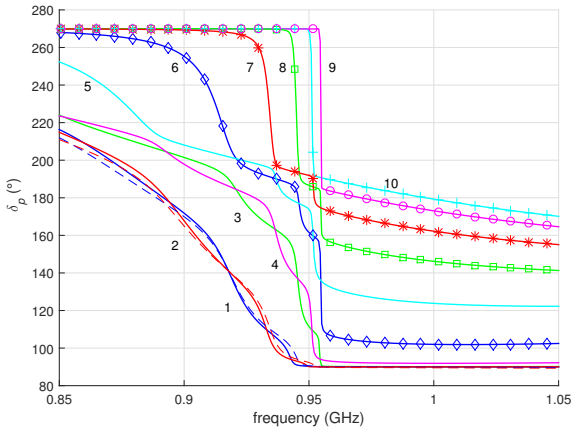

Figure 3.7: Characteristic angles of all CM for the ten-element dipole array. Numbers $1, 2, \cdots, 10$ at curves correspond to number p of CM. FEKO results are shown only for CM $p = 1, 2$ (dashed curves). Reproduced from [65].

FEKO results are shown in Figure 3.7 only for CM $p = 1, 2$ which are the CM with the two lowest resonant frequencies.

It is seen from Figure 3.7 that the CM are quite complex thanks to strong mutual interactions of the array dipoles. Contrary to the classical "continuous" CM analysis, in the "discrete" case, we have to deal with two kinds of resonances: A resonance of an individual array element and a resonance of the whole array. The latter strongly depends on spacing and the mutual orientation of the elements.

The corresponding currents $\mathbf{I}_p$ for the ten element array, where the characteristic angles δ_p of all CM are in Fig. 3.7 related to at the resonant frequencies of the CM are in Fig. 3.8

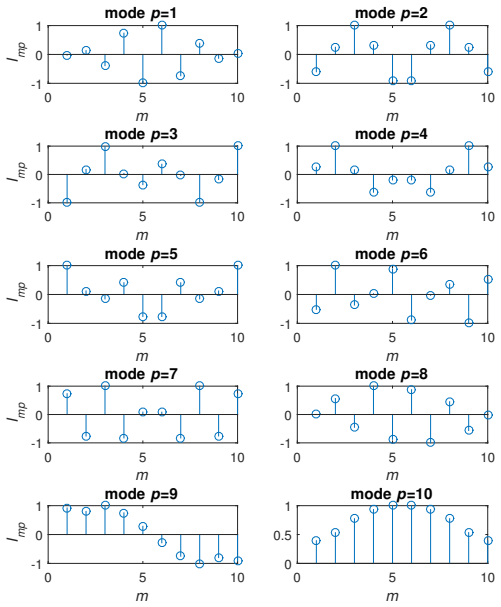

Figure 3.8: Excitation currents (components of eigenvector $\mathbf{I}_p$) of all CM for the ten-element dipole array at resonant frequencies of CM. Components I_{mp} are normalized to $\max(|I_{mp}|)$ for given p. Reproduced from [65].

3.3.2 Excitation of modes

Advantage of the characteristic modes is that they are computed without an excitation, which is represented by an arbitrary impressed field $\mathbf{E}$. On the other hand, it should be noted that when the geometry of the structure is changed, the modes will change as well. Thus, this fact complicates a usage of characteristic modes for designing of the antenna arrays.

To complete the task of excitation of modes we connect the antenna array to arbitrary sources and loads. Thus we can divide the computation to voltage and current sources. When we introduce the circuit diagram for a voltage sources case, shown in Figure 3.9, we denote the matrix of mutual impedances as:

$$\mathbf{Z}_\mathrm{A} = \begin{bmatrix} Z_{\mathrm{A},11} & \cdots & Z_{\mathrm{A},1n} & \cdots & Z_{\mathrm{A},1N} \\ \vdots & \ddots & & & \vdots \\ Z_{\mathrm{A},m1} & & Z_{\mathrm{A},mn} & & Z_{\mathrm{A},mN} \\ \vdots & & & \ddots & \vdots \\ Z_{\mathrm{A},N1} & \cdots & Z_{\mathrm{A},Nn} & \cdots & Z_{\mathrm{A},NN} \end{bmatrix}, \tag{3.56}$$

matrix of load impedances as

$$\mathbf{Z}_{\mathrm{L}} = \begin{bmatrix} Z_{\mathrm{L},11} & \cdots & Z_{\mathrm{L},1n} & \cdots & Z_{\mathrm{L},1N} \\ \vdots & \ddots & & & \vdots \\ Z_{\mathrm{L},m1} & & Z_{\mathrm{L},mn} & & Z_{\mathrm{L},mN} \\ \vdots & & & \ddots & \vdots \\ Z_{\mathrm{L},N1} & \cdots & Z_{\mathrm{L},Nn} & \cdots & Z_{\mathrm{L},NN} \end{bmatrix} \tag{3.57}$$

and the matrix of output impedances, which could be actually the loss matrix defined as

$$\mathbf{Z}_{\mathrm{O}} = \begin{bmatrix} Z_{\mathrm{O},1} & \cdots & 0 & \cdots & 0 \\ \vdots & \ddots & & & \vdots \\ 0 & & Z_{\mathrm{O},m} & & 0 \\ \vdots & & & \ddots & \vdots \\ 0 & \cdots & 0 & \cdots & Z_{\mathrm{O},N} \end{bmatrix}. \tag{3.58}$$

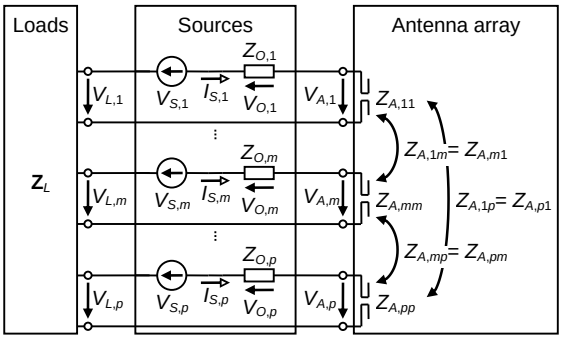

Figure 3.9: Circuit diagram of the antenna array

From the circuit relations we can calculate the source current from known impedances of array $\mathbf{Z}_{\mathrm{A}}$, load impedances $\mathbf{Z}_{\mathrm{L}}$, source impedance $\mathbf{Z}_{\mathrm{S}}$ and voltages set on a generator $\mathbf{V}_{\mathrm{S}}$ see Figure 3.9 as

$$\mathbf{I}_{\mathrm{S}} = \left(\mathbf{Z}_{\mathrm{A}} + \mathbf{Z}_{\mathrm{L}} + \mathbf{Z}_{\mathrm{O}}\right)^{-1} \mathbf{V}_{\mathrm{S}} \tag{3.59}$$

and the corresponding voltages

$$\mathbf{V}_{\mathrm{A}} = \mathbf{Z}_{\mathrm{A}} \cdot \mathbf{I}_{\mathrm{S}}, \mathbf{V}_{\mathrm{L}} = \mathbf{Z}_{\mathrm{L}} \cdot \mathbf{I}_{\mathrm{S}}, \mathbf{V}_{\mathrm{O}} = \mathbf{Z}_{\mathrm{O}} \cdot \mathbf{I}_{\mathrm{S}} \tag{3.60}$$

The available active power corresponding to a power set on generator

$$\mathbf{P}_{\mathrm{AV}} = \frac{1}{8} \mathbf{V}_{\mathrm{S}} \circ \left(\left(\mathrm{Re}\left(\mathbf{Z}_{\mathrm{O}}\right) \right)^{-1} \cdot \mathbf{V}_{\mathrm{S}}^{*} \right), \tag{3.61}$$

where $\circ$ is a function composition. In our case the excitation of the characteristic mode, thanks to the sinusoidal current assumption, is simple.

If calculating with admitances and the antenna array is connected to current sources as depicted in Figure 3.10, the task is similar to voltage sources.

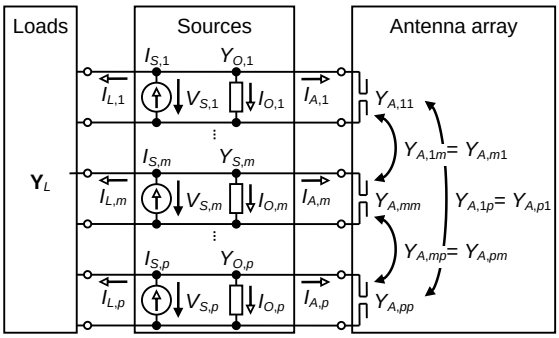

Figure 3.10: Circuit diagram of the antenna array

The matrix of mutual admitances is

$$\mathbf{Y}_\mathrm{A} = \begin{bmatrix} Y_{\mathrm{A},11} & \cdots & Y_{\mathrm{A},1n} & \cdots & Y_{\mathrm{A},1N} \\ \vdots & \ddots & & & \vdots \\ Y_{\mathrm{A},m1} & & Y_{\mathrm{A},mn} & & Y_{\mathrm{A},mN} \\ \vdots & & & \ddots & \vdots \\ Y_{\mathrm{A},N1} & \cdots & Y_{\mathrm{A},Nn} & \cdots & Y_{\mathrm{A},NN} \end{bmatrix}, \tag{3.62}$$

matrix of load impedances as

$$\mathbf{Y}_\mathrm{L} = \begin{bmatrix} Y_{\mathrm{L},11} & \cdots & Y_{\mathrm{L},1n} & \cdots & Y_{\mathrm{L},1N} \\ \vdots & \ddots & & & \vdots \\ Y_{\mathrm{L},m1} & & Y_{\mathrm{L},mn} & & Y_{\mathrm{L},mN} \\ \vdots & & & \ddots & \vdots \\ Y_{\mathrm{L},N1} & \cdots & Y_{\mathrm{L},Nn} & \cdots & Y_{\mathrm{L},NN} \end{bmatrix} \tag{3.63}$$

and the matrix of output impedances, which could be actually the loss matrix defined as

$$\mathbf{Y}_\mathrm{O} = \begin{bmatrix} Y_{\mathrm{O},1} & \cdots & 0 & \cdots & 0 \\ \vdots & \ddots & & & \vdots \\ 0 & & Y_{\mathrm{O},m} & & 0 \\ \vdots & & & \ddots & \vdots \\ 0 & \cdots & 0 & \cdots & Y_{\mathrm{O},N} \end{bmatrix}. \tag{3.64}$$

From the circuit relations the source voltage from known admitances and current

$$\mathbf{V}_\mathrm{S} = \left(\mathbf{Y}_\mathrm{A} + \mathbf{Y}_\mathrm{L} + \mathbf{Y}_\mathrm{O}\right)^{-1} \mathbf{I}_\mathrm{S} \tag{3.65}$$

and the corresponding currents

$$\mathbf{I}_\mathrm{A} = \mathbf{Y}_\mathrm{A} \cdot \mathbf{V}_\mathrm{S}, \mathbf{I}_\mathrm{L} = \mathbf{Y}_\mathrm{L} \cdot \mathbf{V}_\mathrm{S}, \mathbf{I}_\mathrm{O} = \mathbf{Y}_\mathrm{O} \cdot \mathbf{V}_\mathrm{S} \tag{3.66}$$

The available active power corresponding to a power set on generator

$$\mathbf{P}_{\mathrm{AV}} = \frac{1}{8}\mathbf{I}_{\mathrm{S}} \circ \left(\left(\mathrm{Re}\left(\mathbf{Y}_{\mathrm{O}} \right) \right)^{-1} \cdot \mathbf{I}_{\mathrm{S}}^{*} \right). \tag{3.67}$$

The theory in this section will be used to set the proper source voltage of a generator, when feeding the antenna array.

3.4 Array synthesis for different optima

Similar as the CM problem we can formulate the eigenproblem task in several different ways.

1. Radiation modes [120]
$$\mathbf{R}\mathbf{I}_p = \lambda_p \mathbf{I}_p \tag{3.68}$$

2. Magnetic and electric stored energy modes [120]
$$\mathbf{X}^{\mathrm{m}}\mathbf{I}_p = \lambda_p^{\mathrm{m}} \mathbf{I}_p \,, \tag{3.69}$$

$$\mathbf{X}^{\mathrm{e}}\mathbf{I}_p = \lambda_p^{\mathrm{e}} \mathbf{I}_p \,, \tag{3.70}$$

   where $\mathbf{X}^{\mathrm{m}}$ and $\mathbf{X}^{\mathrm{e}}$ correspond to the imaginary part $\mathbf{X}$ of the impedance $\mathbf{Z}_{\mathrm{A}}$ divided into its current and charge components (only Ψ and Υ part in (3.20) are retained respectively).

3. Q-factor modes [31]
$$\omega \mathbf{X}' \mathbf{I}_p = Q_p \mathbf{R}\mathbf{I}_p \,, \tag{3.71}$$

   where $\mathbf{X}'$ is frequency derivative of the imaginary part $\mathbf{X}$ of the impedance matrix $\mathbf{Z}_{\mathrm{A}}$ and Q_p is Q factor (eigenvalue) of p-th mode.

4. Directivity modes

$$4\pi \mathbf{u}\mathbf{I}_p = D\mathbf{p}\mathbf{I}_p. \tag{3.72}$$

   where $\mathbf{u}$ and $\mathbf{p}$ are matrices of the normalized radiation intensities u_{mn} and p_{mn} is a normalization of a mutual radiated power of the m-th and n-th elements explained later in Chapter 4.5.

In this work we aim on the directivity modes.

3.5 Super directivity in antenna arrays

Several authors have treated the problem of expressing the directivity of an array in the closed-form. Such expressions for the directivity can be found for a phased array with prescribed current distributions [121], a Dolph-Chebyshev array [122], or an arbitrary

volumetric array [123]. Nonetheless, no superdirective excitation is considered in these works.

In the following cases, the integrals contained in the relation for the directivity are easy to work out in the closed-form. Furthermore, the quadratic form of the excitation currents involved in the relation for the directivity (3.31) allows, by means of the generalized eigenvalue problem, the optimum to be found, thus producing a maximal directivity of these configurations. The optimum is also derived in the closed-form by following the approach of Uzsoky and Solymar [58] and [63]. In this manner, the "superdirective factor" of 21/15, accounting for the increased directivity between the optimal and out-of-phase excitation of the array of two elementary dipoles, is found. A similar factor of 4/3 is discovered for the array of two isotropic radiators.

It is good to mention that the elementary dipole/loop and isotropic radiator belong to a class of so-called CMSA, i.e., single-mode antennas [72], [73]. They have the important property that the far field of a standalone antenna is identical with the far field of the same antenna embedded as an element of an array and influenced by its other open-circuited elements. In such a case, the self- and mutual radiation intensities, self- and mutual radiated powers and optimal excitation currents of the elements in the array can be derived only from knowledge of the far field of the standalone antenna given by its current distribution. The excitation currents for superdirective radiation can be found based on the procedure presented in this paper for an arbitrary array. However, in the case of non-CMSA elements, the far field of the elements from the numerical full-wave analysis usually have to be used for evaluation of the self- and mutual radiation intensities, self- and mutual radiated powers and optimal excitation currents. The directivity in terms of source currents starts from basic equation of the directivity of a radiating source in angular direction defined in this work (3.21). The intensity U is related to a far electric field $\mathbf{E}_{\mathrm{far}}$ of the source as

$$U(\theta,\phi) = r^2 S_{\mathrm{r}} = r^2 \frac{|\mathbf{E}_{\mathrm{far}}(r,\theta,\phi)|^2}{2Z_0} \tag{3.73}$$

where r is a distance from the origin of the coordinates, S_{r} is a radial power density, $Z_0 = 120\pi = \sqrt{\mu_0/\epsilon_0}$ is an impedance of the free space and ϵ_0 and μ_0 are a permittivity and permeability of vacuum. The far electric field $\mathbf{E}_{\mathrm{far}}$ may be expressed as

$$\mathbf{E}_{\mathrm{far}}(r,\theta,\phi) = \frac{\mathrm{j}k}{\sqrt{\epsilon_0\mu_0}} \mathbf{r}_0 \times (\mathbf{r}_0 \times \mathbf{A}_{\mathrm{far}}(r,\theta,\phi)) \tag{3.74}$$

where $\mathbf{A}_{\mathrm{far}}$ is a vector potential of the source given by

$$\mathbf{A}_{\mathrm{far}}(r,\theta,\phi) = \frac{\mu_0}{4\pi} \frac{\mathrm{e}^{-\mathrm{j}kr}}{r} \int_V \mathbf{J}(\mathbf{r}_m) \mathrm{e}^{\mathrm{j}k\mathbf{r}_0\cdot\mathbf{r}_m} \,\mathrm{d}\mathbf{r}_m. \tag{3.75}$$

In the above equation, the integration is performed over a (finite) volume V of a current density $\mathbf{J}$ of the source. Furthermore, $k = 2\pi/\lambda$ is a wavenumber, the unit vector $\mathbf{r}_0 = (\sin\theta\cos\phi, \sin\theta\sin\phi, \cos\theta)$ determines the direction of radiation and the position vector

$\mathbf{r}_m$ describes the location of the density $\mathbf{J}$.

In the case of the source represented by an array of N elements, the density $\mathbf{J}$ can be written as

$$\mathbf{J}(\mathbf{r}) = \sum_{m=1}^{N} \mathbf{J}_m(\mathbf{r}) = \sum_{m=1}^{N} I_m \mathbf{j}_m(\mathbf{r}) \tag{3.76}$$

where $\mathbf{J}_m$ is a current density existing in a volume V_m of the m-th element and $\mathbf{j}_m$ is a current density normalized to its excitation current I_n. By inserting (3.76) through (3.75) and (3.74) into (3.73) and using $|\mathbf{E}_{\text{far}}|^2 = \mathbf{E}^*_{\text{far}} \cdot \mathbf{E}_{\text{far}}$, we arrive at the expression

$$U(\theta, \phi) = \sum_{m=1}^{N} \sum_{n=1}^{N} U_{mn}(\theta, \phi) \tag{3.77}$$

where

$$\begin{aligned} U_{mn}(\theta, \phi) &= I^*_m I_n \frac{15k^2}{4\pi} \int_{V_m} \int_{V_n} \Lambda(\mathbf{r}_m, \mathbf{r}_n) \mathrm{e}^{-\mathrm{j}k\mathbf{r}_0 \cdot (\mathbf{r}_m - \mathbf{r}_n)} \, \mathrm{d}\mathbf{r}_n \, \mathrm{d}\mathbf{r}_m \\ &= I^*_m I_n u_{mn}(\theta, \phi), \end{aligned} \tag{3.78}$$

is a mutual radiation intensity that accounts for the interaction of the m-th and n-th elements and u_{mn} is its normalization to the currents I_m and I_n and

$$\Lambda(\mathbf{r}_m, \mathbf{r}_n) = \mathbf{j}^*_m(\mathbf{r}_m) \cdot \mathbf{j}_n(\mathbf{r}_n) - \mathbf{r}_0 \cdot \mathbf{j}^*_m(\mathbf{r}_m) \mathbf{r}_0 \cdot \mathbf{j}_n(\mathbf{r}_n). \tag{3.79}$$

The normalized current densities $\mathbf{j}_m$ and $\mathbf{j}_n$ are usually expressed as vectors, where $\mathbf{j}_m = [j_{mx}, j_{my}, j_{mz}]$ and $\mathbf{j}_n = [j_{nx}, j_{ny}, j_{nz}]$ in the Cartesian coordinates similarly as the unit vector $\mathbf{r}_0 = [\sin\theta\cos\phi, \sin\theta\sin\phi, \cos\theta]$, which determines the direction of radiation. This leads to the expression of (3.79) as

$$\begin{aligned} \Lambda = \; & \Lambda_{mx,nx} + \Lambda_{mx,ny} + \Lambda_{mx,nz} \\ & + \Lambda_{my,nx} + \Lambda_{my,ny} + \Lambda_{my,nz} \\ & + \Lambda_{mz,nx} + \Lambda_{mz,ny} + \Lambda_{mz,nz} \end{aligned} \tag{3.80}$$

where

$$\begin{aligned}
\Lambda_{mx,nx} &= j^*_{mx} j_{nx}(\cos^2\theta\cos^2\phi + \sin^2\phi)\\
\Lambda_{mx,ny} &= j^*_{mx} j_{ny}(-\sin^2\theta\cos\phi\sin\phi)\\
\Lambda_{mx,nz} &= j^*_{mx} j_{nz}(-\cos\theta\sin\theta\cos\phi)\\
\Lambda_{my,nx} &= j^*_{my} j_{nx}(-\sin^2\theta\cos\phi\sin\phi)\\
\Lambda_{my,ny} &= j^*_{my} j_{ny}(\cos^2\theta\sin^2\phi + \cos^2\phi)\\
\Lambda_{my,nz} &= j^*_{my} j_{nz}(-\cos\theta\sin\theta\sin\phi)\\
\Lambda_{mz,nx} &= j^*_{mz} j_{nx}(-\cos\theta\sin\theta\cos\phi)\\
\Lambda_{mz,ny} &= j^*_{mz} j_{ny}(-\cos\theta\sin\theta\sin\phi)\\
\Lambda_{mz,nz} &= j^*_{mz} j_{nz}\sin^2\theta.
\end{aligned}$$

The expression of the directivity D (3.31) holds true for an arbitrary array and it is exact, provided the densities $\mathbf{j}_n$ are known exactly. The densities $\mathbf{j}_n$ are necessary for evaluation of the matrices $\mathbf{u}$ and $\mathbf{p}$ through (3.78)–(3.79), (3.30). For an arbitrary array, the exact densities $\mathbf{j}_n$ have usually to be found with the help of a numerical full-wave analysis of the complete array. In the case of an array consisting of elements belonging to the class of CMSA, the exact densities $\mathbf{j}_n$ can be obtained by a full-wave analysis of standalone elements only. For some simple cases, the densities $\mathbf{j}_n$ can be expressed in a closed-form and the integrals in (3.78) and (3.30) may be also evaluated analytically as it will be shown in chapter 4.5

3.6 Array feed optimization based on radiation pattern description

This chapter covers the expression of directivity through different formulation of far fields (loaded, modal) and denotes the strategy to synthesize the incident wave on the antenna array port. The example is shown in chapter 5.2. The principle of the synthesis of a given far field is its decomposition (projection) into the orthogonal basis of functions represented by modal far fields. The projection is given by the scalar product of the given far field and modal far field from the base.

By inserting (3.75) through (3.74) into (3.23) and using (3.76), we arrive at the expressions

$$\mathbf{E}_{\mathrm{far}}(r,\theta,\phi) = C\sqrt{2Z_0}\frac{\mathrm{e}^{-\mathrm{j}kr}}{r}\sum_{n=1}^{N} I_n \mathbf{f}_{on}(\theta,\phi) \tag{3.81}$$

$$U(\theta,\phi) = |C|^2 \sum_{m=1}^{N}\sum_{n=1}^{N} I^*_m \mathbf{f}^*_{om}(\theta,\phi)\cdot I_n \mathbf{f}_{on}(\theta,\phi) \tag{3.82}$$

where

$$\mathbf{f}_{on}(\theta,\phi) = \mathbf{r}_0 \times \left(\mathbf{r}_0 \times \int_{V_n} \mathbf{j}_n(\mathbf{r}')\mathrm{e}^{\mathrm{j}k\mathbf{r}_0\cdot\mathbf{r}'}\,\mathrm{d}\mathbf{r}'\right) \tag{3.83}$$

is a open-circuited normalized far field of the n-th element and

$$C = \frac{\mathrm{j}k}{4\pi}\sqrt{\frac{Z_0}{2}} \tag{3.84}$$

is a constant. The term open-circuited refers to the state when only the n-th element is excited by the current I_n and other elements are open-circuited, i.e., $I_m = 0$ for $m \neq n$,

3.6.1 Expression of directivity through loaded far fields

The directivity D can be expressed through loaded (or also so-called embedded) normalized far-fields to unit radiated power $\mathbf{f}_\mathrm{e} = [\mathbf{f}_{\mathrm{e}1}, \cdots, \mathbf{f}_{\mathrm{e}n}, \cdots, \mathbf{f}_{\mathrm{e}N}]$ where $\mathbf{f}_{\mathrm{e}n}$ is loaded normalized far-field of the n-th element. The term loaded refers to the state when only the n-th element is excited by the normalized incident voltage waves v_{+n} and other elements are loaded by port impedances. In this case, the currents $\mathbf{I}$ can be written as

$$\mathbf{I} = \mathbf{Z}_\mathrm{A}^{-1}\sqrt{\mathbf{Z}_\mathrm{O}}\,(\mathbf{1} + \mathbf{S}_\mathrm{A})\,\mathbf{v}_+ \tag{3.85}$$

Then it holds true

$$\mathbf{f}_\mathrm{o}(\theta,\phi)\mathbf{I} = \mathbf{f}_\mathrm{o}(\theta,\phi)\mathbf{Z}_\mathrm{A}^{-1}\sqrt{\mathbf{Z}_\mathrm{O}}\,(\mathbf{1} + \mathbf{S}_\mathrm{A})\,\mathbf{v}_+ = \mathbf{f}_\mathrm{e}(\theta,\phi)\mathbf{v}_+ \tag{3.86}$$

which implies for the far field $\mathbf{f}_{\mathrm{e}n}$

$$\mathbf{f}_{\mathrm{e}n} = \left[\mathbf{f}_\mathrm{o}(\theta,\phi)\mathbf{Z}_\mathrm{A}^{-1}\sqrt{\mathbf{Z}_\mathrm{O}}\,(\mathbf{1} + \mathbf{S}_\mathrm{A})\right]_n \tag{3.87}$$

where $[]_n$ denotes an operation which gets the n-th column of the vector in the square brackets.

3.6.2 Expression of directivity through modal far fields

The directivity D can be expressed through modal normalized far-fields

$$\mathbf{f}_\mathrm{m} = [\mathbf{f}_{\mathrm{m}1}, \cdots, \mathbf{f}_{\mathrm{m}n}, \cdots, \mathbf{f}_{\mathrm{m}N}] \tag{3.88}$$

where $\mathbf{f}_{\mathrm{m}p}$ is modal normalized far-field of the array corresponding to its p-th mode. The term modal refers to the state when the elements of the array are excited by the currents $\mathbf{I}_p = [I_{1p}, \cdots, I_{np}, \cdots, I_{Np}]^\mathrm{T}$ where I_{np} is an excitation current of n-th element corresponding to p-th mode. Various types of the modes of the array can be considered. Further, the so-called Characteristic Modes are taken into account. In this case, the currents $\mathbf{I}$ can be written as a linear combination of the currents $\mathbf{I}_p$, $p = 1, \cdots, N$

$$\mathbf{I} = \mathbf{I}_\mathrm{m}\mathbf{w} \tag{3.89}$$

where $\mathbf{w} = [w_1, \cdots, w_p, \cdots, w_N]^\mathrm{T}$ is a vector of weights of the modes, w_p is a weight of the p-th mode and $\mathbf{I}_\mathrm{m} = [\mathbf{I}_1, \cdots, \mathbf{I}_p, \cdots, \mathbf{I}_N]$ is a vector of the modal currents which can

be also expanded to the form

$$\mathbf{I}_{\mathrm{m}} = \begin{bmatrix} I_{11} & \cdots & I_{1p} & \cdots & I_{1N} \\ \vdots & \ddots & \vdots & \ddots & \vdots \\ I_{n1} & \cdots & I_{np} & \cdots & I_{nN} \\ \vdots & \ddots & \vdots & \ddots & \vdots \\ I_{N1} & \cdots & I_{Np} & \cdots & I_{NN} \end{bmatrix}. \tag{3.90}$$

Then holds true

$$\mathbf{f}_{\mathrm{o}}(\theta,\phi)\mathbf{I} = \mathbf{f}_{\mathrm{o}}(\theta,\phi)\mathbf{I}_{\mathrm{m}}\mathbf{w} = \mathbf{f}_{\mathrm{m}}(\theta,\phi)\mathbf{w} \tag{3.91}$$

which implies for the far field $\mathbf{f}_{\mathrm{m}p}$

$$\mathbf{f}_{\mathrm{m}p} = \mathbf{f}_{\mathrm{o}}(\theta,\phi)\mathbf{I}_{\mathrm{m}p}. \tag{3.92}$$

A scale of the currents I_p is set through the weight w_p when they are summed in (3.89). It is convenient to pre-scale the currents to fulfill the condition

$$\int_0^{2\pi}\int_0^{\pi} \mathbf{f}^*_{\mathrm{m}p}(\theta,\phi)\cdot\mathbf{f}_{\mathrm{m}p}(\theta,\phi)\sin\theta\,\mathrm{d}\theta\,\mathrm{d}\phi = 1. \tag{3.93}$$

The optimization of radiation pattern, where $\mathbf{f}$ is required radiation pattern should fulfill condition to minimize the mean quadratic error Δ^2

$$|\mathbf{f} - \sum_{n=1}^{N} c_{\mathrm{m}}\mathbf{f}_{\mathrm{m}}|^2 = \Delta^2, \tag{3.94}$$

where c_{m} is a weight coefficient. Using (3.93) and the orthogonal property, we can get the weights coefficient as

$$c_{\mathrm{m}} = \int_0^{2\pi}\int_0^{\pi} \mathbf{f}^*_{\mathrm{m}}(\theta,\phi)\cdot\mathbf{f}(\theta,\phi)\sin\theta\,\mathrm{d}\theta\,\mathrm{d}\phi \tag{3.95}$$

and the required radiation pattern is then

$$\mathbf{f} = \sum_{n=1}^{N} c_{\mathrm{m}}\mathbf{f}_{\mathrm{m}}. \tag{3.96}$$

Chapter 4

Results

4.1 Bandwidth optimization of linear arrays above PEC ground

As mentioned above, the input driving impedance of array of dipoles backed by an infinite electric ground plane consists of contribution of self and mutual impedances, in which the latter are function of the elements positions. The bandwidth potential is evaluated using the impedance quality factor [124]. It follows from previous research [125] that control of mutual radiated power is important for optimizing the bandwidth. This is shown by expressing the mutual radiated power between two elementary radiators, forming result important for small antennas. In next section two different dipole arrays are optimized using in-house Particle Swarm Optimization (PSO) code [126] for minimum Q and the bandwidth is compared with FEKO full-wave MoM simulation [12]. For radiators above electric ground, there is cancellation of radiated power caused by mutual interactions. This is important especially when the structure is small and the radiators are close to the ground. It will be shown, that this power interference, rather than stored energy, is key issue that limits bandwidth of such arrays. For simplicity assume 1D current flowing along the z-axis.

It could be evaluated from [127] that the mutual radiated power for out-of-phase point currents ($I(z)I(z') = -1$) is led by the function

$$P_{12}(kR) = -\frac{\sin kR}{(kR)^3} + \frac{\cos kR}{(kR)^2} \ . \tag{4.1}$$

Here R is the distance between currents. This function is depicted in Figure 4.1 and has maximum (which is important for maximizing the radiated power) for $kR \approx 5.76$. This is equivalent to one point source above infinite ground at height $h = R/2$, hence $kh \approx 2.88$ ($h/\lambda \approx 0.46$). In previous study [125] worked out for $\lambda/2$ dipoles, the optimum was found to be of similar value $h/\lambda \approx 0.33$.

For upcoming two examples we consider length of dipoles $L = \lambda/2$ and radius $a/\lambda = 5 \cdot 10^{-4}$. At first we introduce one dipole above PEC in height h. For small distances the quality factor asymptotically behaves as $(h/\lambda)^{-2}$ and there is optimal separation $h/\lambda \approx 0.33$

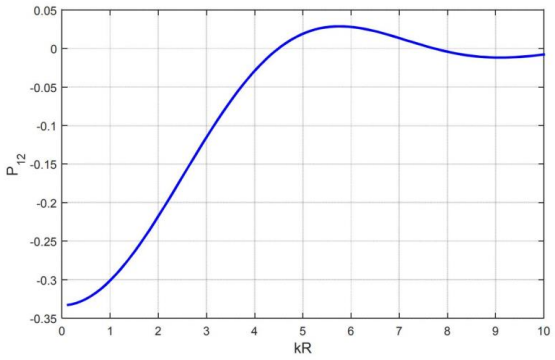

Figure 4.1: Plot of the function P_{12} accounting for mutual radiated power between two point currents. Reproduced from [127].

with $Q_z = 5.04$. The ratio of quality factors between free space and grounded array is thus

$$\frac{Q_z\,(\text{free space})}{Q_z\,(\text{array})} = 0.66. \tag{4.2}$$

Relative bandwidth evaluated from Q_z is, assuming single resonance tuning

$$BW = \frac{1}{Q_z\sqrt{2}} = 13.6\%, \tag{4.3}$$

while simulation in FEKO software gives relative bandwidth

$$BW = \frac{f_+ - f_-}{\sqrt{f_+ f_-}} = 13.4\%. \tag{4.4}$$

The two in-phase dipoles above ground is another interesting structure appreciated for great bandwidth, also known as the "Eleven feed" [128]. The dipoles are for all cases fed in-phase voltage gaps located at height h and separated by s.

At first the Q_z is shown as a function of both height and separation in Figure 4.2. There is one minimum at $h/\lambda \approx 0.37$ and $s/\lambda \approx 50.37$ resulting in $Q_z = 2.52$

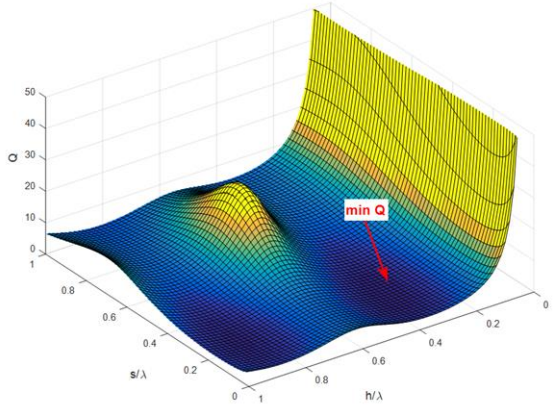

Figure 4.2: Plot of quality factor of array of two in-phase fed dipoles separated by s and located at h above infinite electric ground plane.

The ratio of quality factors between free space and grounded array is in this case 0.33. The relative bandwidth evaluated from Q_{z} is, assuming now double resonance tuning

$$BW = \frac{\sqrt{3}}{Q_{\mathrm{z}}} = 68\% \ , \tag{4.5}$$

while FEKO simulation gives

$$BW = \frac{f_+ - f_-}{\sqrt{f_+ f_-}} = 71\% \ . \tag{4.6}$$

From the above results it is observed that optimal heights for both arrays are similar, leading to conclusion that it is the radiated power cancellation caused by opposite currents due to electric ground.

4.2 Three element array

A frequency where eigenvalue $\lambda_p = 0$ is further referred to as a resonant frequency of a p-th CM of the array. The CMs are ordered and numbered by p according to their resonant frequencies ascendingly, i.e., the highest p corresponds to the highest resonant frequency.

For excitation of an dipole array in FEKO, voltage gaps are used at the centers of the dipoles. Relevant excitation voltages $\mathbf{V}_p = [V_{1p}, \cdots, V_{mp}, \cdots, V_{Np}]^{\mathrm{T}}$ of a p-th CM are then given by [27]:

$$\mathbf{V}_p = \mathbf{Z}_{\mathrm{A}} \mathbf{I}_p. \tag{4.7}$$

As a first example, let us consider an antenna array consisting of three parallel thin-wire dipoles placed horizontally above an infinite electric ground plane, equally spaced, each with the same length $L_1 = L_2 = L_3 = L = \lambda/2$, where $\lambda = 0.3$ m is a wavelength at the frequency 1 GHz. A spacing between each two dipoles is $s_{12} = s_{23} = s = 0.25\lambda$ and a height above the ground plane is $h = 0.25\lambda$, see Figure 3.4.

The characteristic angles δ_p of all CM and the corresponding currents $\mathbf{I}_p$ at the resonant frequencies of the CM are shown in Figure 4.3. The agreement is perfect up to the fundamental resonance of the individual dipoles which occurs at a frequency of 1 GHz approximately. Further, it starts to deviate as the one-term sinusoidal current distribution (3.32) becomes inaccurate. Improvement of accuracy is possible, e.g., by incorporating to (3.32) a three-term approximation [20].

The currents $\mathbf{I}_p$ of all CM are also presented in Figure 4.4. Due to the symmetry of the dipole array, see Figure 3.4, the magnitudes of the currents I_{mp} are the same for the dipoles $m = 1$ and $m = 3$. The currents $\mathbf{I}_p$ are normalized in the usual way

$$\frac{1}{2} \mathbf{I}_p^{\mathrm{H}} \mathbf{R} \mathbf{I}_p = 1 \ (\mathrm{W}). \tag{4.8}$$

Finally, the directivities D_p of all CM are depicted in Fig. 4.5. Their maximal values in linear scale for CM $p = 1, 2, 3$ are 8.4, 9.2, 12.5 and 8.5, 7.4, 11 for calculation in MATLAB and FEKO respectively. The differences can be addressed to the slightly different current

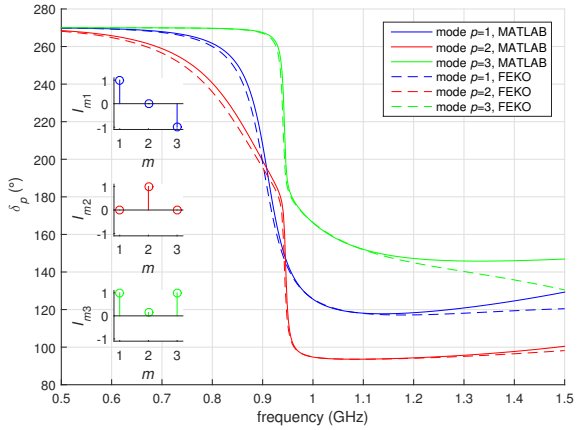

Figure 4.3: Characteristic angles and excitation currents (eigenvector $\mathbf{I}_p$) of all CM for the three-element dipole array. Components I_{mp} are plotted at resonant frequencies of CM and normalized to $\max(|I_{mp}|)$ for given p.

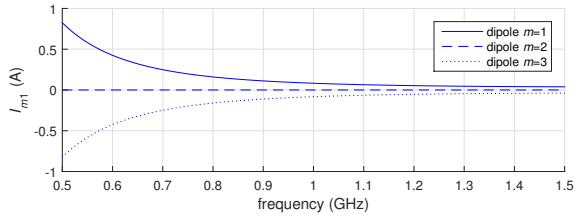

(a) mode $p = 1$

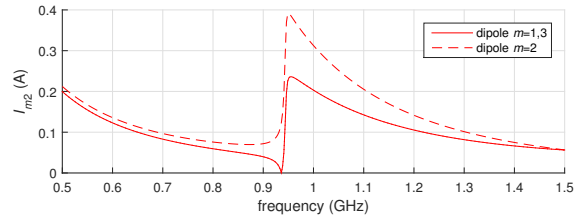

(b) mode $p = 2$

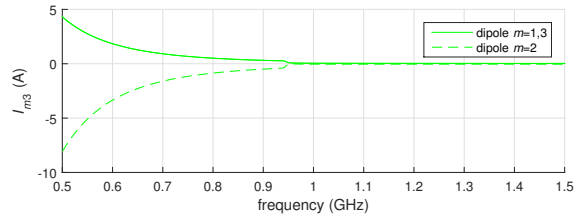

(c) mode $p = 3$

Figure 4.4: Excitation currents (components of eigenvector $\mathbf{I}_p$) of all CM for the three-element dipole array.

distributions on the dipoles (one-term sinusoidal vs. obtained through full MoM in FEKO).

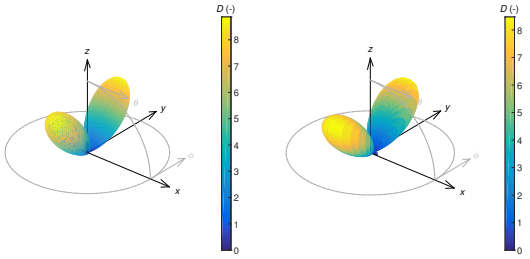

(a) mode $p = 1$, MATLAB (b) mode $p = 1$, FEKO

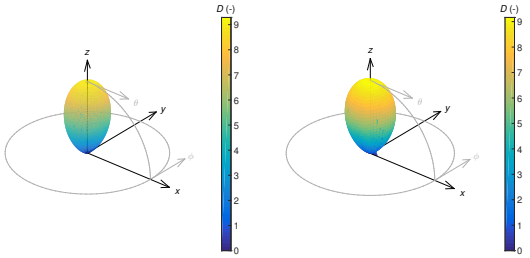

(c) mode $p = 2$, MATLAB (d) mode $p = 2$, FEKO

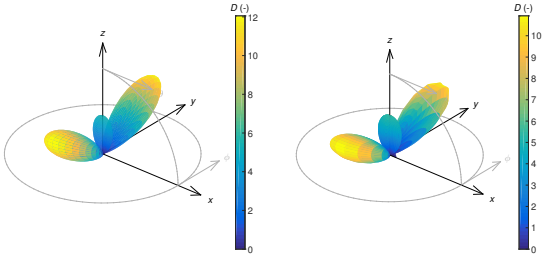

(e) mode $p = 3$, MATLAB (f) mode $p = 3$, FEKO

Figure 4.5: Directivity of the three-element dipole array for all CM at their resonant frequencies. Directivity is plotted in linear scale and for half-space xyz^+ only since it is symmetrical by the xy plane for this array.

4.3 Yagi-Uda optimization

The Yagi-Uda antenna parameters are optimized with respect to total directivity. The purpose of this example is to present the usefulness of the developed method on an arrays of any geometrical configuration, including unequally spaced elements and different lengths.

The radiation of the antenna array is oriented in y direction, while the elements itself are oriented in z direction as depicted in Figure 4.6.

The length of the reflector is L_0, length of the active element is L_1, and the length of directors is L_2 and L_3 respectively. The spacings of the elements are noted S_0, S_1 and S_2, and the radius of the dipoles is chosen $a = 0.005\lambda$ and $\lambda = c_0/f$ is the free-space wavelength at the center frequency 1 GHz. The active element is optimized in length to achieve small reflection coefficient. The optimization steps are as follows: find the optimum spacing and length of the reflector and the active element in free space, optimize

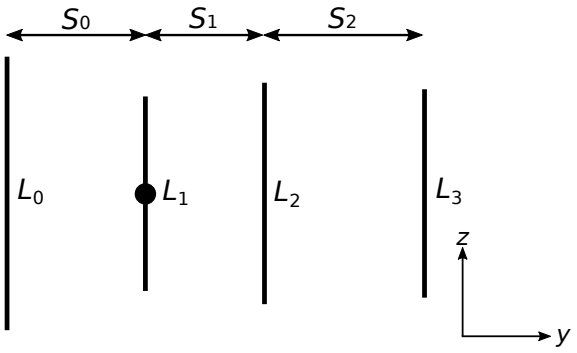

Figure 4.6: Geometry of the Yagi-Uda antenna.

and analyze one director followed by the second director. This design steps are then completed by optimization of a whole structure, this optimization contains 6 variables (L_0, L_2, L_3,S_0, S_1 and S_2).

To test the correctness of the calculated directivity it is compared with FEKO. From the comparison we can see good agreement for length of dipole up to $L_0 = 0.8\lambda$ as shown in Figure 4.7. On the figure the directivity is in linear scale as a function of spacing S_0 for two dipole elements.

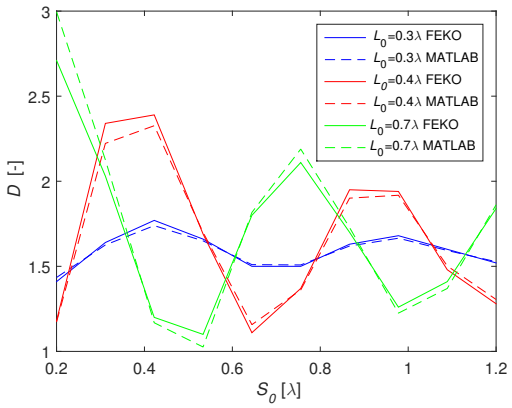

Figure 4.7: Directivity comparison as a function of the spacing S_0 from MATLAB and FEKO for three fixed reflector lengths.

When we evaluate the directivity depending on mutual spacing and length of the reflector, we can observe a maximum directivity for $L_0 = 0.477\lambda$ and $S_0 = 0.2\lambda$. The directivity for the array consisting of reflector and active element is depicted in Figure 4.8. In this figure, the directivity is increasing from blue colour to yellow, up to $D = 2.5$.

The cut of radiation pattern for this two-element structure for optimal current feeding, when only one element is actively fed is depicted in Figure 4.9 in linear scale.

These steps can be extended to a full array, a complete four element Yagi-Uda antenna. The directivity result of a sweep in length L_4 and spacing S_3 is showed in Figure 4.10.

From Figure 4.10 and previous results the final optimized dimensions of the Yagi-Uda antenna for directivity maximization are: $L_0 = 0.5\lambda$, $L_1 = 0.404\lambda$, $L_2 = 0.451\lambda$ and $L_3 = 0.443\lambda$. The spacing between elements are $S_0 = 0.22\lambda$, $S_1 = 0.214\lambda$ and

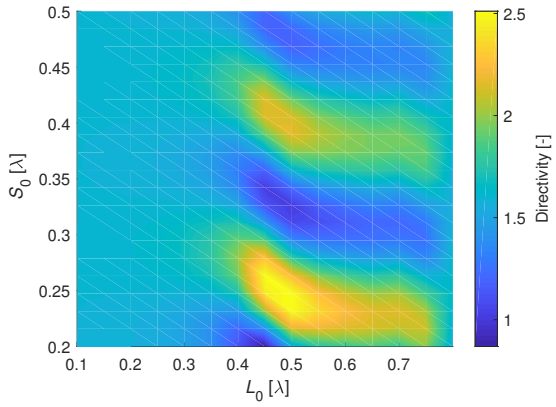

Figure 4.8: Maximum achievable directivity of the array with active element and reflector element calculated in MATLAB.

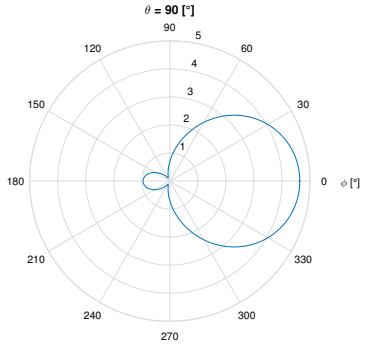

Figure 4.9: Cut of radiation pattern for active and reflector element for $\theta = 90°$ in linear scale.

$S_2 = 0.326\lambda$. The total radiation pattern is depicted in Figure 4.11 and its vertical cut in Figure 4.12, where the total directivity is $D = 13.29$ and $D = 13.28$ in MATLAB and FEKO respectively.

The comparison of the radiation pattern in the cut for $\theta = 90°$ is depicted in Figure 4.12. We can see the excellent agreement of the calculated directivity from MATLAB and from FEKO.

4.4 Circular array

The circular array is composed of five z-oriented dipoles uniformly spaced with distance s, see Figure 4.13. The length of each the dipole is $L = \lambda/2$ and radius $a = 0.005\lambda$. The mutual spacing between the dipoles is denoted as s, where the radius of the circle is $R = s/\left(2\sin\left(\pi/N\right)\right)$ and N is total number of elements.

The maximum directivity in direction of x-axis ($\phi = 0$) as a function of separation s is depicted in Figure 4.14. For each particular separation, decomposition (3.71) is performed with radiation intensity $\mathbf{u}$ fixed to $(\theta = \pi/2, \phi = 0)$.

The calculated directivity by our code and FEKO for spacing $s = 0.1\ \lambda$ is shown in Figure 4.15 showing good agreement.

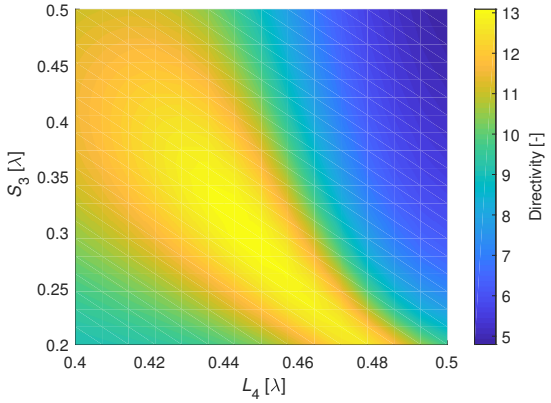

Figure 4.10: Directivity of the array with 4 elements calculated in MATLAB.

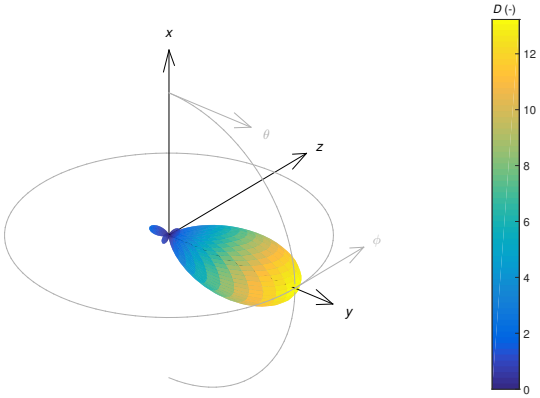

Figure 4.11: Total directivity for 4 element Yagi-Uda antenna.

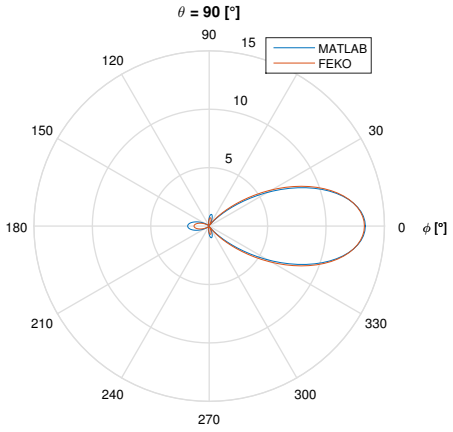

Figure 4.12: Cut of radiation pattern for 4 dipoles for $\theta = 90°$.

Due to the rotational symmetry, we are able to obtain the same directivity in any ϕ direction. It is notable that for the maximization of directivity in direction $\phi = 0, \pi/2, \pi, 3\pi/2$, the amplitude of the feeding current is exactly the same, only the phase is changing.

This method is able to find the optimum current distribution in any direction, which

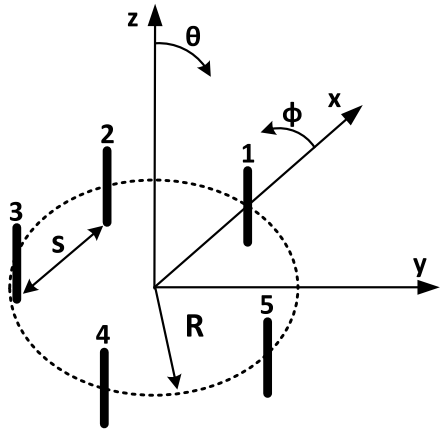

Figure 4.13: A five-element circular dipole array.

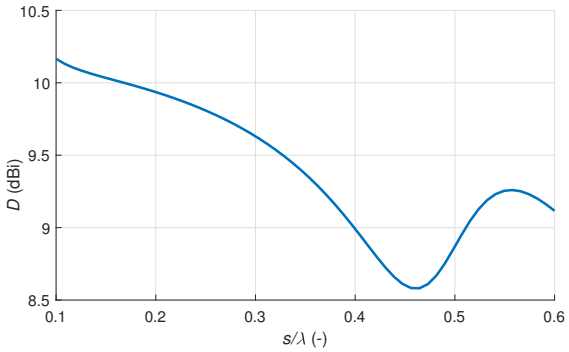

Figure 4.14: Maximum directivity in x ($\phi = 0°$) axis for different distance between 5 dipoles.

is fixed in the $\mathbf{u}(\theta, \phi)$ matrix. Using (4.7), where $\mathbf{Z}_\mathrm{A}$ is the impedance matrix of the array, corresponding voltage excitation vector $\mathbf{V}$ is obtained. These voltages were actually used as inputs for FEKO in Figure 4.15.

Table 4.1 shows a normalized current and calculated voltage distribution for maximization of directivity of the circular array with the radiation pattern in Figure 4.15.

For the circular array, the CM decomposition was also used and the array was extended to nine dipoles in circle. The excitation currents (components of eigenvector $\mathbf{I}_p$) of all CM

N	$\lvert I\rvert$(A)	$I(°)$	$\lvert V\rvert$(V)	$V(°)$
1	1	-81.07	23.56	32.2
2	0.84	90.15	17.56	158.4
3	0.32	-104.23	3.95	-21.9
4	0.32	-104.23	3.95	-21.9
5	0.84	90.15	17.56	158.4

Table 4.1: Complex feed currents and voltages for maximizing directivity of circular array with $s = 0.1\lambda$.

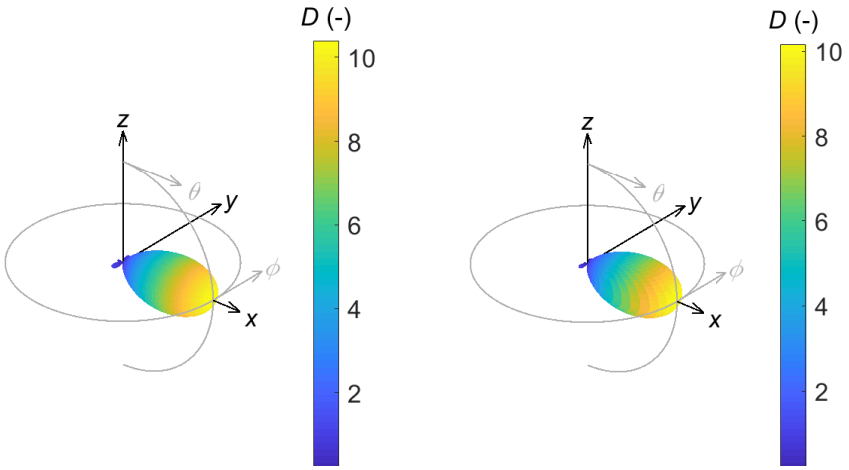

(a) MATLAB $D = 10.16$ dBi (b) FEKO $D = 10.07$ dBi

Figure 4.15: Radiation pattern for circular array with 5 dipoles fed by optimal currents.

for the nine element circular array are in Figure 4.16 noted with blue colour. With the red line there is approximation via cosine function. The period of the cosine function is increasing with every two modes, means mode 2 and 3 has the same cosine distribution, but with phase shift. It should be mentioned, that these discrete characteristic modes when approximated with the cosine function behaves as excitation currents of elementary loop.

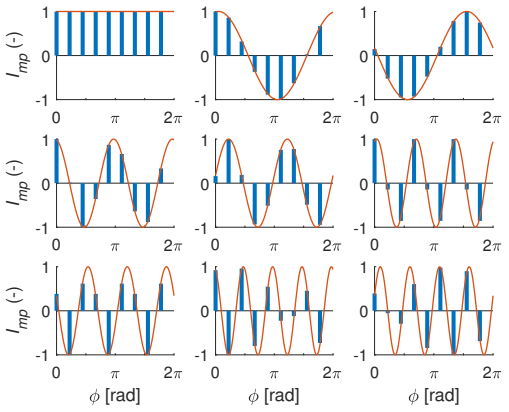

Figure 4.16: The excitation currents (components of eigenvector $\mathbf{I}_p$) of all CM for the nine element circular array.

4.5 End-fire superdirective array

In this chapter the directivity D, according to (3.31), is calculated for an array of two elementary dipoles with end-fire radiation and the Uzkov's limit N^2 for the end-fire directivity of N isotropic radiators [46] is verified for $N = 2$. Finally the array of two isotropic radiators above PEC ground is treated. This necessitates the finding of entries u_{mn} and p_{mn} of the matrices $\mathbf{u}$ and $\mathbf{p}$ in (3.78) and (3.30).

Firstly, we consider an elementary dipole of the length $L \to 0$ in the origin of the coordinates oriented in the z-axis with a constant current density $\mathbf{J}_1 = I_1\delta(x)\delta(y)\mathbf{z}_0 = I_1 j_{1z}\mathbf{z}_0$, see Fig. Figure 4.17 a).

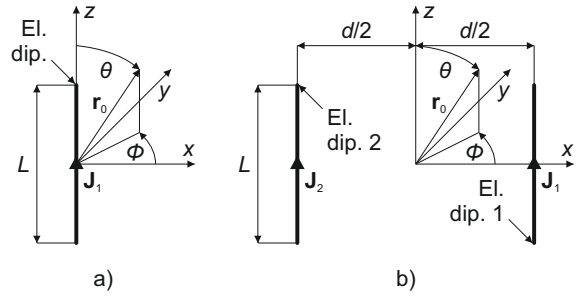

Figure 4.17: Geometry: a) elementary dipole, b) array of two elementary dipoles. Reproduced from [129].

4.5.1 Two elementary dipoles

Now we have basic knowledge about radiation intensity and power of a single elementary dipole. Now, we can consider an array of two elementary dipoles of the length $L \to 0$ oriented in the z-axis and spaced in the x-coordinate by a distance d with constant current densities $\mathbf{J}_1 = I_1\delta(x-d/2)\delta(y)\mathbf{z}_0$ and $\mathbf{J}_2 = I_2\delta(x+d/2)\delta(y)\mathbf{z}_0$, see Figure 4.17 b). It is well known that this arrangement produces end-fire radiation if the dipoles are closely-spaced ($d < \lambda/2$) and excited by the out-of-phase currents, i.e., $I_1 = -I_2 = I$ [53].

In this case, the self-intensities $u_{11} = u_{22}$, since they cannot depend either on the placement in the coordinates, nor on the mutual placement of the dipoles, and due to the dipoles being identical. From (3.78)–(3.79), it follows for the mutual intensities u_{12} and u_{21} that $u_{12} = u_{21}^*$ and

$$\begin{aligned} u_{12}(\theta,\phi,s) &= \frac{15k^2}{4\pi}\int_{-L/2}^{L/2}\int_{-L/2}^{L/2} \sin^2\theta \mathrm{e}^{-\mathrm{j}k\mathbf{r}_0\cdot(\mathbf{r}-\mathbf{r}')}\,\mathrm{d}z'\,\mathrm{d}z \\ &\approx \frac{15k^2}{4\pi}\int_{-L/2}^{L/2}\int_{-L/2}^{L/2} \sin^2\theta \mathrm{e}^{-\mathrm{j}kd\sin\theta\cos\phi}\,\mathrm{d}z'\,\mathrm{d}z \\ &= \frac{15k^2L^2}{4\pi}\sin^2\theta \mathrm{e}^{-\mathrm{j}kd\sin\theta\cos\phi} \\ &= u_{11}(\theta,\phi)\mathrm{e}^{-\mathrm{j}s\sin\theta\cos\phi}. \end{aligned} \tag{4.9}$$

In the above equation, the Dirac δ-functions reduce the 3D volume integrals from (3.78) to the 1D line integrals and effectively simplify (3.12), (3.79) and, finally, the approximation $z - z' \approx 0$ for $L \to 0$ is used with a normalized spacing $s = kd$ being defined. Since the elementary dipole belongs to the class of CMSA the character of the densities $\mathbf{J}_1$ and $\mathbf{J}_2$ of two dipoles in the array is considered the same as for a standalone dipole. Then, it is seen from (4.9) that the mutual intensity u_{12} of two dipoles in the array is determined by the self-intensity u_{11} of a standalone dipole through the phase shift $-s\sin\theta\cos\phi$ which is

the above mentioned property of CMSA.

The self-powers p_{11} and p_{22}, i.e., $p_{11} = p_{22}$, since the intensities u_{11} and u_{22} are equal. From (3.30), it follows for the mutual powers p_{12} and p_{21} that $p_{12} = p_{21}^*$ since it holds true that $u_{12} = u_{21}^*$, for the intensities u_{12} and u_{21}. In addition, the power p_{12} is real, thus, $p_{12} = p_{21}$. This property follows from power p_{12} (4.10). Note that this result holds true for all radiators whose normalized far field pattern f is rotationally symmetrical, i.e., it is a function of the coordinate θ only.

Further, the relation (3.30) for the power p_{12} using (4.9) reads

$$p_{12}(s) = \frac{15k^2L^2}{4\pi} \int_0^{2\pi} \int_0^{\pi} \sin^3\theta \mathrm{e}^{-\mathrm{j}s\sin\theta\cos\phi}\,\mathrm{d}\theta\,\mathrm{d}\phi. \tag{4.10}$$

The above integral was evaluated elsewhere [57], [60]. It is noted that exactly the same result can be obtained by the EMF method [130], where all terms containing $z - z'$ are discarded. It yields

$$p_{12}(s) = 15k^2L^2 \left(\frac{\sin s}{s} + \frac{\cos s}{s^2} - \frac{\sin s}{s^3} \right), \tag{4.11}$$

where the term in brackets in (4.11) can be written with the help of spherical Bessel functions as $\mathrm{j}_0(s) - \mathrm{j}_1(s)/s$. For the given array, considering the out-of-phase excitation currents $\mathbf{I} = [I, -I]^{\mathrm{T}}$ with a magnitude I and using the above found entries of the matrices $\mathbf{u}$ and $\mathbf{p}$, the directivity D (3.31) becomes

$$D(\theta, \phi, s) = \frac{3\sin^2\theta(1 - \cos(s\sin\theta\cos\phi))}{2 - 3\left(\frac{\sin s}{s} + \frac{\cos s}{s^2} - \frac{\sin s}{s^3}\right)}. \tag{4.12}$$

The value of the magnitude I is insignificant when calculating the directivity D since it is ultimately canceled in (3.31). Further, considering the spacing $d < \lambda/2$ (i.e., $s < \pi$), the maximal (end-fire) radiation occurs for the direction ($\theta = 90°, \phi = 0°$) and the corresponding directivity D is

$$D(90°, 0°, s) = \frac{3(1 - \cos s)}{2 - 3\left(\frac{\sin s}{s} + \frac{\cos s}{s^2} - \frac{\sin s}{s^3}\right)} \tag{4.13}$$

with the limit $15/4 = 3.75$ (5.74 dBi) for the spacing $d \to 0$ (i.e., $s \to 0$).

In the directivity D (4.12), the currents $\mathbf{I} = [I, -I]^{\mathrm{T}}$ are considered. However, the general expression of the directivity D (3.31) is a quadratic form in terms of the currents $\mathbf{I}$ and can be used to find their optimum $\mathbf{I}_{\mathrm{opt}}$ which maximizes the directivity D for a given direction (θ, ϕ) and spacing s by solving the related weighted eigenvalue equation [62]

In this particular case, the currents $\mathbf{I}_{\mathrm{opt}} = [I_{1,\mathrm{opt}}, I_{2,\mathrm{opt}}]^{\mathrm{T}}$ can be found analytically by following the procedure in [58], [63]. They are given by the solution

$$\mathbf{I}_{\mathrm{opt}}(\theta, \phi, s) = \frac{1}{4\pi}\mathbf{p}^{-1}(s)\mathbf{V}(\theta, \phi, s) \tag{4.14}$$

where

$$\mathbf{p}^{-1}(s) = \frac{1}{p_{11}^2 - p_{12}^2(s)} \begin{bmatrix} p_{11} & -p_{12}(s) \\ -p_{12}(s) & p_{11} \end{bmatrix} \tag{4.15}$$

$$\mathbf{V}(\theta, \phi, s) = \begin{bmatrix} \mathrm{e}^{-\mathrm{j}s/2 \sin\theta\cos\phi} f\,(\theta, \phi) \\ \mathrm{e}^{\mathrm{j}s/2 \sin\theta\cos\phi} f\,(\theta, \phi) \end{bmatrix} \tag{4.16}$$

$$f\,(\theta, \phi) = \sin\theta \tag{4.17}$$

and f is a normalized far field pattern of the elementary dipole. Thus, the currents $\mathbf{I}_{\mathrm{opt}}$ (4.14) can be written with the help of the previously found matrix $\mathbf{p}$ as

$$\mathbf{I}_{\mathrm{opt}}(\theta, \phi, s) = \begin{bmatrix} I\mathrm{e}^{-\mathrm{j}\alpha(\theta,\phi,s)/2} \\ I\mathrm{e}^{\mathrm{j}\alpha(\theta,\phi,s)/2} \end{bmatrix} \tag{4.18}$$

where the magnitude I is the same for the currents $I_{1,\mathrm{opt}}$ and $I_{2,\mathrm{opt}}$ and α is their phase difference, which reads

$$\alpha(\theta, \phi, s) = -s \sin\theta \cos\phi + 2 \arg\left(\rho_{\mathrm{Re}}(\theta, \phi, s) + \mathrm{j}\rho_{\mathrm{Im}}(\theta, \phi, s)\right) \tag{4.19}$$

where

$$\rho_{\mathrm{Re}}(\theta, \phi, s) = 2\cos\left(s \sin\theta \cos\phi\right) - 3\left(\frac{\sin s}{s} + \frac{\cos s}{s^2} - \frac{\sin s}{s^3}\right) \tag{4.20}$$

$$\rho_{\mathrm{Im}}(\theta, \phi, s) = 2\sin\left(s \sin\theta \cos\phi\right). \tag{4.21}$$

For the given array, considering the optimal excitation currents $\mathbf{I}_{\mathrm{opt}}$ (4.18) and using the above found entries of the matrices $\mathbf{u}$ and $\mathbf{p}$, the directivity D (3.31) becomes

$$D(\theta, \phi, s) = \frac{3 \sin^2\theta(\cos\alpha + \cos\left(s \sin\theta \cos\phi\right))}{2\cos\alpha + 3\left(\frac{\sin s}{s} + \frac{\cos s}{s^2} - \frac{\sin s}{s^3}\right)}. \tag{4.22}$$

This relation expresses the maximal directivity D for the given direction (θ, ϕ) and spacing s which is achieved by the excitation of the given array by the currents $\mathbf{I}_{\mathrm{opt}}$ set for the direction (θ, ϕ) and spacing s according to (4.18). Further, considering the spacing $d < \lambda/2$ (i.e., $s < \pi$), the maximal (end-fire) radiation occurs for the direction $(\theta = 90°, \phi = 0°)$ and the corresponding directivity D is

$$D(90°, 0°, s) = \frac{3(\cos\alpha + \cos s)}{2\cos\alpha + 3\left(\frac{\sin s}{s} + \frac{\cos s}{s^2} - \frac{\sin s}{s^3}\right)} \tag{4.23}$$

where the phase difference α (4.19) is now

$$\alpha(90°, 0°, s) = 2\pi - s + 2\arctan\left(\frac{2\tan s}{2 - 3\left(\frac{\tan s}{s} + \frac{1}{s^2} - \frac{\tan s}{s^3}\right)}\right). \tag{4.24}$$

The directivity D (4.23) has a limit of $21/4 = 5.25$ (7.20 dBi) when the spacing $d \to 0$ (i.e., $s \to 0$). Compared to the out-of-phase excitation, this represents an increase by the

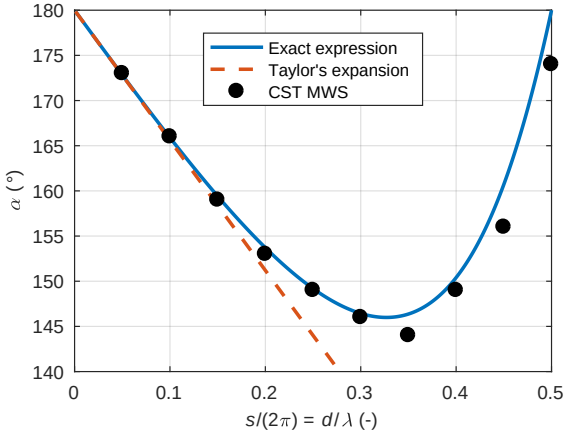

Figure 4.18: Phase difference of optimal excitation currents for maximal directivity of end-fire radiation of array of two elementary dipoles: exact expression (blue-solid), Taylor's expansion (red-dashed), CST MWS simulation (black-dot). Reproduced from [129].

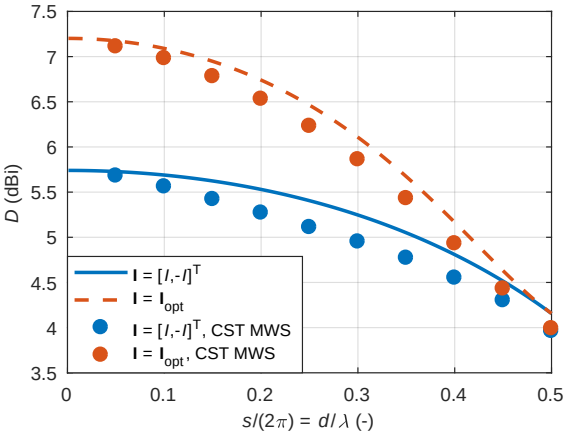

Figure 4.19: Directivity of end-fire radiation of array of two elementary dipoles with out-of-phase (blue-solid) and optimal for maximal directivity (red-dashed) excitation. CST MWS simulation (dot). Reproduced from [129].

"superdirective factor" of $21/15 = 1.4$ (1.46 dB). As seen from Figure 4.18, the phase difference α is almost linear for a close spacing s. This motivates its Taylor's expansion, which, by taking the first two terms, gives a simple relation

$$\alpha(90^\circ, 0^\circ, s) \approx \pi - \frac{2}{5}s. \tag{4.25}$$

The phase difference α (4.24) is notably similar to that obtained numerically by Yaghjian [47] and Altshuler [49].

The calculated directivities D (4.13) and (4.23) for both out-of-phase and optimal excitation are shown in Figure 4.19. The results are also validated by the time-domain simulation in CST MWS [14], in which the given array is modeled by two thin dipoles of the length $L = \lambda/30$. The optimal phase difference α of their excitation currents $\mathbf{I}_{\text{opt}}$ is set manually in the simulation by varying the phases of the currents in the post-processing

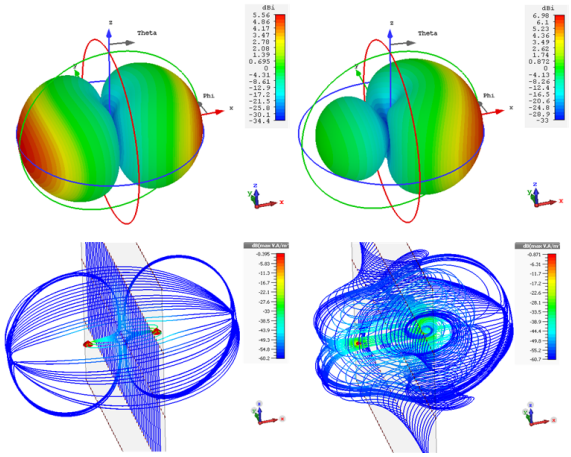

Figure 4.20: Radiation pattern of end-fire radiating array of two elementary dipoles with spacing 0.1 λ for out-of-phase (top-left) and optimal for maximal directivity (top-right) excitation. Corresponding streamlines of Poynting vector are shown below. Reproduced from [129].

stage and checking the end-fire radiation for the maximal directivity, see Figure 4.18. The differences in the values of the directivities D and phase difference α obtained by (4.13), (4.23), (4.24) and by the simulation can be addressed to the fact that the simulation approximates the infinitely small elementary dipoles with the constant current distributions assumed for the analytical relations by the dipoles of finite dimensions. For the array with the spacing $d = 0.1\ \lambda$ (i.e., $s = 0.2\pi$), the equation (4.24) gives the phase difference $\alpha = 166°$. It is seen from Figure 4.20 that the radiation patterns of this array for the out-of-phase and optimal excitation are quite distinct. Streamlines of the Poynting vector [131], [132] are also shown. The interaction between the two dipoles is much stronger for the superdirective case and the power density represented by the streamlines is more closely bound to the dipoles. Indeed, the fine structure of the power flow is remarkable.

4.5.2 Two isotropic radiators

We can further follow this approach and can verify the Uzkov's limit N^2 for the end-fire directivity of N isotropic radiators [46] for $N = 2$. We consider an array of two isotropic radiators spaced in the x-coordinate by a distance d in the same manner as the elementary dipoles in Figure 4.17 a).

Similarly, as for the case of the array of two elementary dipoles, it holds true for the intensities $u_{11} = u_{22}$, $u_{12} = u_{21}^*$ and

$$u_{12}(\theta, \phi, s) = u_{11} \mathrm{e}^{-\mathrm{j}s \sin\theta \cos\phi}. \tag{4.26}$$

However, the intensity u_{11} cannot depend on the direction (θ, ϕ) of radiation for the isotropic radiator. From (3.30), the relation of the intensity u_{11} and power p_{11} can be found as

$$p_{11} = u_{11} \int_0^{2\pi} \int_0^{\pi} \sin\theta \, \mathrm{d}\theta \, \mathrm{d}\phi = 4\pi u_{11} \tag{4.27}$$

$$u_{11} = \frac{p_{11}}{4\pi}. \tag{4.28}$$

It holds true for the powers $p_{11} = p_{22}$ and $p_{12} = p_{21}^* = p_{21}$ since the intensities u_{11} and u_{22} are equal, $u_{12} = u_{21}^*$ and the power p_{12} is real. Further, the relation (3.30) for the power p_{12} using (4.26) and (4.28) reads

$$p_{12}(s) = \frac{p_{11}}{4\pi} \int_0^{2\pi} \int_0^{\pi} \sin\theta \mathrm{e}^{-\mathrm{j}s\sin\theta\cos\phi} \,\mathrm{d}\theta \,\mathrm{d}\phi = p_{11} \frac{\sin s}{s}. \tag{4.29}$$

For the given array, considering the out-of-phase excitation currents $\mathbf{I} = [I, -I]^{\mathrm{T}}$ and using the above found entries of the matrices $\mathbf{u}$ and $\mathbf{p}$, the directivity D (3.31) becomes

$$D(\theta, \phi, s) = \frac{1 - \cos(s\sin\theta\cos\phi)}{1 - \frac{\sin s}{s}}. \tag{4.30}$$

Further, considering the spacing $d < \lambda/2$ (i.e., $s < \pi$), the maximal (end-fire) radiation occurs for the direction $(\theta = 90°, \phi = 0°)$ and the corresponding directivity D is

$$D(90°, 0°, s) = \frac{1 - \cos s}{1 - \frac{\sin s}{s}} \tag{4.31}$$

with the limit 3 (4.77 dBi) for the spacing $d \to 0$ (i.e., $s \to 0$).

In this case, the optimal currents $\mathbf{I}_{\mathrm{opt}}$ producing the maximal directivity D for a given direction (θ, ϕ) and spacing s can be also found in the manner given by (4.14) and (4.16) but the normalized far field pattern f of the isotropic radiator is

$$f(\theta, \phi) = 1. \tag{4.32}$$

The currents $\mathbf{I}_{\mathrm{opt}}$ have the same form as (4.18) but the phase difference α is now

$$\alpha(\theta, \phi, s) = -s\sin\theta\cos\phi + 2\arg\left(\rho_{\mathrm{Re}}(\theta, \phi, s) + \mathrm{j}\rho_{\mathrm{Im}}(\theta, \phi, s)\right) \tag{4.33}$$

where

$$\rho_{\mathrm{Re}}(\theta, \phi, s) = \cos(s\sin\theta\cos\phi) - \frac{\sin s}{s} \tag{4.34}$$

$$\rho_{\mathrm{Im}}(\theta, \phi, s) = \sin(s\sin\theta\cos\phi). \tag{4.35}$$

For the given array, considering the optimal excitation currents $\mathbf{I}_{\mathrm{opt}}$ (4.18) and using the above found entries of the matrices $\mathbf{u}$ and $\mathbf{p}$, the directivity D (3.31) becomes

$$D(\theta, \phi, s) = \frac{\cos\alpha + \cos(s\sin\theta\cos\phi)}{\cos\alpha + \frac{\sin s}{s}}. \tag{4.36}$$

Further, considering the spacing $d < \lambda/2$ (i.e., $s < \pi$), the maximal (end-fire) radiation

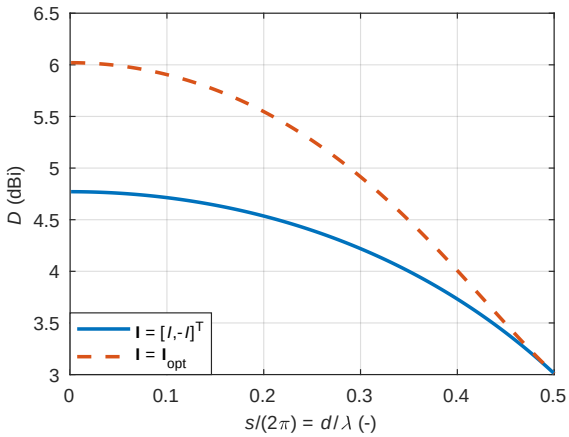

Figure 4.21: Directivity of end-fire radiation of array of two isotropic radiators with out-of-phase (blue-solid) and optimal for maximal directivity (red-dashed) excitation. Reproduced from [129].

occurs for the direction $(\theta = 90°, \phi = 0°)$ and the corresponding directivity D is

$$D(90°, 0°, s) = \frac{\cos\alpha + \cos s}{\cos\alpha + \frac{\sin s}{s}} \tag{4.37}$$

where the phase difference α (4.33) is now

$$\alpha(90°, 0°, s) = 2\pi - s + 2\arctan\left(\frac{\tan s}{1 - \frac{\tan s}{s}}\right) \tag{4.38}$$

with first two terms of Taylor's expansion for a close spacing s

$$\alpha(90°, 0°, s) \approx \pi - \frac{1}{3}s. \tag{4.39}$$

The directivity D (4.37) has a limit 4 (6.02 dBi) for the spacing $d \to 0$ (i.e., $s \to 0$) corresponding with Uzkov's limit N^2 for $N = 2$ [46]. The calculated directivities D (4.31) and (4.37) for both out-of-phase and optimal excitation are shown in Figure 4.21. A comparison of the phase differences α (4.24) and (4.38) for the arrays of two elementary dipoles and two isotropic radiators is given in Figure 4.22.

4.6 Two isotropic radiators backed by PEC ground

The increase in directivity for two isotropic radiators when close to each other implies, that the arrays backed by PEC, when the height h is close to zero may have the greatest directivity. To verify this, we present two isotropic dipoles above PEC ground. The array of two isotropic radiators is spaced in the x coordinate by a distance d in the same manner as the elementary dipoles in Figure 4.17 a), but shifted in y coordinate by distance h. The PEC ground is presented here by additional two isotropic radiators shifted in y direction by a distance $-h$.

Similarly, as for the case of the array of two isotropic elements, it holds true for the

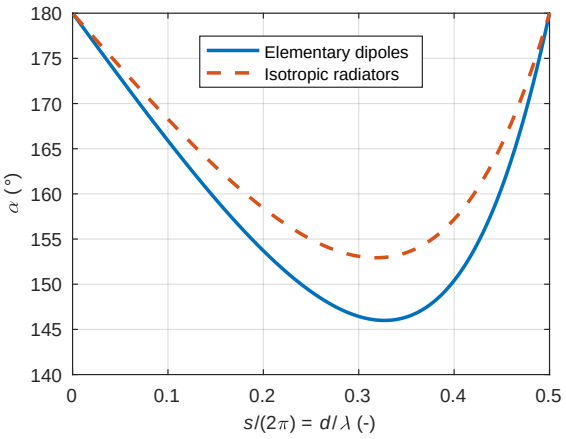

Figure 4.22: Comparison of phase difference of optimal excitation currents for maximal directivity of end-fire radiation of arrays of two elementary dipoles (blue-solid) and two isotropic radiators (red-dashed). Reproduced from [129].

intensities $u_{11} = u_{22}$, $u_{12} = u_{21}^*$. Here also the distance h comes in play and the intensity u_{13} will be

$$u_{13}(\theta, \phi, h) = u_{11} \mathrm{e}^{-\mathrm{j}v \sin\theta \sin\phi}, \tag{4.40}$$

where $v = kh$ and

$$u_{14}(\theta, \phi, s, h) = u_{11} \mathrm{e}^{-\mathrm{j}s \sin\theta \cos\phi - v \sin\theta \sin\phi}. \tag{4.41}$$

When we calculate the additional intensities for the remaining elements and vice versa, we get the intensities that holds true $u_{11} = u_{22} = u_{33} = u_{44}$, $u_{12} = u_{21}^* = u_{34} = u_{43}^*$, $u_{13} = u_{31}^* = u_{24} = u_{43}^*$, $u_{14} = u_{41}^*$ and $u_{23} = u_{32}^*$ and for the powers $p_{11} = p_{22} = p_{33} = p_{44}$, $p_{12} = p_{21} = p_{34} = p_{43}$, $p_{13} = p_{31} = p_{24} = p_{42}$ and $p_{14} = p_{41} = p_{23} = p_{44}$, thus the power matrix is symmetric.

For the given array, considering the in-phase excitation currents $\mathbf{I} = [I, I, -I, -I]^{\mathrm{T}}$ where the first two current are for the elements above PEC ground and second pair of currents is for mirror elements and using the above found entries of the matrices $\mathbf{u}$ and $\mathbf{p}$, the directivity D (3.31) becomes

$$D(\theta, \phi, s, h) = \frac{kdh\sqrt{d^2+h^2}\cos\left(kh\sin\theta\sin\phi - 1\right)\left(\cos\left(kd\sin\theta\cos\phi\right)\right)}{dh\sin\left(k\sqrt{d^2+h^2}\right) + \sqrt{d^2+h^2}\left(d\sin\left(kh\right) - h\sin\left(kd\right) - dkh\right)}. \tag{4.42}$$

Further considering the maximum radiation in the direction $(\theta = 90°, \phi = 90°)$ the corresponding directivity D is

$$D(\theta, \phi, s, h) = \frac{2kdh\left(\cos\left(kh\right) - 1\right)\sqrt{d^2+h^2}}{dh\sin\left(k\sqrt{d^2+h^2}\right) + \sqrt{d^2+h^2}\left(d\sin\left(kh\right) - h\sin\left(kd\right) - dkh\right)} \tag{4.43}$$

with first four terms of Taylor's expansion for a small height h shows the limit 6.56 (8.17 dBi) for the height $h \to 0$ and spacing $d = 0.93\lambda$. The directivity D 4.43 is shown in Figure 4.23 and the directivity D for a limit when $h \to 0$ is given in Figure 4.24.

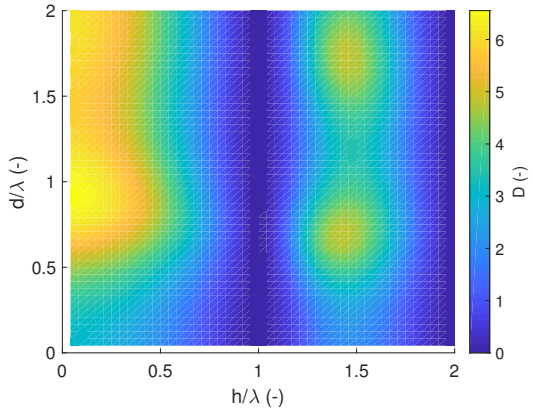

Figure 4.23: Directivity for two isotropic radiators above PEC ground.

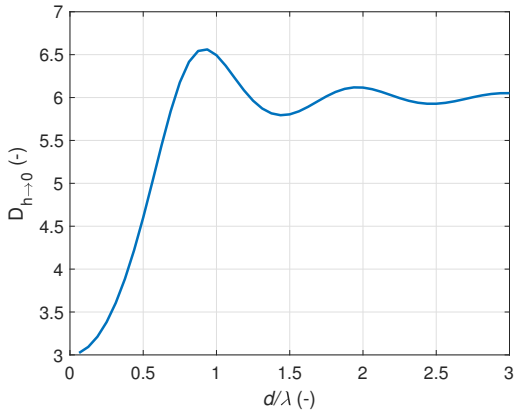

Figure 4.24: Directivity for two isotropic radiators for $h \to 0$.

The optimal currents here are difficult, but generally possible, to find analytically by the procedure described in previous chapter.

4.7 PSO optimization for antenna arrays

Because the developed computational method is very fast, we can evaluate the maximum achievable broadside directivity for an array of N thin horizontal dipoles above PEC ground by the PSO [133]. These dipoles have the same length of $L = \lambda/2$ and radius as in the three element array example in chapter 4.2 and are oriented in z direction. The height of the dipoles above the PEC ground is h and spacing is first fixed $s_n = s$ and then let arbitrary s_n. Due to constraint of broadside radiation ($\theta = 0$), arrays with two and three elements will have the same separation. However for arrays with more dipoles, this is not generally true.

The maximum obtainable broadside directivity for the array of ten dipoles with constant spacing is depicted in Figure 4.26 Maximum directivity $D = 20.75$ dBi occurs for $s = 0.658\ \lambda$ and $h = 0.907\ \lambda$.

It is noted that thanks to the presence of the ground plane, the superdirective currents

are real (equiphase). It follows from the symmetry of the u and p matrices and the fact that the original $\mathbf{I}_o = \mathrm{Re}\mathbf{I}_o + \mathrm{jIm}\mathbf{I}_o$ and image $\mathbf{I}_i = \mathrm{Re}\mathbf{I}_i + \mathrm{jIm}\mathbf{I}_i$ currents resulting from the modal decomposition are complex conjugated $\mathbf{I}_i = \mathbf{I}_o^*$.

The results for different number of dipoles with constant separation are summarized in Table 4.2 and the results from PSO with different spacings between elements are in Table 4.3

number of elements N	D (dBi)	$h/\lambda(-)$	$s/\lambda(-)$
2	12.82	0.677	0.628
3	14.9	0.677	0.752
4	16.33	0.658	0.814
5	17.45	0.658	0.845
10	20.76	0.658	0.907
25	25.03	0.658	0.932
50	27.95	0.628	0.907

Table 4.2: Maximum directivity and its optima for different number of elements in the array. Separations are kept constant.

	$N = 4$	$N = 5$	$N = 10$
D(dBi)	16.44	17.57	21
$h/\lambda(-)$	0.663	0.662	0.657
$s_1/\lambda(-)$	0.753	0.774	0.795
$s_2/\lambda(-)$	0.875	0.878	0.915
$s_3/\lambda(-)$	s_1	s_2	0.918
$s_4/\lambda(-)$		s_1	0.93
$s_5/\lambda(-)$			0.933

Table 4.3: Array parameters for maximum directivities with PEC ground. Height and separations are optimized

It is interesting that the optimal heights and mutual spacings are very similar. The separation tends to increase with number of dipoles. This finding suggests that the height of linear array above PEC ground has its optimum for any array with a different number of elements.

This idea is supported by evaluation of optimal current for two isotropic radiators above the PEC ground and inserting them into 3.31. The result is depicted in Figure 4.27 Contrary to the dipole case, there are two peaks. The first one is for zero height (probably due to the fact that isotropic radiators lack any polarization properties), but for the second we obtain similar numbers as for dipoles.

In Fig.4.25 we show normalized current amplitudes for arrays with $N = 10, 25$ and 50 elements (optimized both height and constant spacing as from Table 4.2), where the center dipole is denoted as $N = 0$. It is interesting that the optimal height h and spacing s for various numbers N are very similar and the spacing s tends to increase with the number N. This finding suggests that the height h has optimum for an arbitrary number N. In Figure 4.25, it is apparent that the magnitudes of the currents $\mathbf{I}_{\mathrm{opt}}$ are not uniform, but tapered. For higher number N, the magnitudes changes along the array in an oscillatory

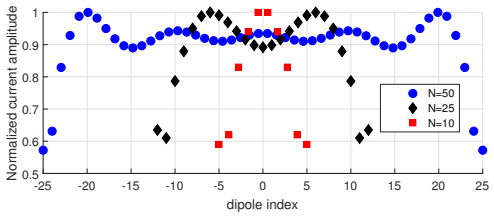

Figure 4.25: Feeding currents that maximize directivity for array with 10, 25 and 50 elements.

way, probably due to some kind of "resonance".

Finally, in Figure 4.28 we show the radiation pattern of the array with three dipoles placed at optimal height and spacing and fed by optimal current to achieve the maximum directivity. Agreement with FEKO is excellent.

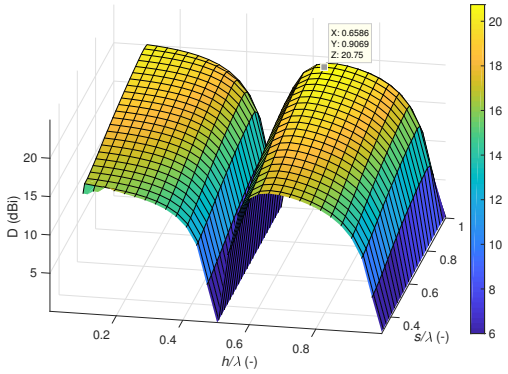

Figure 4.26: Maximum directivity of 10 element dipole array above PEC ground.

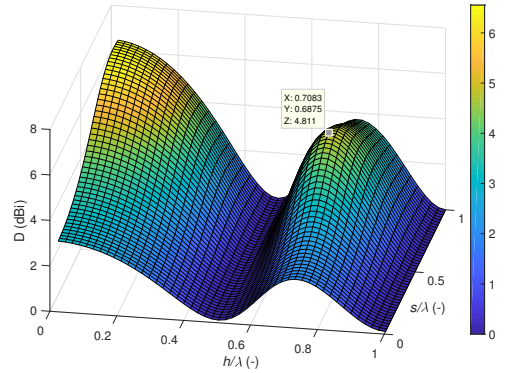

Figure 4.27: Maximum directivity of 2 isotropic element array above PEC ground.

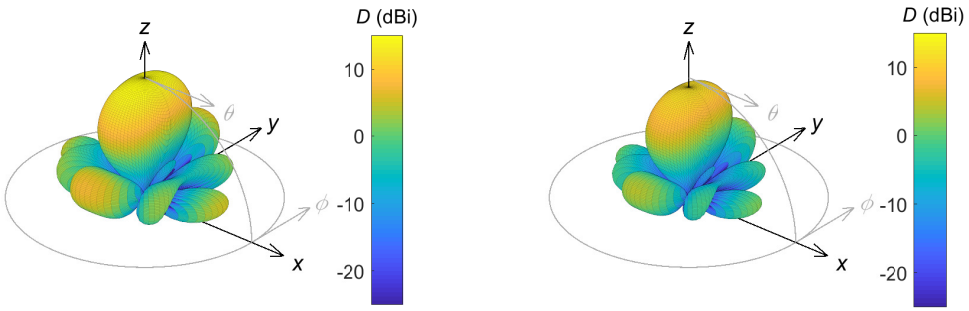

(a) FEKO 3x1

(b) MATLAB 3x1

Figure 4.28: Radiation pattern of 3 × 1 array above PEC optimized for maximum directivity.

Chapter 5

Beamforming

The array beamforming problem is the process of forming a strong beam or multiple beams in a given direction using a collection of antennas that do not necessarily have any preferential direction. By controlling the amplitude and phase of each antenna, their individual radiation patterns can be made to constructively interfere in a chosen direction, forming a main beam. At the same time, their radiation patterns interfere destructively in other directions, ensuring that most of the emitted power travels along the main beam. Basic approaches to the beamforming problem assume control over element positions, transmit amplitudes, and transmit phases [134].

Multiuser M-MIMO systems are projected to play a vital role in 5G communication. The bandwidth requirements for 5G are expected to rise 100 times more than the current 4G systems. These requirements now can be achieved only with beamforming.

5.1 Design of a 24-28 GHz array

For the antenna array using with 5G system a three different antenna arrays was designed. They differ with maximum observable gain and bandwidth and on the other hand were were selected by the manufacturing cost and durability. The maximum gain can be achieved with Vivaldi array, moderate gain with waveguide array and lowest gain with dipole array.

5.1.1 Vivaldi array

A Vivaldi antenna is antenna that is characterized by wide bandwidth, high gain and an end-fire radiation pattern [135]. On the Figure 5.2 is a reflection coefficient and realized gain of the Vivaldi antenna with a microstrip line feed depicted in Figure 5.1. This antenna was designed on both sides of a Rogers RT/Duroid 5880. Because the Vivaldi antenna requires a feed with a slot-line transmission line, which is balanced , it is necessary to use balun, that acts as a microstrip-to-slot-line transformer. This balun must operate over a frequency range of at least two octaves, and up to several octaves. Kayani [136] proposed a simple, compact Vivaldi antenna in 2005 and this design was used in our antenna design. The main advantage of this design is that the antenna can be made smaller compared

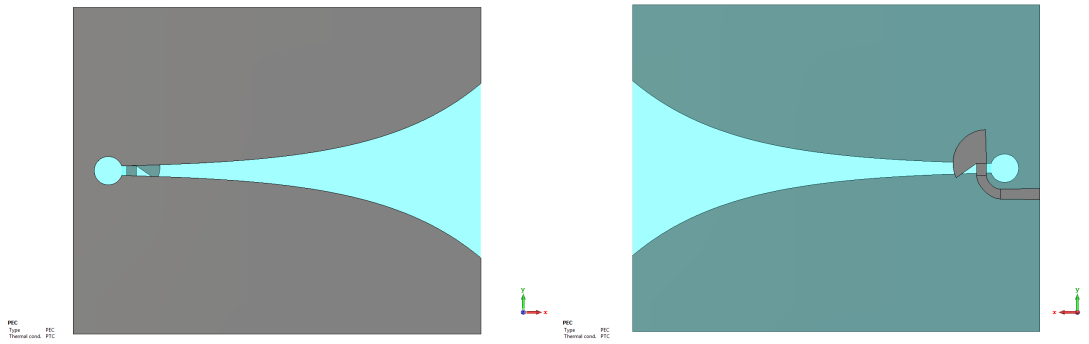

(a) front of the vivaldi antenna (b) back of the vivaldi antenna

Figure 5.1: Vivaldi with microstrip feed with dimensions $x \approx 1.7\lambda$, $y \approx 1.3\lambda$

phase\element	1	2	3	4	5
A	0	0	0	0	0
B	-100	-50	0	50	100
C	-200	-100	0	100	200
D	-300	-150	0	150	300

Table 5.1: Phase distribution on the elements of the array

to an antipodal Vivaldi antenna. The realized gain is evaluated for the radiation in x direction ($\theta = \pi, \phi = 0$).

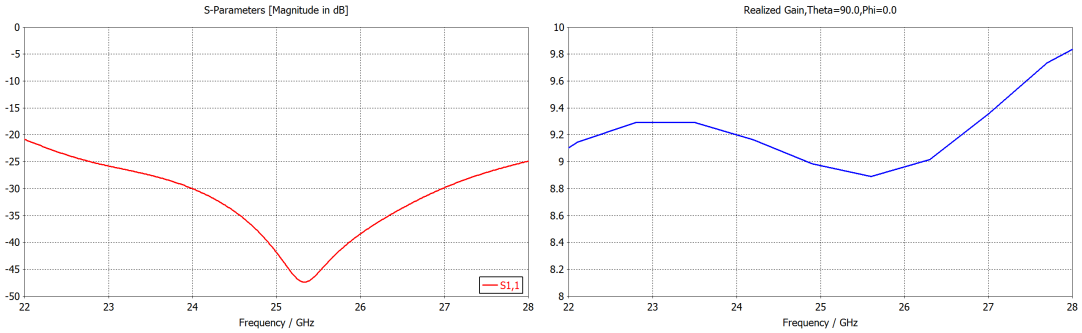

(a) S parameters (b) realized gain

Figure 5.2: Simulated S parameters and gain of the Vivaldi antenna

The antenna from Figure 5.1 was used to create an antenna array. The distance between the elements was changed to achieve optimal results (minimal grating-lobes, minimal mutual coupling and maximal steering angle). As an initial distance was set $d = 6$ mm. This value was calculated from (5.1), when fullfilling this expression, the closest unwanted grating lobe will be not appear in visible space [137].

$$\frac{d}{\lambda} < \frac{1}{1 + \sin|\theta_0|}, \tag{5.1}$$

where d is mutual distance between elements, λ is wavelength and θ_0 is scanning angle.

In the Figure 5.3 is depicted basic arrangement of the Vivaldi array with mutual

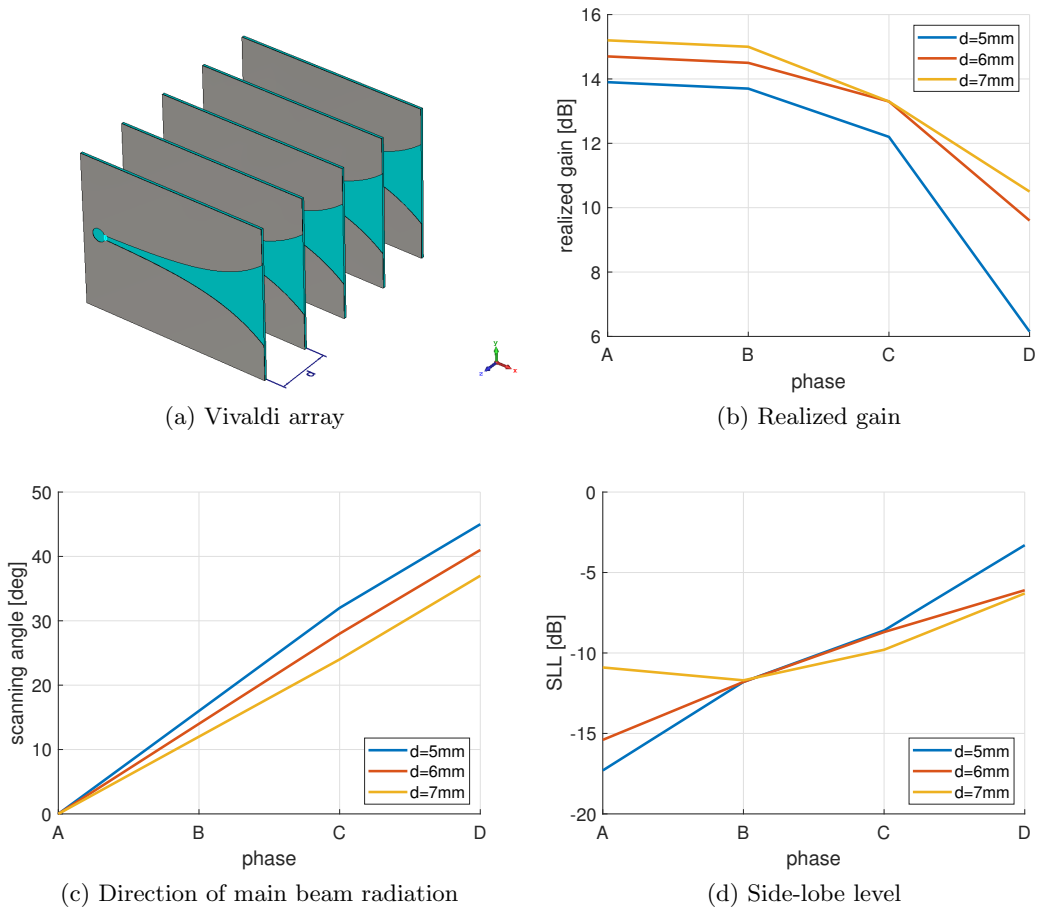

(a) Vivaldi array

(b) Realized gain

(c) Direction of main beam radiation

(d) Side-lobe level

Figure 5.3: Parameters of the Vivaldi array with five elements, based on spacing between the elements

distance d. This mutual distance is changed from $d = 5$ mm to $d = 7$ mm with the results of the realized gain, scanning angle and side-lobe level (SLL) is depicted in Figure 5.3. The parameters are calculated for different feeding, constant amplitude and phase in degrees from Table 5.1. From the Figure 5.3 we can see, that with increasing mutual distance d the realized gain is lower, but the scanning angle is wider, so the optimal mutual spacing for our array of antennas is $d = 6$ mm.

The amplitude analysis for having narrow beams with low sidelobes was performed with basic linear weight distribution distribution.

Often it is desirable to lower the highest sidelobes, at the expense of raising the lower sidelobes. The optimal sidelobe level (for a given beamwidth) will occur when the sidelobes are all equal in magnitude with Dolph-Chebyshev distribution [135],[20].

Taylor-Kaiser arrays are another used technique for designing array beam patterns. In contrast to Chebyshev, the relation between mainlobe width and sidelobe attenuation is not optimum in this technique. The mainlobe width is larger than in Chebyshev arrays with the same sidelobe level [138] The array excitation coefficients can be calculated in the folllowing way:

$$I_m = I_0 \left(\gamma \sqrt{1 - m^3/M^2} \right), \tag{5.2}$$

where $m = \pm 1, \pm 2, \ldots, \pm M$, or $m = 0, \pm 1, \pm 2, \ldots, \pm M$, for even or odd number of array elements, I_0 stands for the modified Bessel function of 1^{st} kind and zero order and γ is the shape parameter.

The binomial array has the amplitudes arranged in such a way that the resultant radiation pattern has no minor lobes, but wide mainlobe. The weights of an N-element binomial array are the binomial coefficients:

$$w(m) = \frac{(N-1)!}{m!(N-1-m)!}, \tag{5.3}$$

where $m = 0, 1, \ldots, N-1$.

The weights for the specific array with five elements and mutual distance $d = 6$ mm are depicted in Table 5.2.

distribution\element	1	2	3	4	5
linear	1	1	1	1	1
Dolph-Chebyshev	1	1.61	1.93	1.61	1
Taylor-Kaiser	1	2.27	2.84	2.27	1
binomial	1	4	6	4	1

Table 5.2: Weights distribution on the elements of the array

These weights were used as input for the realized gain calculation on the array. The realized gains are depicted in Figure 5.4 and Figure 5.5 respectively, for the broadside radiation and for maximum phase distribution D from Table 5.1.

5.1.2 Waveguide array

The final mounting and set precise element spacing of each antenna with Vivaldi elements is complicated, thus the waveguide antenna was designed and is depicted in Figure 5.6. The advantage of a waveguide antenna is easy manufacturing and possibility of transmitting high power, thus increasing transmission distance and improving SNR. The realized gain and reflection coefficient of the waveguide antenna is shown on Figure 5.7. From the simulation one can notice that the reflection coefficient and realized gain is inferior compared to Vivaldi results. Specifically the reflection coefficient in the monitored band $(24 - 28$ GHz) is better then $s_{11} = -14$ dB and realized gain is over 7 dBi. The reflection coefficient was improved by adding the metal disc to the end of the coaxial feed probe.

To enhance the realized gain of the waveguide antenna another part of "cavity" was added to top and bottom of the waveguide. The final design of a single antenna element is depicted in Figure 5.8. The reflection coefficient and realized gain of this antenna are in Figure 5.9. The realized gain has increased in the band $24 - 31$ GHz and is approaching the results of the Vivaldi antenna. The reflection coefficient in the monitored band has improved by 2 dBi. On this design many parameters was optimized with respect to feasibility of manufacturing. For this case the inside of the waveguide is blended with radius R = 1mm. The feeding of the waveguide is from top side with SMP male threaded limited detent connector SC5510 from Fairview Microwave [139]

The model of the antenna from Figure 5.8 was used to create the antenna array with five elements. The problematic part here was to minimize the spacing between each antenna element. Due to this factor the metal thickness of the vertical wall between the elements is reduced to one millimeter. In the Figure 5.10 is depicted total reflection coefficient and realized gain for feeding of the elements with equal amplitude and phase. Due to the symmetry, only three curves of reflection coefficient are showed, while $s_{1,1+2+3+4+5} = s_{5,1+2+3+4+5}$ and $s_{2,1+2+3+4+5} = s_{4,1+2+3+4+5}$. The realized gain with this antenna array is slightly better then with Vivaldi array. In the monitored band we obtain average gain 15 dBi. Also the waveguide array can operate in large frequency band.

But as mentioned above, the 5G networks will use M-MIMO. To ensure this property we need to be able to stack up this array on each other. Thus the feeding from top or side of the waveguide is not possible in this case. The only possible feeding of an $N \times N$ waveguide array is from behind. In literature there are many different techniques to feed the waveguide with this way. Many authors use substrate integrated waveguide (SIW) to waveguide transition such as [140], [141] or directly inserts the substrate into the waveguide [142]. The design of the transition from microstrip to waveguide by Iizuka [143], followed by Seo [144] and second approach by Sakakibara [145] was implemented in

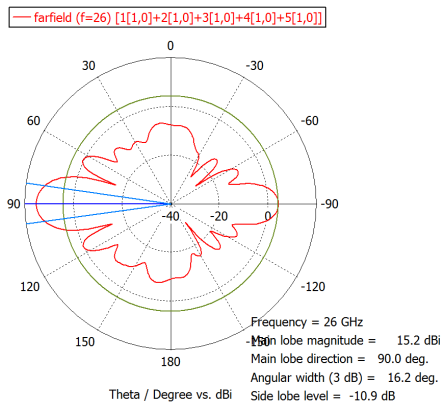

(a) Uniform distribution, no steering

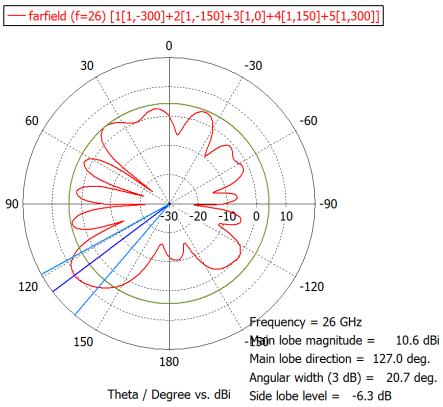

(b) Uniform distribution, max steering

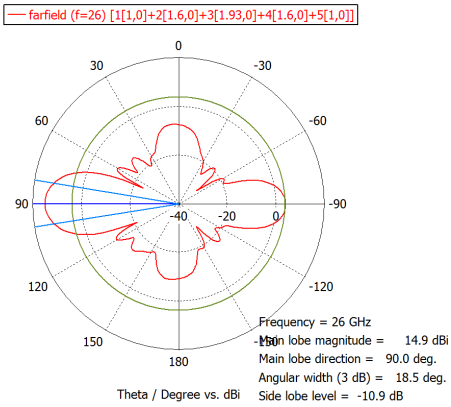

(c) Dolph-Chebyshev distribution, no steering

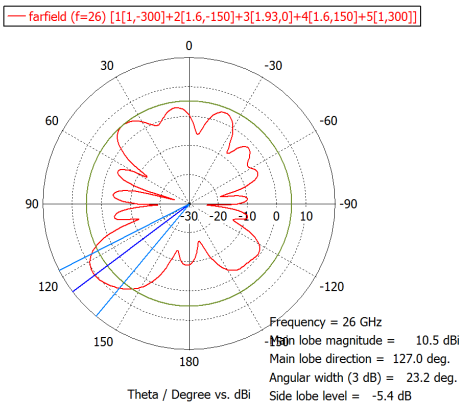

(d) Dolph-Chebyshev, max steering

Figure 5.4: Different amplitude distribution for none and maximum steering

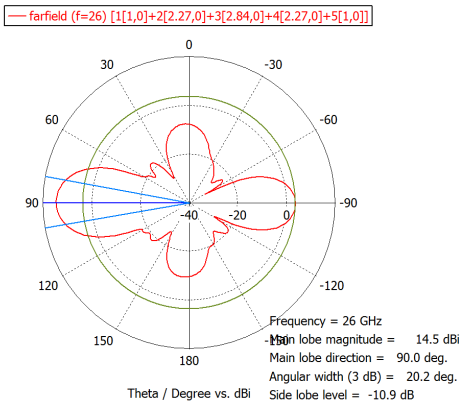

(a) Taylor-Kaiser distribution, no steering

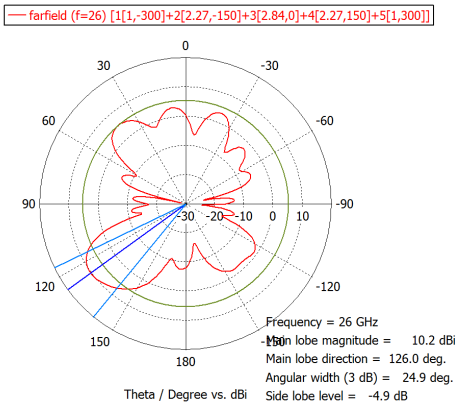

(b) Taylor-Kaiser, max steering

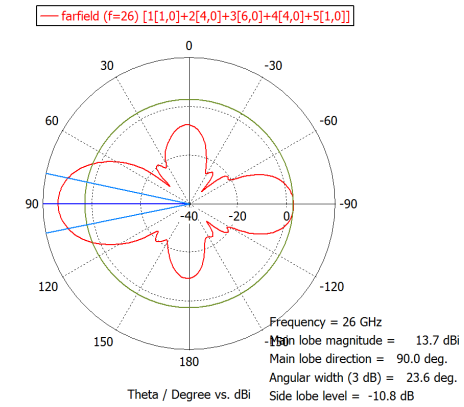

(c) Binomial distribution, no steering

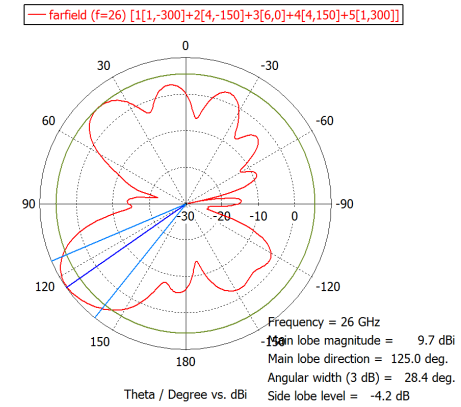

(d) Binomial, max steering

Figure 5.5: Different amplitude distribution for none and maximum steering

CST. The designed structures are shown in Figure 5.11

Both design were applied to a central frequency 76.5 GHz. Iizuka developed a planar proximity coupling transition. This transition can be composed of only a single dielectric substrate attached to the waveguide end and suitable for mass production. The conductor pattern with a notch and the microstrip line are located on the upper plane of the dielectric substrate. A rectangular patch element and a surrounding ground are patterned on the lower plane of the dielectric substrate. Via holes are surrounding the aperture of the waveguide on the lower plane of the dielectric substrate to connect the surrounding ground and the waveguide short electrically. The microstrip line is inserted into the waveguide and overlaps on the rectangular patch element. The overall bandwidth is only 6.5%.

Sakakibara present design with substrate attached on a back short waveguide and to WR-10 waveguide on top of the structure. This design is more difficult to manufacture and consist from more parts. Also stacking up multiple layers is not possible with this design. A topside waveguide-to-microstrip transition with double layer substrate has been also developed. The substrate is set on the flat metal plate and the waveguide is set on it perpendicularly. All the design parameters are in the substrate. Any special structures are not necessary in the metal parts. However, the double layer substrate is necessary and

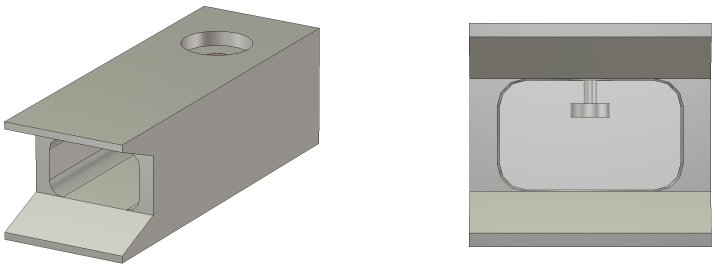

(a) (b)

Figure 5.6: Waveguide antenna with coaxial feeding with dimensions $x \approx 0.7\lambda$, $y \approx 0.65\lambda$, $z \approx 3.3\lambda$,

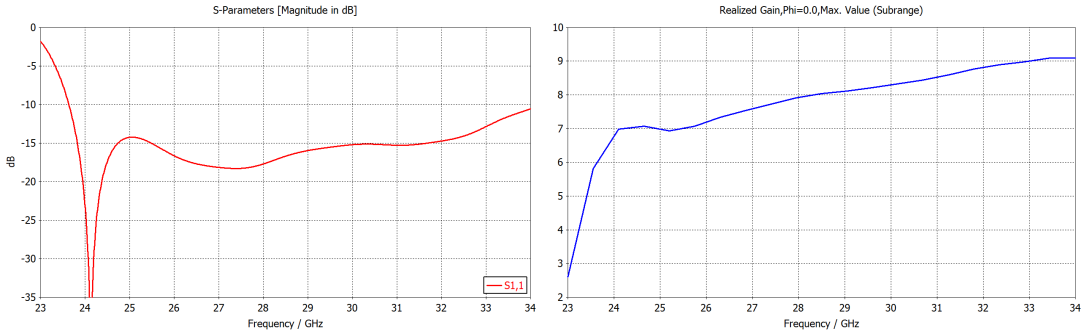

(a) S parameters (b) realized gain

Figure 5.7: Simulated S parameters and gain of the waveguide

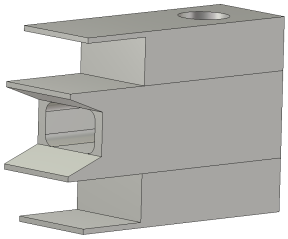

Figure 5.8: Waveguide antenna with coaxial feeding and 'cavity'

the bandwidth is limited because it operates by patch resonance. The bandwidth in this case is only 6%.

This solutions are not applicable to our case because of required bandwidth, which should be 15%.

5.1.3 Dipole array

Due to manufacturing problems, the dipole based dipole array on the PCB was designed, where the design was inspired by [146].

Figure 5.12 shows the geometry of the printed dipole antenna, which was designed on substrate Rogers RT/Duroid 5880 ($h = 0.254$ mm, $\varepsilon_r = 2.2$, and $\tan\delta = 0.0009$).

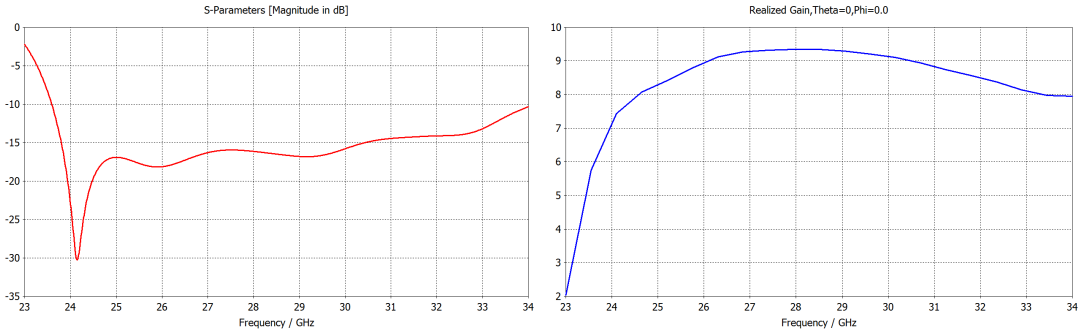

(a) S parameters (b) realized gain

Figure 5.9: Simulated S parameters and gain of the waveguide antenna with 'cavity'

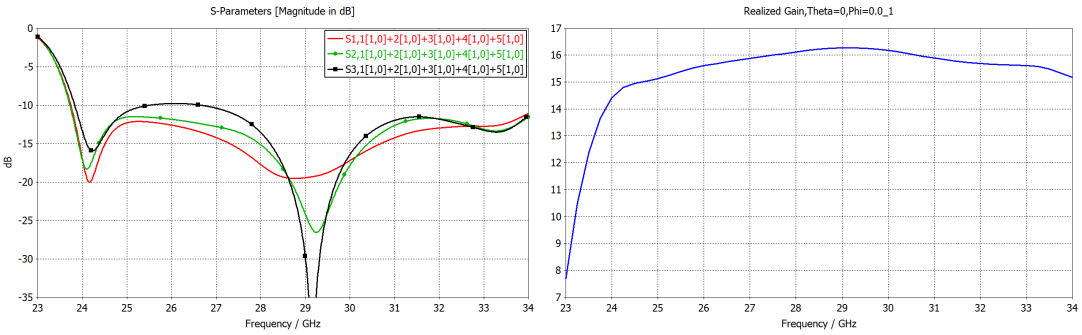

(a) S parameters (b) realized gain

Figure 5.10: Simulated S parameters and gain of the waveguide antenna array with 'cavity'

The antenna consists from a printed dipole, integrated balun, microstrip-line feed and mini SMP full detent right angle connector type 187662 from Rosenberger [147]. The feedline was on the top layer of the substrate, whereas the dipole and the ground plane were on the bottom layer. Impedance matching was realized by adjusting the folded line and rectangular slot. Also, the gap of the slotline and the stripline are crucial design parameters of impedance matching. The printed dipole was angled to achieve a compact size, as well as to realize a wide pattern in the E-plane. The simulated reflection coefficient and a realized gain is depicted in Figure 5.13. Here the reflection coefficient is comparable with reflection coefficient of the waveguide antenna, but the realized gain is lower by $1-2$ dBi with decline around 29 and 32 GHz, which is outside the designed frequency band. The dipole is fed by a slot line and the balun acts as a microstrip-to-slot-line transformer. This arrangement does not allow for a completely symmetrical antenna, so the main lobe direction of the far field is 5° with 3 dB beamwidth and -8.3 dB side-lobe-level.

As already mentioned, the designing of an antenna array is tradeoff between low mutual coupling and low sidelobes with maximization of scanning angle. To obtain low mutual coupling between dipole elements a microstrip stub was inserted in between the two elements with $d = 6$ mm spacing. The function of the stub is similar to the radio frequency choke [148]. We implemented an 4-element dipole array as shown in Figure 5.14. The final dimensions of this four element antenna array is in Appendix A.

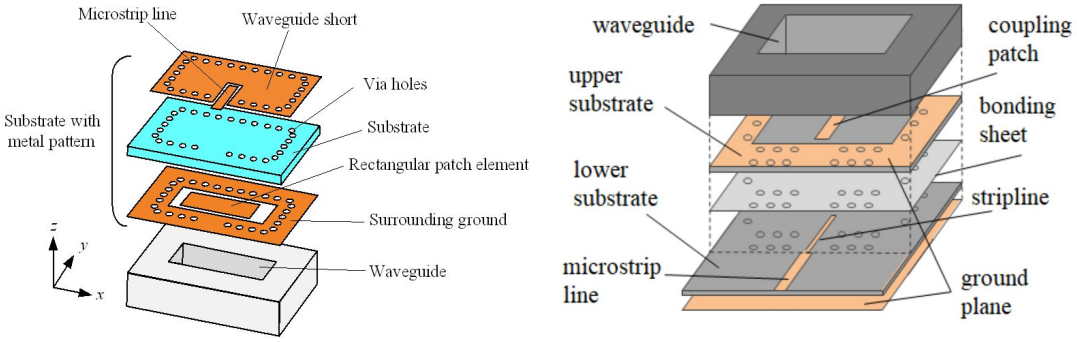

(a) design by Iizuka [143]

(b) design by Sakakibara [145]

Figure 5.11: Waveguide to microstrip transition with double layer substrate

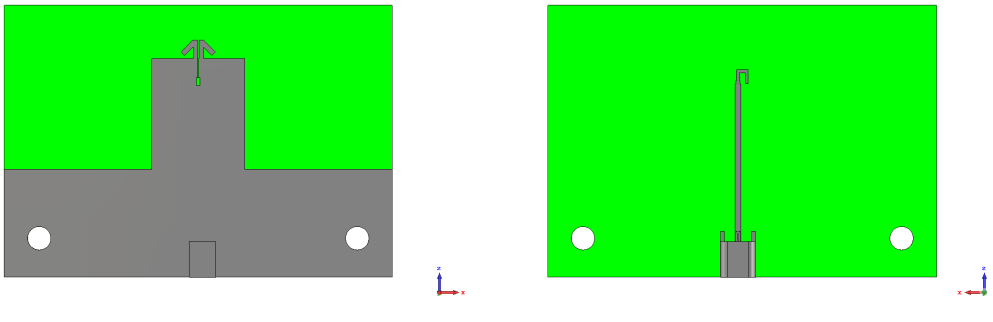

(a) front of the dipole antenna

(b) back of the dipole antenna

Figure 5.12: Dipole antenna with microstrip feed with dimensions $x = 4\lambda$, $y = 2.8\lambda$.

The simulated reflection coefficient and realized gain is depicted in Figure 5.15 for constant feeding in amplitude and phase. Because of the asymmetry of the single element design, when the microstrip is offset against the dipole, the calculated s parameters are also not symmetrical. The reflection coefficient of the dipole array is better than waveguide array, but worse compared to Vivaldi array. The realized gain is lowest from all the simulated antenna arrays. But the advantage of this array is its simple manufacturing on one Printed Circuit Board (PCB), so the manufacturing cost is lower than with waveguide array.

The manufactured antenna arrays were on PCB substrate with size 200×240 mm. To use all the expensive substrate, three versions from each array were manufactured. Because the gap of the slotline and the stripline are crucial design parameters, this parameters were varied by a few percent in each design. The manufactured arrays include 1,3,4,5 and 8 elements and 4 elements with simple power divider. The figure of all the manufactured antennas is in Appendix B.

The manufactured antenna with only one dipole elements was used to measure and verify the design. On the Figure 5.16 is comparison from CST simulation with simple model of mini SMP connector and measurement of the same manufactured antenna. Also one manufactured sample was mounted with end-launch connector and measured. From

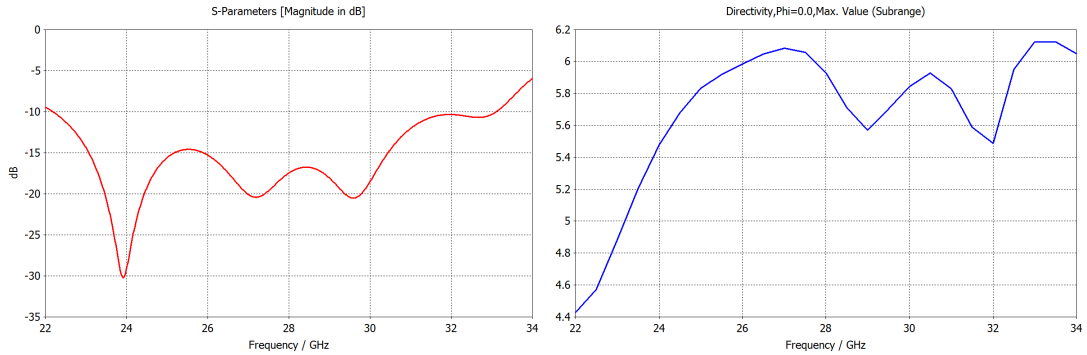

(a) S parameters (b) realized gain

Figure 5.13: Simulated S parameters and gain of the dipole antenna.

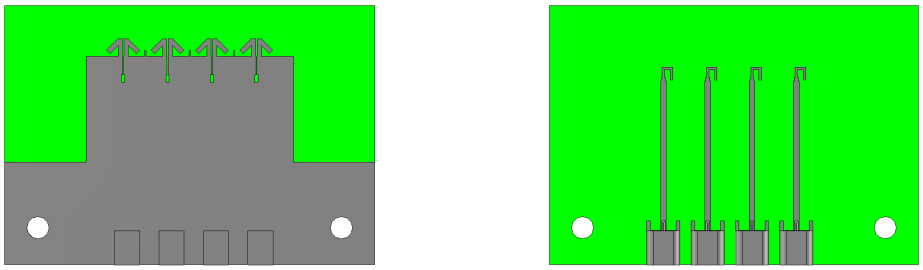

(a) front of the dipole antenna array (b) back of the dipole antenna array

Figure 5.14: Dipole antenna array with microstrip feed

this comparison we can see, that the results are very close to the simulation. The differences are probably due to poor mini SMP model in CST and also due to high sensitivity in dimension change of the slotline and stripline.

Because of differencies in simulation and manufactured antenna, the one element PCB was measured with microscope ASH OMNI [149] with resolution up to 0.001 mm. The results with crucial dimensions are shown in Figure 5.17. The maximum variation in dimensions is up to 15% in middle gap. This variation can cause the inaccuracy in measurement and software simulation.

The manufactured four element dipole array was assembled by mini SMP connectors and measured with vector network analyzer (VNA) Rohde & Schwarz ZVA50 and mini SMP calibration kit. The measured results are depicted in Figure 5.18. Compared to simulation, the antenna has not the best reflection coefficient. The lowest s_{11} is in frequency band from 21-23 GHz, while in simulation it was on frequencies around 24 GHz. This frequency shift could be due to different substrate parameters, ϵ_r, or by slightly different dimensions caused by manufacturing tolerances. This type of antenna is also sensitive to misalignment of the two metallic planting. Strange behavior has port number 4, which reflection coefficient is the highest and differs from other elements. This is probably due to mistake in calibration.

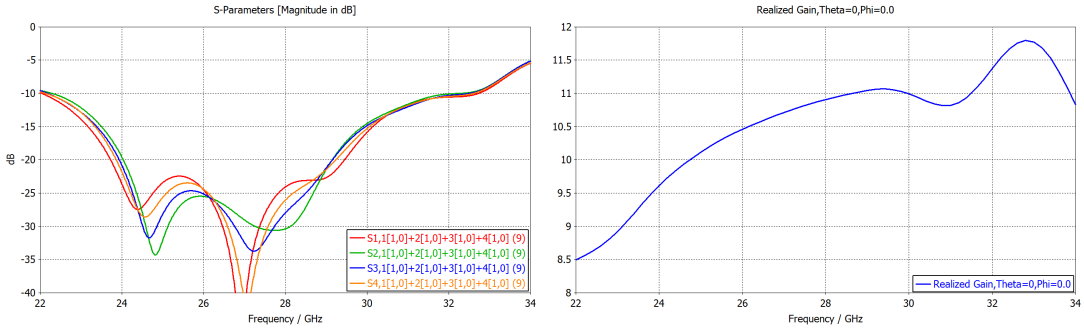

(a) S parameters (b) realized gain

Figure 5.15: Simulated S parameters and gain of the dipole antenna array

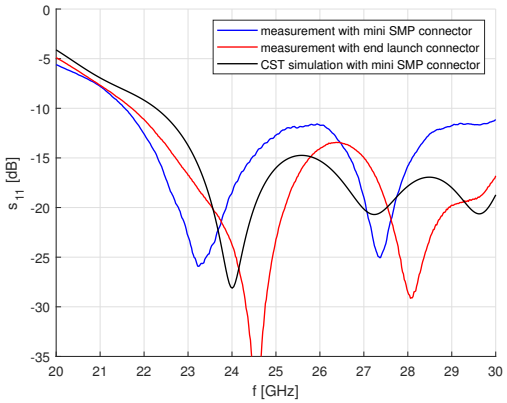

Figure 5.16: Comparison of s_{11} from simulation and measurement

Another problem with this measurement are the mini SMP connectors itself. These connectors are not precise and so the measurement repeatability is poor. In the best case we get ± 4 dBi variations when re-connecting the antenna. The repeated connecting of the antenna with four elements and four different re-connection is depicted in Figure 5.19. The s_{11} is a reflection coefficient of the first (left) element, while all connectors of the antenna were connected to VNA.

5.2 Synthesis of feeding coefficients

The antenna array structure from Figure 5.14 was used to optimize the radiation pattern based on prescribed one in MATLAB. For this antenna array the desired farfield was prescribed in MATLAB by the functions (5.4) and (5.5). The direction of a main lobe was steered in θ by 30 degrees and no side lobes were considered. The results from CST (impedance matrix and radiation patterns), which are noted as loaded far fields were integrated to MATLAB. These inputs were used along with modal decomposition to get the vector of weights of the modes, vector of the modal currents and modal normalized

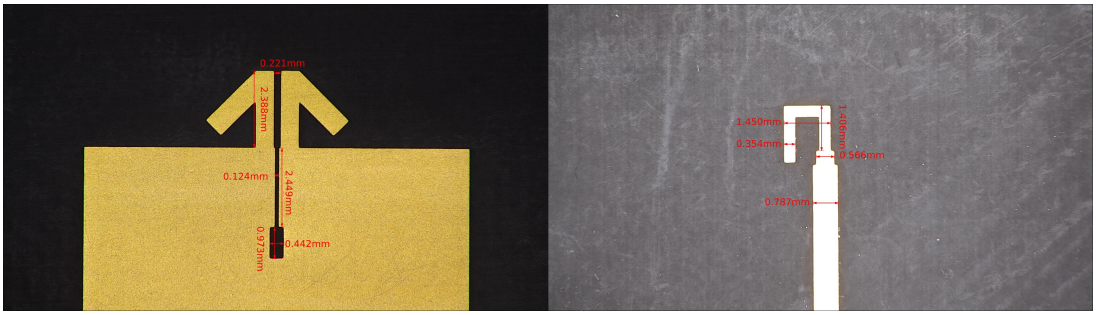

Figure 5.17: Printed dipole antenna under the microscope

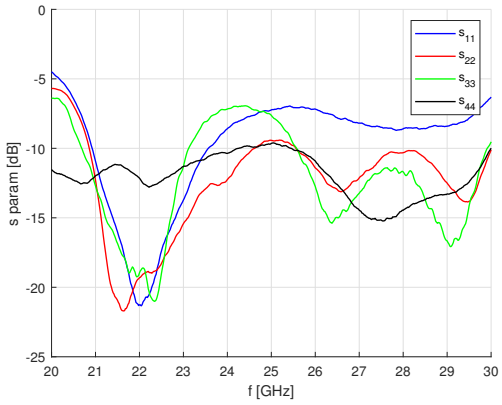

Figure 5.18: s parameters of the manufactured antenna array with miniSMP calibration

farfields, see the MATLAB code in appendix C.

$$\mathbf{f}_{on}(\theta) = \cos\left(\theta - \pi/2 + 30\pi/180\right)^{22} \tag{5.4}$$

$$\mathbf{f}_{on}(\phi) = \cos\left(((\phi - \pi/2) + 1)/2\right)^{2} \tag{5.5}$$

The optimal parameters of a incident wave on the antenna ports are depicted in Table 5.3. The amplitude on edge elements is lower to suppress the side lobes of the farfield, while the phase on each element is not intuitive at all. The required normalized farfield from functions (5.4) and (5.5) and farfield optimized by MATLAB are depicted in Figure 5.20.

element number	amplitude (V)	phase (°)
1	0.0165	173.7
2	0.0248	82.2
3	0.0257	-8
4	0.0188	-101.6

Table 5.3: Optimal incident wave on the antenna port

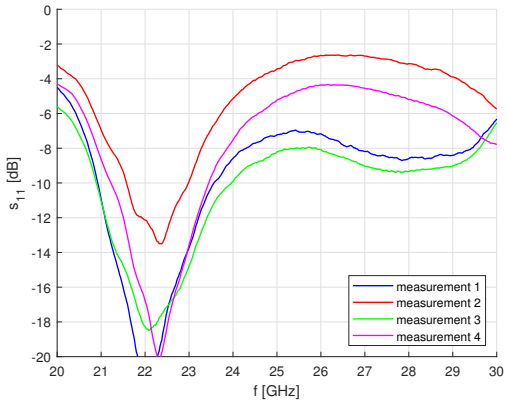

Figure 5.19: Repeated connecting of the four element antenna array with mini SMP connector

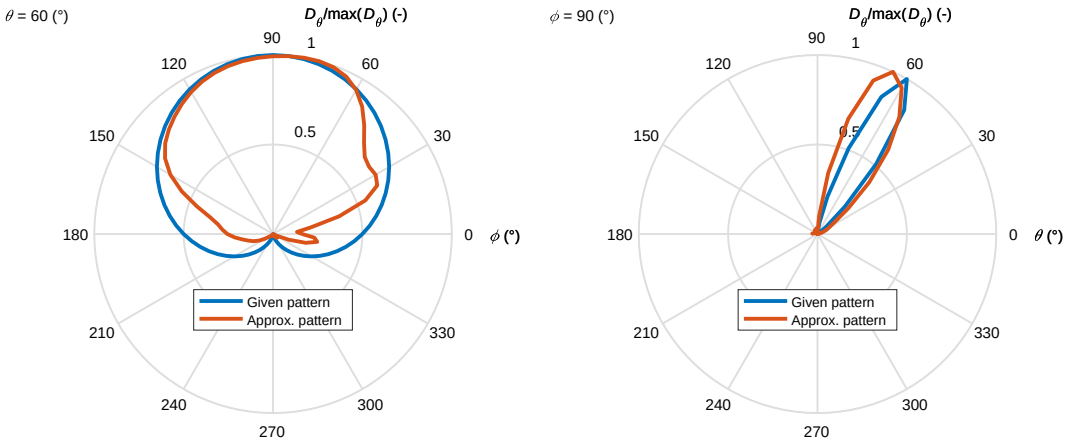

(a) farfield θ cut

(b) farfield ϕ cut

Figure 5.20: Required and optimized radiation patterns for 5GHz dipole antenna array. Note that the farfields are minimized by the minimum-square method, therefore the farfield is optimized as a whole resulting in slightly different maxima.

5.3 Practical realization and beam steering using RoF

This chapter and the results are done under the project MPO FV30427. To verify the developed theory, the RoF method was used to feed the antenna array. The complete system block diagram of the proposed scheme is depicted in Figure 5.21. The emitted signal by a continuous wave (CW) 4 port laser (IDPhotonics TLCoBrite DX4) is launched into the dense wavelength division multiplexer (DWDM). The signal is then launched to the Mach-Zehnder Modulator (MZM) through polarize controller (PC) to set the defined polarization. A RF signal at the frequency of 24 GHz from RF generator is used to modulate the optical carrier. The optical channel is formed by single mode fiber (SMF) with variable lengths. The optical channels are then separated by using another DWDM. Direct detection of the signal is realized by using a high-speed photodetector (PD) (PD–Optilab PD 40) and the RF signal is send into the antenna. The phase shift between the elements

is then controlled by varying the wavelength of the optical signal from CW laser. Due to chromatic dispersion there is a different delay between the wavelengths. The s-parametrs of the PD are in Figure 5.22.

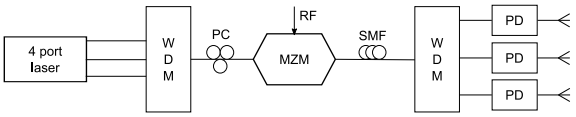

Figure 5.21: System block diagram

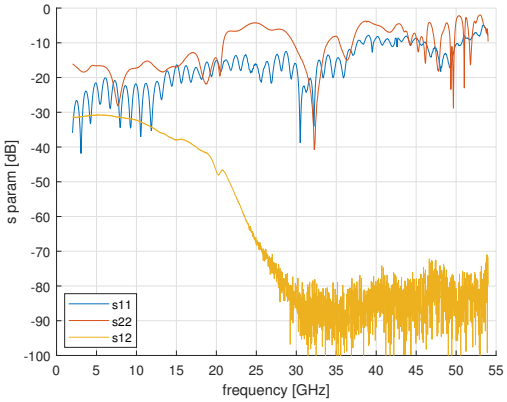

Figure 5.22: s-parameters of PD-Optilab PD 40

From the RF point of view is important the connection from the output of PD to input of the antenna array. This could be done by directly integrating the PD with the PCB of the antenna array. But this solution is very expensive. The cable connection was realized with 6 inch long cables with miniSMP female to 2.92 male connectors. In this case the relative phase shift of all cables relative to cable no.1 is crucial and must be know to eliminate the error in feeding of the antenna. This relative phase is depicted in Table 5.4.

cable number	1	2	3	4	5	6	7	8	9	10
relative phase shift (°)	-	0.2	0.6	2.6	10	9.7	7.6	−10.8	−11.1	−7.9

Table 5.4: Relative phase shift of the 6 inch long, miniSMP to 2.92 cables relative to cable no.1

The practical realization was first done without the antennas itself to verify the capability of phase shift and possible output power A different length of SMF was used. The realization is depicted in Figure 5.23.

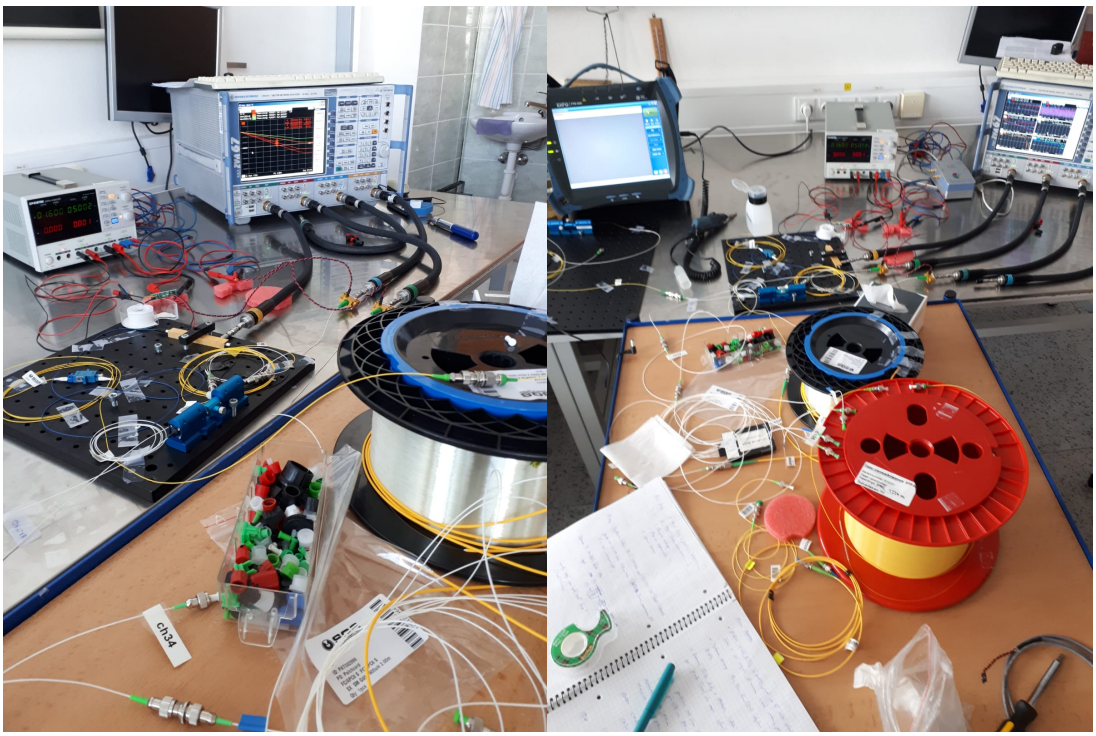

(a) (b)

Figure 5.23: Practical realization of RoF without antenna sector.

Chapter 6

Conclusion

6.1 Discussion of results

The antenna array can be optimized from many points of view and for a different optima. In this thesis I have focused on characterization of an arbitrary dipole arrays with discrete impedance matrix, including mutual coupling between elements. This matrix description was extended to directivity and gain.

A simple one-term sinusoidal current distribution with central excitation of the dipoles was applied for increasing calculation speed and the infinite electric ground plane was modeled by the method of images. The results of the proposed method, which was implemented in MATLAB, were confirmed by examples and compared with good agreement with a full-wave simulator FEKO using the method of moments. The MATLAB code was extended with a more realistic King's three-term approximation of the current distribution on the dipoles.

The described theory can be used to solve complex and arbitrary oriented antenna arrays with different elements in the array. This method is also suitable for all problems, where one can prescribe analytically the current of an element. A four element Yagi-Uda antenna was optimized as an example for gain and low side lobes level in the main axis and to present the correctness of this method on elements with different length.

From the example with three dipoles above PEC ground we can see, that the antenna array is very sensitive to a current deviations when in resonance. It was shown, that the directivity maximization for a circular array with 5 elements can be achieved in all ϕ scanning angles.

By using the generalized concept of the directivity of an antenna array based on the self- and mutual radiation intensities, self- and mutual radiated powers and excitation currents of array elements, analytical expressions for the directivity of the out-of-phase excited arrays of two closely-spaced elementary dipoles and two isotropic radiators were derived. Further, the optimal excitations to maximize the directivity of the arrays for a given direction and spacing of their elements were also found analytically. It was shown, that the analytical expressions can be derived for the arrays consisting of more than two elements represented by the isotropic radiators since the necessary relations for the mutual intensities and powers were stated for an arbitrary spacing of the elements. However, the

expressions are expected to be extremely complicated, especially, due to the inverse of the matrix of the self- and mutual powers contained in the derivation.

By employing the PSO it could find the exact optimal spacing and height for each antenna element separately. But the maximized directivity with the optimized parameters was slightly higher than in array with constant spacing between elements.It was shown that for arrays above PEC ground, the optimal currents are purely real.

This methods contributed to design of 5G antenna array and synthesis of feeding coefficients.

6.2 Contributions of the thesis

The most important contributions of the thesis are listed below:

- Derivation of generalized impedance, directivity and radiation intensity for arbitrary oriented array elements with sinus and with a more realistic King's three-term approximation of the current distribution on the dipoles.
- Modal decomposition in antenna arrays with use of so called discrete modes applied to different optima.
- Super directivity arrays with elementary dipoles and isotropic radiators backed by PEC ground.
- Antenna array optimization based on required radiation pattern.
- Implementing the developed method into MATLAB and connecting with CST software to synthesize radiation pattern, beamforming.
- PSO optimization of linear arrays with different number of elements.
- Design and manufacturing of a 5G array and synthesis of feeding coefficients.

6.3 Future suggestions

The introduction of 5G networks is approaching rapidly. The developing of synthesis for antenna arrays is essential. Beamforming is indispensable to achieve strict parameters of these networks. Nowadays the beamforming is done by changing the phase of the signal based on simple, but old theory. When designing the antenna arrays, engineers now must design this array and with use of some software they can calculate phases on each segment of antenna. But no possibility to prescribe the required radiation pattern and synthesize feeding coefficients, amplitude and phase. Including this theory into some commercial software should be done to help with antenna array design. Extension of the input geometry could be done with elements, where the current is analytically known. Also using the antenna array as a passive elements could bring some interesting results and will be easy to manufacture.

In this work, the proposed method for arbitrary oriented array elements was mainly applied on a periodical and linear arrays. Some smart optimization should be implemented to find optimal space distribution of array elements.

The RoF is promising technology to help with fast spreading of 5G networks. Low loss and low price of the optical cables are nowadays redeemed with the high price of optical to radio converters. This converters should be included directly into PCB of the antenna.

Bibliography

[1] L. Jelinek and M. Capek, "Optimal currents on arbitrarily shaped surfaces", 2016, eprint arXiv:1602.05520.

[2] M. Capek, P. Hazdra, M. Masek, and V. Losenicky, "Analytical representation of characteristic mode decomposition", *IEEE Transactions on Antennas and Propagation*, vol. 65, no. 2, pp. 713–720, 2017, ISSN: 0018-926X. DOI: 10.1109/TAP.2016.2632725.

[3] G. A. E. Vandenbosch, "Reactive energies, impedance, and Q factor of radiating structures", *IEEE Trans. Antennas Propag.*, vol. 58, no. 4, pp. 1112–1127, 2010. DOI: 10.1109/TAP.2010.2041166.

[4] K. Schab, L. Jelinek, M. Capek, C. Ehrenborg, D. Tayli, G. A. E. Vandenbosch, and M. Gustafsson, "Energy stored by radiating systems", *IEEE Access*, vol. 6, pp. 10 553–10 568, 2018, ISSN: 2169-3536. DOI: 10.1109/ACCESS.2018.2807922.

[5] J. G. Andrews, S. Buzzi, W. Choi, S. V. Hanly, A. Lozano, A. C. K. Soong, and J. C. Zhang, "What will 5g be?", *IEEE Journal on Selected Areas in Communications*, vol. 32, no. 6, pp. 1065–1082, 2014, ISSN: 0733-8716. DOI: 10.1109/JSAC.2014.2328098.

[6] S. Kanchi, S. Sandilya, D. Bhosale, A. Pitkar, and M. Gondhalekar, "Overview of lte-a technology", in *2013 IEEE Global High Tech Congress on Electronics*, 2013, pp. 195–200. DOI: 10.1109/GHTCE.2013.6767272.

[7] A. Gupta and R. K. Jha, "A survey of 5g network: Architecture and emerging technologies", *IEEE Access*, vol. 3, pp. 1206–1232, 2015, ISSN: 2169-3536. DOI: 10.1109/ACCESS.2015.2461602.

[8] T. Asai, "5g radio access network and its requirements on mobile optical network", in *2015 International Conference on Optical Network Design and Modeling (ONDM)*, 2015, pp. 7–11. DOI: 10.1109/ONDM.2015.7127265.

[9] H. Al-Raweshidy and S. Komaki, *Radio Over Fiber Technologies for Mobile Communications Networks*, ser. Artech House universal personal communications series. Artech House, 2002, ISBN: 9781580531481. [Online]. Available: https://books.google.cz/books?id=2qO9cKo-w8kC.

[10] A. F. Peterson, S. L. Ray, and R. Mittra, *Computational Methods for Electromagnetics*. Wiley – IEEE Press, 1998.

[11] W. Chew, *Fast and efficient algorithms in computational electromagnetics*. Boston: Artech House, 2001, ISBN: 1-58053-152-0.

[12] (2016). FEKO, Altair, [Online]. Available: www.feko.info.

[13] (2017). User manual for HFSS, Ansoft corporation, Pittsburg, USA.

[14] CST Computer Simulation Technology. (2014). CST MWS, [Online]. Available: http://www.cst.com/.

[15] A. O. Boryssenko and D. H. Schaubert, "Physical aspects of mutual coupling in finite broadband tapered slot (vivaldi) arrays", in *2005 5th International Conference on Antenna Theory and Techniques*, tom, 2005, pp. 74–79. DOI: 10.1109/ICATT.2005.1496887.

[16] B. Munk, R. Taylor, T. Durharn, W. Croswell, B. Pigon, R. Boozer, S. Brown, M. Jones, J. Pryor, S. Ortiz, J. Rawnick, K. Krebs, M. Vanstrum, G. Gothard, and D. Wiebelt, "A low-profile broadband phased array antenna", in *IEEE Antennas and Propagation Society International Symposium. Digest. Held in conjunction with: USNC/CNC/URSI North American Radio Sci. Meeting (Cat. No.03CH37450)*, vol. 2, 2003, 448–451 vol.2. DOI: 10.1109/APS.2003.1219272.

[17] R. Garbacz, "Modal expansions for resonance scattering phenomena", *Proc. IEEE*, vol. 53, no. 8, pp. 856–864, 1965, ISSN: 0018-9219. DOI: 10.1109/PROC.1965.4064.

[18] J. Allen, "Gain and impedance variation in scanned dipole arrays", *IRE Transactions on Antennas and Propagation*, vol. 10, no. 5, pp. 566–572, 1962, ISSN: 0096-1973. DOI: 10.1109/TAP.1962.1137903.

[19] W. L. Stutzman, *Antenna Theory and Design, 3rd Edition*. Wiley, 2012.

[20] S. J. Orfanidis. (). Electromagnetic waves & antennas, [Online]. Available: www.ece.rutgers.edu/~orfanidi/ewa.

[21] S. P. Skobelev, *Phased Array Antennas with Optimized Element Patterns (Artech House Antennas and Propagation Library)*. Artech House Publishers, 2011.

[22] "Ieee standard for definitions of terms for antennas", *IEEE Std 145-2013 (Revision of IEEE Std 145-1993)*, pp. 1–50, 2014. DOI: 10.1109/IEEESTD.2014.6758443.

[23] B. A. Munk, *Finite Antenna Arrays and FSS (Wiley - IEEE)*. Wiley-IEEE Press, 2008.

[24] R. C. Hansen, "Comments on "the active element pattern"", *IEEE Transactions on Antennas and Propagation*, vol. 43, no. 6, pp. 634–, 1995, ISSN: 0018-926X. DOI: 10.1109/8.387184.

[25] K.-C. Lee and T.-H. Chu, "A circuit model for mutual coupling analysis of a finite antenna array", *IEEE Transactions on Electromagnetic Compatibility*, vol. 38, no. 3, pp. 483–489, 1996, ISSN: 0018-9375. DOI: 10.1109/15.536079.

[26] R. J. Garbacz, "A generalized expansion for radiated and scattered fields", PhD thesis, Department of Electrical Engineering, Ohio State University, 1968.

[27] R. F. Harrington and J. R. Mautz, "Theory of characteristic modes for conducting bodies", *IEEE Trans. Antennas Propag.*, vol. 19, no. 5, pp. 622–628, 1971. DOI: 10.1109/TAP.1971.1139999.

[28] ——, "Computation of characteristic modes for conducting bodies", *IEEE Trans. Antennas Propag.*, vol. 19, no. 5, pp. 629–639, 1971. DOI: 10.1109/TAP.1971.1139990.

[29] J. B. J. Fourier, "Mémoire sur la théorie analytique de la chaleur", in *Oeuvres de Fourier: Publiées par les soins de Gaston Darboux*, J. G. Darboux, Ed., ser. Cambridge Library Collection - Mathematics. Cambridge University Press, 2013, vol. 2, 145–182. DOI: 10.1017/CBO9781139568159.007.

[30] G. W. Hanson and A. B. Yakovlev, *Operator Theory for Electromagnetics: An Introduction*. Springer, 2001, ISBN: 0387952780.

[31] R. F. Harrington and J. R. Mautz, "Control of radar scattering by reactive loading", *IEEE Trans. Antennas Propag.*, vol. 20, no. 4, pp. 446–454, 1972. DOI: 10.1109/TAP.1972.1140234.

[32] K. P. Murray and B. A. Austin, "Synthesis of vehicular antenna nvis radiation patterns using the method of characteristic modes", *IEE Proceedings - Microwaves, Antennas and Propagation*, vol. 141, no. 3, pp. 151–154, 1994, ISSN: 1350-2417. DOI: 10.1049/ip-map:19941030.

[33] B. A. Austin and K. P. Murray, "The application of characteristic-mode techniques to vehicle-mounted nvis antennas", *IEEE Antennas Propag. Mag.*, vol. 40, pp. 7–21, 1998. DOI: 10.1109/74.667319.

[34] R. Harrington and J. Mautz, "Modal analysis of loaded n-port scatterers", in *1972 Antennas and Propagation Society International Symposium*, vol. 10, 1972, pp. 267–267. DOI: 10.1109/APS.1972.1146982.

[35] R. F. Harrington and J. R. Mautz, "Pattern synthesis for loaded N-port scatterers", *IEEE Trans. Antennas Propag.*, vol. 22, no. 2, pp. 184–190, 1974. DOI: 10.1109/TAP.1974.1140785.

[36] R. Harrington, "Reactively controlled directive arrays", *IEEE Transactions on Antennas and Propagation*, vol. 26, no. 3, pp. 390–395, 1978, ISSN: 0018-926X. DOI: 10.1109/TAP.1978.1141852.

[37] D. Liu, R. J. Garbacz, and D. M. Pozar, "Antenna synthesis and optimization using generalized characteristic modes", *IEEE Trans. Antennas Propag.*, vol. 38, no. 6, pp. 862–868, 1990. DOI: 10.1109/8.55583.

[38] J. Wang, C. Choi, and R. Moore, "Precision experimental characterization of the scattering and radiation properties of antennas", *IEEE Transactions on Antennas and Propagation*, vol. 30, no. 1, pp. 108–112, 1982, ISSN: 0018-926X. DOI: 10.1109/TAP.1982.1142745.

[39] S. Uda and Y. Mushiake, *Yagi-Uda Antenna*. Research Institute of Electrical Communication, Tohoku University, 1954. [Online]. Available: https://books.google.cz/books?id=kygIAQAAIAAJ.

[40] D. G. Reid, "The gain of an idealized yagi array", *Electrical Engineers - Part IIIA: Radiolocation, Journal of the Institution of*, vol. 93, no. 3, pp. 564–566, 1946. DOI: 10.1049/ji-3a-1.1946.0144.

[41] D. K. Cheng, "Gain optimization for yagi-uda arrays", *IEEE Antennas and Propagation Magazine*, vol. 33, no. 3, pp. 42–46, 1991, ISSN: 1045-9243. DOI: 10.1109/74.88220.

[42] E. A. Jones and W. T. Joines, "Design of yagi-uda antennas using genetic algorithms", *IEEE Transactions on Antennas and Propagation*, vol. 45, no. 9, pp. 1386–1392, 1997, ISSN: 0018-926X. DOI: 10.1109/8.623128.

[43] J. Y. Li, "Optimizing design of antenna using differential evolution", in *2007 Asia-Pacific Microwave Conference*, 2007, pp. 1–4. DOI: 10.1109/APMC.2007.4554614.

[44] W. W. Hansen and J. R. Woodyard, "A new principle in directional antenna design", *Proceedings of the Institute of Radio Engineers*, vol. 26, no. 3, pp. 333–345, 1938. DOI: 10.1109/JRPROC.1938.228128.

[45] A. Bloch, R. Medhurst, and S. Pool, "A new approach to the design of superdirective aerial arrays", *Proc. IEE*, vol. 100, 303–314, 1953.

[46] A. I. Uzkov, "An approach to the problem of optimum directive antennae design", *Comptes Rendus (Doklady) de l'Academie des Sciences de l'URSS*, vol. 53, no. 1, pp. 35–38, 1946.

[47] A. D. Yaghjian, T. H. O'Donnell, E. E. Altshuler, and S. R. Best, "Electrically small supergain end-fire arrays", *Radio Science*, vol. 43, no. 3, pp. 1–13, 2008, ISSN: 1944-799X. DOI: 10.1029/2007RS003747.

[48] A. Haskou, A. Sharaiha, and S. Collardey, "Design of small parasitic loaded superdirective end-fire antenna arrays", *IEEE Transactions on Antennas and Propagation*, vol. 63, no. 12, pp. 5456–5464, 2015, ISSN: 0018-926X. DOI: 10.1109/TAP.2015.2496112.

[49] E. E. Altshuler, T. H. O'Donnell, A. D. Yaghjian, and S. R. Best, "A monopole superdirective array", *IEEE Trans. Antennas Propag.*, vol. 53, no. 8, pp. 2653–2661, 2005. DOI: 10.1109/TAP.2005.851810.

[50] A. Noguchi and H. Arai, "3-element super-directive endfire array with decoupling network", in *2014 International Symposium on Antennas and Propagation Conference Proceedings*, Kaohsiung, Taiwan, 2014, pp. 455–456. DOI: 10.1109/ISANP.2014.7026723.

[51] S. R. Best, E. E. Altshuler, A. D. Yaghjian, J. M. McGinthy, and T. H. O'Donnell, "An impedance-matched 2-element superdirective array", *IEEE Antennas and Wireless Propagation Letters*, vol. 7, pp. 302–305, 2008, ISSN: 1536-1225. DOI: 10.1109/LAWP.2008.921372.

[52] A. Clemente, M. Pigeon, L. Rudant, and C. Delaveaud, "Design of a super directive four-element compact antenna array using spherical wave expansion", *IEEE Transactions on Antennas and Propagation*, vol. 63, no. 11, pp. 4715–4722, 2015, ISSN: 0018-926X. DOI: 10.1109/TAP.2015.2475617.

[53] J. D. Kraus, *Antennas*. McGraw-Hill, 1988.

[54] M. Gustafsson, M. Cismasu, and B. L. G. Jonsson, "Physical bounds and optimal currents on antennas", *IEEE Trans. Antennas Propag.*, vol. 60, no. 6, pp. 2672–2681, 2012. DOI: 10.1109/TAP.2012.2194658.

[55] T. S. Angell, A. Kirsch, and R. E. Kleinman, "Antenna control and optimization", *Proceedings of the IEEE*, vol. 79, no. 10, pp. 1559–1568, 1991, ISSN: 0018-9219. DOI: 10.1109/5.104230.

[56] M. Gustafsson, "Antenna current optimization and optimal design", in *2016 International Symposium on Antennas and Propagation (ISAP)*, 2016, pp. 132–133.

[57] D. Margetis, G. Fikioris, J. M. Myers, and T. T. Wu, "Highly directive current distributions: General theory", *Phys. Rev. E*, vol. 58, p. 2531, 1998.

[58] M. Uzsoky and L. Solymár, "Theory of super-directive linear arrays", *Acta Physica Academiae Scientiarum Hungaricae*, vol. 6, no. 2, pp. 185–205, 1956. DOI: 10.1007/BF03157322.

[59] D. K. Cheng, "Optimization techniques for antenna arrays", *Proceedings of the IEEE*, vol. 59, no. 12, pp. 1664–1674, 1971, ISSN: 0018-9219. DOI: 10.1109/PROC.1971.8523.

[60] Y. T. Lo, S. W. Lee, and Q. H. Lee, "Optimization of directivity and signal-to-noise ratio of an arbitrary antenna array", *Proceedings of the IEEE*, vol. 54, no. 8, pp. 1033–1045, 1966, ISSN: 0018-9219. DOI: 10.1109/PROC.1966.4988.

[61] O. Einarsson, "Optimization of planar arrays", *IEEE Transactions on Antennas and Propagation*, vol. 27, no. 1, pp. 86–92, 1979, ISSN: 0018-926X. DOI: 10.1109/TAP.1979.1142036.

[62] R. F. Harrington, *Field Computation by Moment Methods*. Wiley – IEEE Press, 1993.

[63] E. Shamonina and L. Solymar, "Maximum directivity of arbitrary dipole arrays", *IET Microw. Antenna P.*, vol. 9, 101–107, 2015.

[64] D. K. Cheng and C. A. Chen, "Directivity optimization for large circular arrays with many parallel dipoles", *Radio Science*, vol. 16, no. 6, pp. 1071–1075, 1981. DOI: 10.1029/RS016i006p01071. eprint: https://agupubs.onlinelibrary.wiley.com/doi/pdf/10.1029/RS016i006p01071. [Online]. Available: https://agupubs.onlinelibrary.wiley.com/doi/abs/10.1029/RS016i006p01071.

[65] T. Lonsky, P. Hazdra, and J. Kracek, "Characteristic modes of dipole arrays", *IEEE Antennas and Wireless Propagation Letters*, vol. 17, no. 6, pp. 998–1001, 2018, ISSN: 1536-1225. DOI: 10.1109/LAWP.2018.2828986.

[66] (2016). The Matlab, The MathWorks, [Online]. Available: www.mathworks.com.

[67] Y. Chen and C.-F. Wang, "Synthesis of reactively controlled antenna arrays using characteristic modes and de algorithm", *IEEE Antennas Wireless Propag. Lett.*, vol. 11, pp. 385–388, 2012. DOI: 10.1109/LAWP.2012.2191584.

[68] S. Sugiura and H. Iizuka, "Reactively steered ring antenna array for automotive application", *IEEE Transactions on Antennas and Propagation*, vol. 55, no. 7, pp. 1902–1908, 2007, ISSN: 0018-926X. DOI: 10.1109/TAP.2007.900251.

[69] R. F. Harrington, "Antenna excitation for maximum gain", *IEEE Trans. Antennas Propag.*, vol. 13, no. 6, pp. 896–903, 1965. DOI: 10.1109/TAP.1965.1138539.

[70] J. Mautz and R. Harrington, "Modal analysis of loaded n-port scatterers", *IEEE Transactions on Antennas and Propagation*, vol. 21, no. 2, pp. 188–199, 1973, ISSN: 0018-926X. DOI: 10.1109/TAP.1973.1140431.

[71] I. Tzanidis, K. Sertel, and J. L. Volakis, "Characteristic excitation taper for ultra-wideband tightly coupled antenna arrays", *IEEE Transactions on Antennas and Propagation*, vol. 60, no. 4, pp. 1777–1784, 2012, ISSN: 0018-926X.

[72] W. Wasylkiwskyj and W. K. Kahn, "Theory of mutual coupling among minimum-scattering antennas", *IEEE Transactions on Antennas and Propagation*, vol. 18, no. 2, pp. 204–216, 1970, ISSN: 0018-926X. DOI: 10.1109/TAP.1970.1139649.

[73] P. Rogers, "Application of the minimum scattering antenna theory to mismatched antennas", *IEEE Transactions on Antennas and Propagation*, vol. 34, no. 10, pp. 1223–1228, 1986, ISSN: 0018-926X. DOI: 10.1109/TAP.1986.1143747.

[74] C. A. Balanis, *Antenna Theory Analysis and Design*, 3rd ed. Wiley, 2005.

[75] J. D. Jackson, *Classical Electrodynamics*, 3rd ed. Wiley, 1998.

[76] R. E. Collin, *Field Theory of Guided Waves*. Wiley – IEEE Press, 1990.

[77] J. Qiao, X. S. Shen, J. W. Mark, Q. Shen, Y. He, and L. Lei, "Enabling device-to-device communications in millimeter-wave 5g cellular networks", *IEEE Communications Magazine*, vol. 53, no. 1, pp. 209–215, 2015, ISSN: 0163-6804. DOI: 10.1109/MCOM.2015.7010536.

[78] M. Matin, "Review on millimeter wave antennas- potential candidate for 5g enabled applications", *Advanced Electromagnetics*, vol. 5, p. 98, Dec. 2016. DOI: 10.7716/aem.v5i3.448.

[79] Y. Huo, X. Dong, and W. Xu, "5g cellular user equipment: From theory to practical hardware design", *IEEE Access*, vol. 5, pp. 13 992–14 010, 2017, ISSN: 2169-3536. DOI: 10.1109/ACCESS.2017.2727550.

[80] *Making 5g nr a reality*, 2016. [Online]. Available: https://www.qualcomm.com/documents/making-5g-nr-reality.

[81] P. T. Dat, A. Kanno, and T. Kawanishi, "Radio-on-radio-over-fiber: Efficient fronthauling for small cells and moving cells", *IEEE Wireless Communications*, vol. 22, no. 5, pp. 67–75, 2015, ISSN: 1536-1284. DOI: 10.1109/MWC.2015.7306539.

[82] M. Peng, Y. Li, Z. Zhao, and C. Wang, "System architecture and key technologies for 5g heterogeneous cloud radio access networks", *IEEE Network*, vol. 29, no. 2, pp. 6–14, 2015, ISSN: 0890-8044. DOI: 10.1109/MNET.2015.7064897.

[83] C. Tsai, H. Cho, T. K. Shih, J. Pan, and J. J.P. C. Rodrigues, "Metaheuristics for the deployment of 5g", *IEEE Wireless Communications*, vol. 22, no. 6, pp. 40–46, 2015, ISSN: 1536-1284. DOI: 10.1109/MWC.2015.7368823.

[84] N. Wang, E. Hossain, and V. K. Bhargava, "Backhauling 5g small cells: A radio resource management perspective", *IEEE Wireless Communications*, vol. 22, no. 5, pp. 41–49, 2015, ISSN: 1536-1284. DOI: 10.1109/MWC.2015.7306536.

[85] K. N.R.S. V. Prasad, E. Hossain, and V. K. Bhargava, "Energy efficiency in massive mimo-based 5g networks: Opportunities and challenges", *IEEE Wireless Communications*, vol. 24, no. 3, pp. 86–94, 2017, ISSN: 1536-1284. DOI: 10.1109/MWC.2016.1500374WC.

[86] I. A. Alimi, A. L. Teixeira, and P. P. Monteiro, "Toward an efficient c-ran optical fronthaul for the future networks: A tutorial on technologies, requirements, challenges, and solutions", *IEEE Communications Surveys Tutorials*, vol. 20, no. 1, pp. 708–769, 2018, ISSN: 1553-877X. DOI: 10.1109/COMST.2017.2773462.

[87] S. Park, C. Chae, and S. Bahk, "Large-scale antenna operation in heterogeneous cloud radio access networks: A partial centralization approach", *IEEE Wireless Communications*, vol. 22, no. 3, pp. 32–40, 2015, ISSN: 1536-1284. DOI: 10.1109/MWC.2015.7143324.

[88] K. Kibaroglu, M. Sayginer, and G. M. Rebeiz, "A low-cost scalable 32-element 28-ghz phased array transceiver for 5g communication links based on a 2x2 beamformer flip-chip unit cell", *IEEE Journal of Solid-State Circuits*, vol. 53, pp. 1260–1274, 2018.

[89] L. Aluigi, G. Orecchini, and L. Larcher, "A 28 ghz scalable beamforming system for 5g automotive connectivity: An integrated patch antenna and power amplifier solution", in *2018 IEEE MTT-S International Microwave Workshop Series on 5G Hardware and System Technologies (IMWS-5G)*, 2018, pp. 1–3. DOI: 10.1109/IMWS-5G.2018.8484325.

[90] T. Varum, A. Ramos, and J. N. Matos, "Planar microstrip series-fed array for 5g applications with beamforming capabilities", in *2018 IEEE MTT-S International Microwave Workshop Series on 5G Hardware and System Technologies (IMWS-5G)*, 2018, pp. 1–3. DOI: 10.1109/IMWS-5G.2018.8484697.

[91] M. Sun, Y. P. Zhang, K. M. Chua, L. L. Wai, D. Liu, and B. P. Gaucher, "Integration of yagi antenna in ltcc package for differential 60-ghz radio", *IEEE Transactions on Antennas and Propagation*, vol. 56, no. 8, pp. 2780–2783, 2008, ISSN: 0018-926X. DOI: 10.1109/TAP.2008.927577.

[92] H. Hsu and T. Huang, "A koch-shaped log-periodic dipole array (lpda) antenna for universal ultra-high-frequency (uhf) radio frequency identification (rfid) handheld reader", *IEEE Transactions on Antennas and Propagation*, vol. 61, no. 9, pp. 4852–4856, 2013, ISSN: 0018-926X. DOI: 10.1109/TAP.2013.2264451.

[93] W. Hong, K. Baek, Y. Lee, Y. Kim, and S. Ko, "Study and prototyping of practically large-scale mmwave antenna systems for 5g cellular devices", *IEEE Communications Magazine*, vol. 52, no. 9, pp. 63–69, 2014, ISSN: 0163-6804. DOI: 10.1109/MCOM.2014.6894454.

[94] Z. Ahmed, P. McEvoy, and M. J. Ammann, "Comparison of grid array and microstrip patch array antennas at 28 ghz", in *2018 IEEE MTT-S International Microwave Workshop Series on 5G Hardware and System Technologies (IMWS-5G)*, 2018, pp. 1–3. DOI: 10.1109/IMWS-5G.2018.8484539.

[95] J. Helander, K. Zhao, Z. Ying, and D. Sjöberg, "Performance analysis of millimeter-wave phased array antennas in cellular handsets", *IEEE Antennas and Wireless Propagation Letters*, vol. 15, pp. 504–507, 2016, ISSN: 1536-1225. DOI: 10.1109/LAWP.2015.2455040.

[96] H. Zhou, "Phased array for millimeter-wave mobile handset", in *2014 IEEE Antennas and Propagation Society International Symposium (APSURSI)*, 2014, pp. 933–934. DOI: 10.1109/APS.2014.6904795.

[97] D. Psychoudakis, Z. Wang, and F. Aryanfar, "Dipole array for mm-wave mobile applications", in *2013 IEEE Antennas and Propagation Society International Symposium (APSURSI)*, 2013, pp. 660–661. DOI: 10.1109/APS.2013.6710990.

[98] H. Zhou and F. Aryanfar, "Millimeter-wave open ended siw antenna with wide beam coverage", in *2013 IEEE Antennas and Propagation Society International Symposium (APSURSI)*, 2013, pp. 658–659. DOI: 10.1109/APS.2013.6710989.

[99] Y. Cheon and Y. Kim, "Millimeter-wave phased array antenna with wide beam coverage", in *2016 10th European Conference on Antennas and Propagation (EuCAP)*, 2016, pp. 1–3. DOI: 10.1109/EuCAP.2016.7481337.

[100] B. Yang, Z. Yu, Y. Dong, J. Zhou, and W. Hong, "Compact tapered slot antenna array for 5g millimeter-wave massive mimo systems", *IEEE Transactions on Antennas and Propagation*, vol. 65, no. 12, pp. 6721–6727, 2017, ISSN: 0018-926X. DOI: 10.1109/TAP.2017.2700891.

[101] N. Ojaroudiparchin, M. Shen, and G. F. Pedersen, "Multi-layer 5g mobile phone antenna for multi-user mimo communications", in *2015 23rd Telecommunications Forum Telfor (TELFOR)*, 2015, pp. 559–562. DOI: 10.1109/TELFOR.2015.7377529.

[102] J. Yao, "Microwave photonics", *Journal of Lightwave Technology*, vol. 27, no. 3, pp. 314–335, 2009, ISSN: 0733-8724. DOI: 10.1109/JLT.2008.2009551.

[103] J. Bohata, M. Komanec, J. Spacil, S. Zvanovec, Z. Ghassemlooy, and R. Slavik, "Hybrid rof-rofso system using directly modulated laser for 24-26 ghz 5g networks", Jul. 2018, pp. 1–5. DOI: 10.1109/CSNDSP.2018.8471867.

[104] D. Wake, A. Nkansah, N. J. Gomes, G. de Valicourt, R. Brenot, M. Violas, Z. Liu, F. Ferreira, and S. Pato, "A comparison of radio over fiber link types for the support of wideband radio channels", *Journal of Lightwave Technology*, vol. 28, no. 16, pp. 2416–2422, 2010, ISSN: 0733-8724. DOI: 10.1109/JLT.2010.2046136.

[105] X Zhang, R Zhu, D Shen, and T Liu, "Linearization technologies for broadband radio-over-fiber transmission systems", *Photon.*, vol. 14, pp. 455–472, Jan. 2014.

[106] J. Kreissl, V. Vercesi, U. Troppenz, T. Gaertner, W. Wenisch, and M. Schell, "Up to 40 gb/s directly modulated laser operating at low driving current: Buried-heterostructure passive feedback laser (bh-pfl)", *IEEE Photonics Technology Letters*, vol. 24, no. 5, pp. 362–364, 2012, ISSN: 1041-1135. DOI: 10.1109/LPT.2011.2179530.

[107] J. Bohata, M. Komanec, J. Spacil, Z. Ghassemlooy, S. Zvanovec, and R. Slavik, "24–26 ghz radio-over-fiber and free-space optics for fifth-generation systems", *Optics Letters*, vol. 43, Feb. 2018.

[108] Y. Lo and S. Lee, *Antenna Handbook: Antenna theory*. Springer, 1993, ISBN: 0442015933.

[109] R. F. Harrington, *Time-Harmonic Electromagnetic Fields*, 2nd ed. Wiley – IEEE Press, 2001.

[110] E. C. Jordan and K. G. Balmain, *Electromagnetic Waves and Radiating Systems*. Pearson Education, 2nd ed., 2015.

[111] A. W. Rudge, *The Handbook of Antenna Design, Vol. 2*. Institution of Engineering and Technology, 1983.

[112] Z. Miers, H. Li, and B. K. Lau, "Design of bandwidth-enhanced and multiband mimo antennas using characteristic modes", *IEEE Antennas Wireless Propag. Lett.*, vol. 12, pp. 1696–1699, 2013, ISSN: 1536-1225. DOI: 10.1109/LAWP.2013.2292562.

[113] E. Newman, "Small antenna location synthesis using characteristic modes", *IEEE Trans. Antennas Propag.*, vol. 27, no. 4, pp. 530–531, 1979. DOI: 10.1109/TAP.1979.1142116.

[114] R. J. Garbacz and R. H. Turpin, "A generalized expansion for radiated and scattered fields", *IEEE Trans. Antennas Propag.*, vol. 19, no. 3, pp. 348–358, 1971. DOI: 10.1109/TAP.1971.1139935.

[115] M. Cabedo-Fabres, "Systematic design of antennas using the theory of characteristic modes", PhD thesis, UPV, 2007.

[116] A. D. Yaghjian and S. R. Best, "Impedance, bandwidth and Q of antennas", *IEEE Trans. Antennas Propag.*, vol. 53, no. 4, pp. 1298–1324, 2005. DOI: 10.1109/TAP.2005.844443.

[117] A. J. King, "Characteristic mode theory for closely spaced dipole arrays", PhD thesis, University of Illinois, 2015.

[118] R. Elliot, *Antenna Theory and Design*. IEEE Press, 2003.

[119] M. Capek, L. Jelinek, and P. Hazdra, "On the functional relation between quality factor and fractional bandwidth", *IEEE Trans. Antennas Propag.*, vol. 63, no. 6, pp. 2787–2790, 2015. DOI: 10.1109/TAP.2015.2414472.

[120] K. R. Schab and J. T. Bernhard, "Radiation and energy storage current modes on conducting structures", *IEEE Trans. Antennas Propag.*, vol. 63, no. 12, pp. 5601–5611, 2015. DOI: 10.1109/TAP.2015.2490664.

[121] A. Kedar and L. P. Ligthart, "Wide scanning characteristics of sparse phased array antennas using an analytical expression for directivity", *IEEE Transactions on Antennas and Propagation*, vol. 67, no. 2, pp. 905–914, 2019, ISSN: 0018-926X. DOI: 10.1109/TAP.2018.2880006.

[122] A. Safaai-Jazi, "Directivity of Chebyshev arrays with arbitrary element spacing", *Electronics Letters*, vol. 31, no. 10, pp. 772–774, 1995, ISSN: 0013-5194. DOI: 10.1049/el:19950538.

[123] B. F. Costa and T. Abrao, "Closed-form directivity expression for arbitrary volumetric antenna arrays", *IEEE Transactions on Antennas and Propagation*, vol. 66, no. 12, pp. 7443–7448, 2018, ISSN: 0018-926X. DOI: 10.1109/TAP.2018.2869243.

[124] M. Capek, L. Jelinek, P. Hazdra, and J. Eichler, "The measurable Q factor and observable energies of radiating structures", *IEEE Trans. Antennas Propag.*, vol. 62, no. 1, pp. 311–318, 2014. DOI: 10.1109/TAP.2013.2287519.

[125] P. Hazdra, M. Capek, J. Eichler, and M. Mazanek, "The radiation Q-factor of a horizontal $\lambda/2$ dipole above ground plane", *IEEE Antennas Wireless Propag. Lett.*, vol. 13, pp. 1073–1075, 2014. DOI: 10.1109/LAWP.2014.2329421.

[126] M. Capek, P. Hazdra, M. Mazanek, Z. Raida, and J. Rymus, "The antenna toolbox for matlab (atom)", in *Proceedings of the 9th European Conference on Antennas and Propagation (EUCAP)*, Lisbon, Portugal, 2015.

[127] P. Hazdra, T. Lonsky, and M. Capek, "Bandwidth optimization of linear arrays above ground", in *2016 10th European Conference on Antennas and Propagation (EuCAP)*, 2016, pp. 1–2. DOI: 10.1109/EuCAP.2016.7481267.

[128] P. Hazdra, M. Capek, and J. Eichler, "Comments to 'Reactive Energies, Impedance, and Q Factor of Radiating Structures' by G. Vandenbosch", *IEEE Trans. Antennas Propag.*, vol. 61, no. 12, pp. 6266–6267, 2013. DOI: 10.1109/TAP.2013.2281566.

[129] P. Hazdra, T. Lonsky, and J. Kracek, "On the end-fire super directivity of arrays of two elementary dipoles and isotropic radiators", *IET Microwaves Antennas & Propagation*, 2019. DOI: 10.1049/iet-map.2018.6013.

[130] M. Polivka and D. Vrba, "Input resistance of electrically short not-too-closely spaced multielement monopoles with uniform current distribution", *IEEE Antennas and Wireless Propagation Letters*, vol. 11, pp. 1576–1579, 2012, ISSN: 1536-1225. DOI: 10.1109/LAWP.2012.2235058.

[131] E. Shamonina, V. A. Kalinin, K. H. Ringhofer, and L. Solymar, "Short dipole as a receiver: Effective aperture shapes and streamlines of the poynting vector", *IEE Proceedings - Microwaves, Antennas and Propagation*, vol. 149, no. 3, pp. 153–159, 2002, ISSN: 1350-2417. DOI: 10.1049/ip-map:20020388.

[132] J. Diao and K. F. Warnick, "Poynting streamlines, effective area shape, and the design of superdirective antennas", *IEEE Transactions on Antennas and Propagation*, vol. 65, no. 2, pp. 861–866, 2017, ISSN: 0018-926X. DOI: 10.1109/TAP.2016.2632618.

[133] J. Robinson and Y. Rahmat-Samii, "Particle swarm optimization in electromagnetics", *IEEE Trans. Antennas Propag.*, vol. 52, no. 2, pp. 397–407, 2004. DOI: 10.1109/TAP.2004.823969.

[134] B. Steinberg, *Principles of Aperture and Array System Design: Including Random and Adaptive Arrays*. Wiley, 1978. [Online]. Available: https://books.google.cz/books?id=NArVoAEACAAJ.

[135] J. Mandeep, *Design an x-band vivaldi antenna*, 2016. [Online]. Available: https://www.mwrf.com/markets/design-x-band-vivaldi-antenna.

[136] J. K. Kayani, "Design and testing of vivaldi antenna for uwb application", 2005.

[137] V. Rabinovich and N. Alexandrov, *Antenna Arrays and Automotive Applications*. Springer New York, 2013.

[138] G. Rainer, *Adaptive resource allocation schemes in MIMO-OFDM based cellular communication systems*. Cuvillier, 2007, pp. 43–47.

[139] Fairview Microwave. (2019). Smp male limited detent connector stub terminal solder attachment thread-in, [Online]. Available: http://www.fairviewmicrowave.com/smp-male-standard-limited-detent-stub-terminal-connector-sc5510-p.aspx.

[140] X. Dai, "An integrated millimeter-wave broadband microstrip-to-waveguide vertical transition suitable for multilayer planar circuits", *IEEE Microwave and Wireless Components Letters*, vol. 26, no. 11, pp. 897–899, 2016, ISSN: 1531-1309. DOI: 10.1109/LMWC.2016.2614973.

[141] U. Jankovic and D. Budimir, "Stepped bend substrate integrated waveguide to rectangular waveguide transitions", in *2016 IEEE International Symposium on Antennas and Propagation (APSURSI)*, 2016, pp. 1231–1232. DOI: 10.1109/APS.2016.7696323.

[142] C. Rave and A. F. Jacob, "A design approach for tapered waveguide to substrate-integrated waveguide transitions", *IEEE Transactions on Microwave Theory and Techniques*, vol. 64, no. 8, pp. 2502–2510, 2016, ISSN: 0018-9480. DOI: 10.1109/TMTT.2016.2584605.

[143] H. Iizuka, T. Watanabe, and K. Nishikawa, "Millimeter-wave microstrip line to waveguide transition fabricated on a single layer dielectric substrate", *IEICE Transactions on Communications*, vol. vol.85, pp. 1169–1177, 2002.

[144] K. Seo, "Planar microstrip-to-waveguide transition in millimeter-wave band", in. Mar. 2013, pp. 249–277, ISBN: 978-953-51-1019-4. DOI: 10.5772/54662.

[145] N. T.K.N.H. T. Sakakibara K., "Bandwidth comparison of topside waveguide-to microstrip transitions with back-short waveguide and with double-layer substrate in millimeter-wave band", in *Proceedings of the 13th European Conference on Antennas and Propagation (EUCAP)*, 2019.

[146] S. X. Ta, H. Choo, and I. Park, "Broadband printed-dipole antenna and its arrays for 5g applications", *IEEE Antennas and Wireless Propagation Letters*, vol. 16, pp. 2183–2186, 2017, ISSN: 1536-1225. DOI: 10.1109/LAWP.2017.2703850.

[147] Rosenberger. (2019). Rosenberger right angle 50ohm pcb mount smp connector plug, solder termination gold full detent, [Online]. Available: https://catalog.rosenberger.com/u/detail?itemID=451.

[148] S. Lim, C. woo cheol, and Y. Yoon, "Miniaturized radio frequency choke using modified stubs for high isolation in mimo systems", *Journal of electromagnetic engineering and science*, vol. 15, pp. 219–223, Oct. 2015. DOI: 10.5515/JKIEES.2015.15.4.219.

[149] Ash. (2019). Ash omni - digital microscope and measurement system, [Online]. Available: `https://ash-vision.com/products/digital-microscopes/omni/omni-core/`.

Appendix A

5G dipole antenna aray with 4 elements drawing

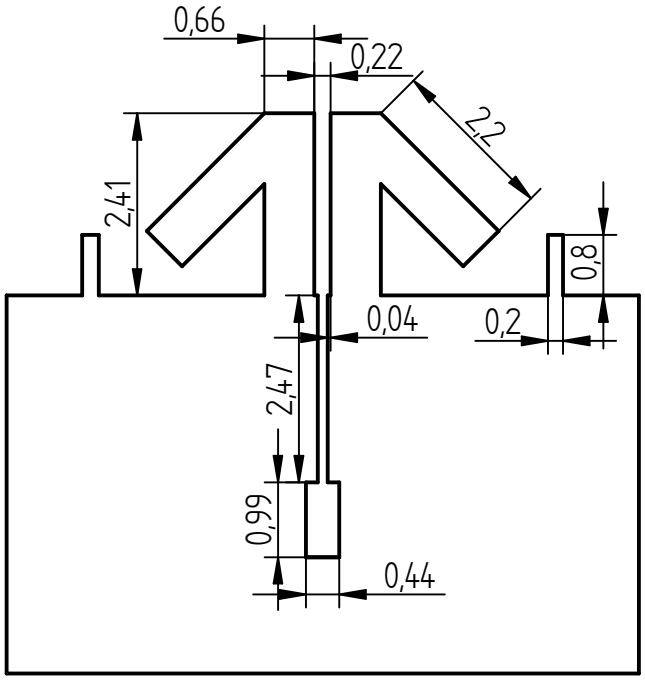

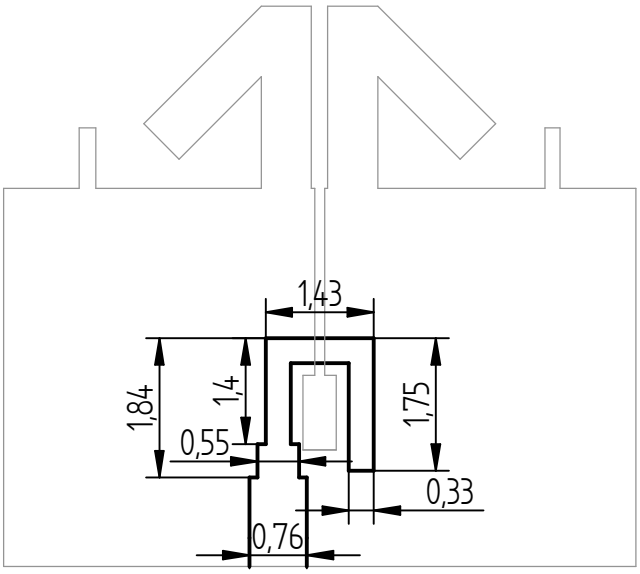

	NAME	DATE
DRAWN	Lonsky	01/12/18

MATERIAL: ROGERS RT 5880
thickness: 0.254 mm

TITLE: 5G dipole antenna

SIZE	DWG NO	REV
A4	1-1.12.18	

FILE NAME: 5g_dipole_antenna.dft

SCALE:10:1	WEIGHT:	SHEET 1 OF 2

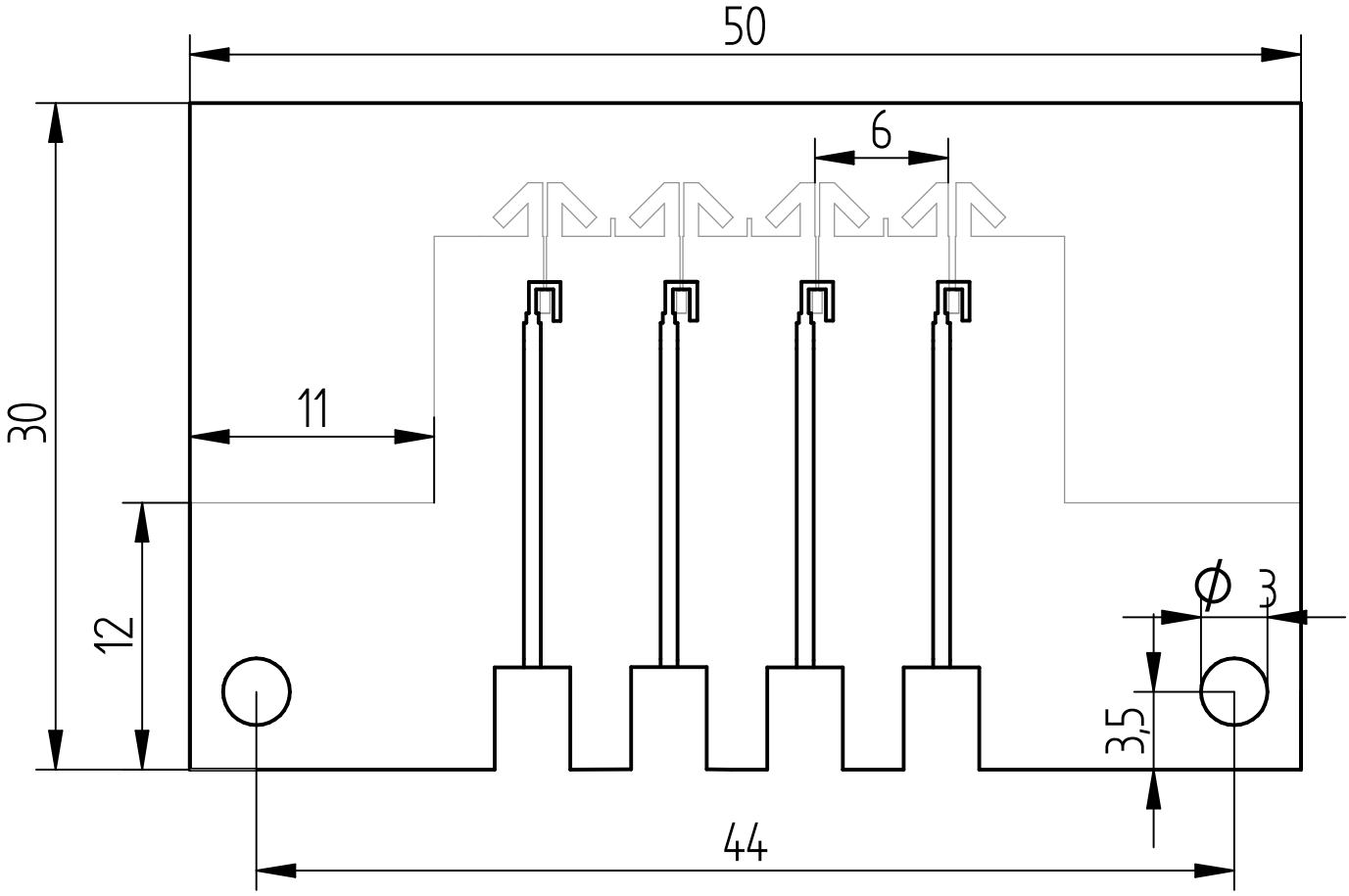

	NAME	DATE
DRAWN	Lonsky	01/12/18

MATERIAL: ROGERS RT 5880
thickness: 0.254 mm

TITLE: 5G dipole antenna

SIZE	DWG NO	REV
A4	1-1.12.18	

FILE NAME: 5g_dipole_antenna.dft

SCALE:10:1	WEIGHT:	SHEET 2 OF 2

Appendix B

Picture of manufactured antenna arrays

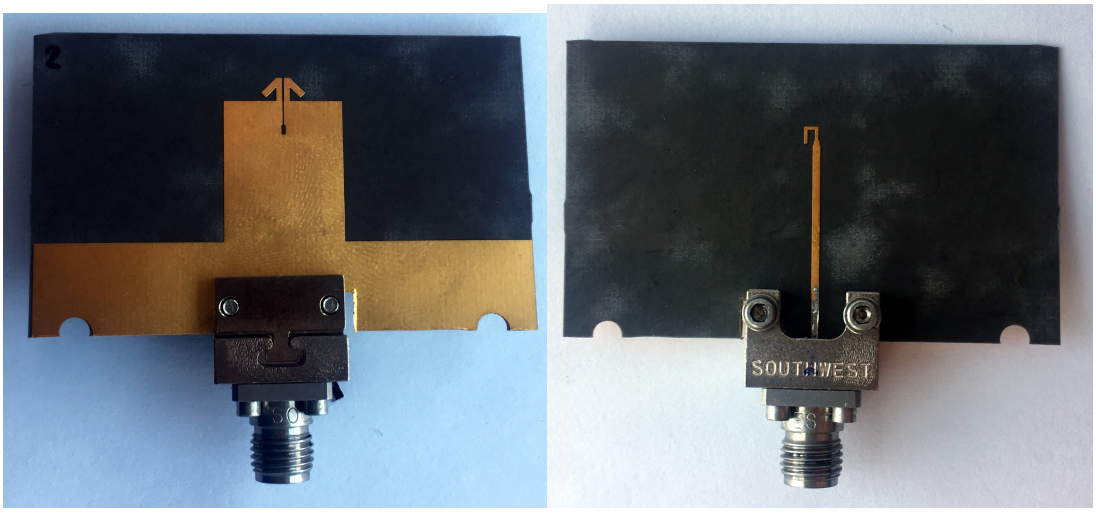

(a) front (b) back

Figure B.1: Photo of the manufactured dipole antenna

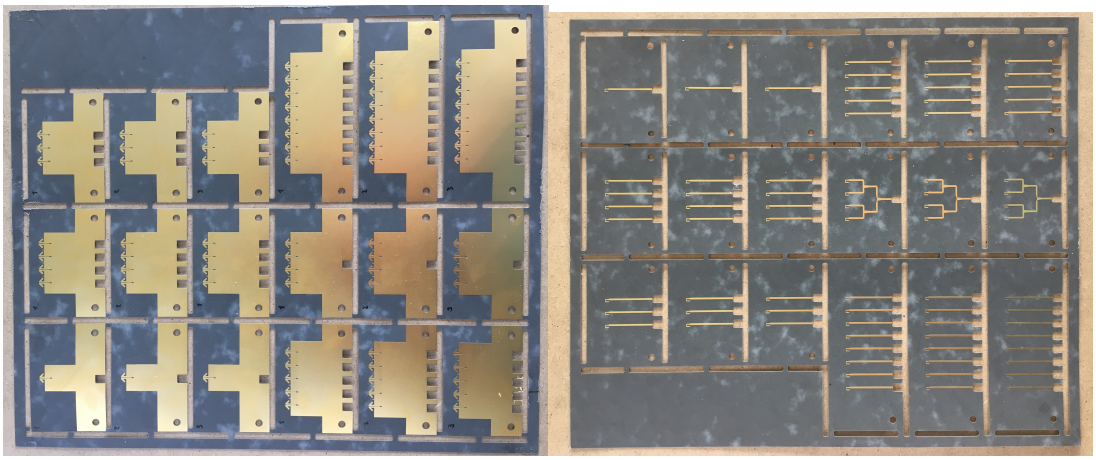

(a) front (b) back

Figure B.2: Photo of the manufactured dipole arrays

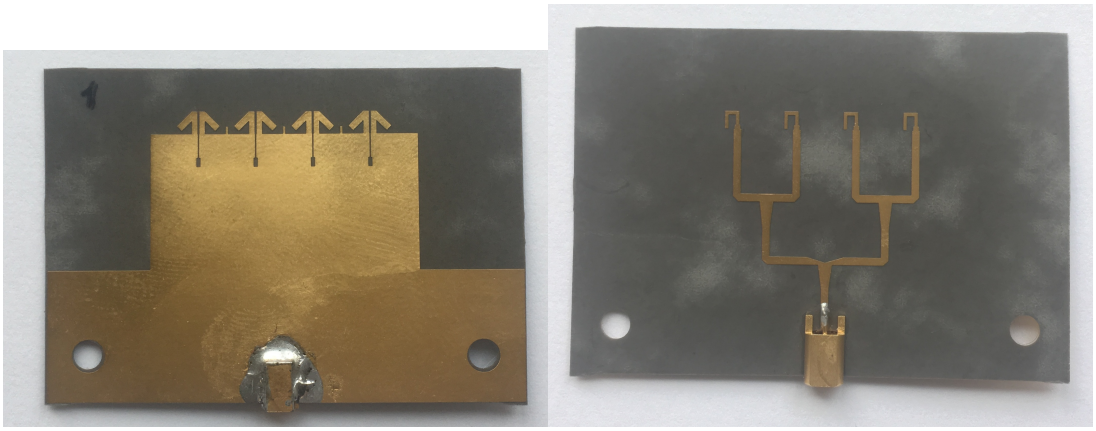

(a) front (b) back

Figure B.3: Photo of the manufactured dipole array with four elements and a feeding network

Appendix C

Description of the developed MATLAB code

The input geometry for the calculation can be directly coded in MATLAB, for simple dipole geometry, or modeled in CST microwave studio for any other antenna type. This means that the first level of calculation, impedance matrix and a radiation intensity vector, is done in MATLAB for dipole array. This level, the impedance matrix and the radiation patterns of elements, can be solely evaluated in CST and imported into MATLAB. Based on the feeding port in CST, there is a need to convert radiation patterns of elements to a modal patterns. The advantage of the calculation of array in MATLAB is that the radiation intensity vector is calculated and one can calculate the total radiation pattern including requested feeding (amplitude and phase).

The native theory of modal decomposition routine needs as an input only impedance matrix for characteristic mode decomposition, radiation intensity vector for directivity decomposition and optional vectors of loading impedance and output impedance for loss calculation. As an additional input, impedance matrix of loads $\mathbf{Z}_{load}$ and sources $\mathbf{Z}_{output}$ can be inserted into the computing routine. Beyond classical characteristic modes, the output from the modal decomposition is maximum achievable directivity D_{modal}, minimum observable quality factor Q_{modal} or efficiency of the modes. Also appropriate current distribution of an array for observing these values.

The term modal normalized pattern of the array refers to the state when the elements of the array are excited by the currents $\mathbf{I}_p = [I_{1p}, \cdots, I_{np}, \cdots, I_{Np}]^{\mathrm{T}}$ where I_{np} is an excitation current of n-th element corresponding to p-th mode. Various types of the modes of the array can be considered. The routine "conversion to modal pattern" transforms the loaded (or also so-called embedded) normalized far-fields to modal normalized far-fields. With these results and prescribed required far-field from user, the code will calculate the weights of the modes to obtain the proper radiation pattern. A simple schematic diagram of the antenna array program is depicted in Figure C.1 with simplified MATLAB code for three element dipole array far-field calculation in Figure C.2.

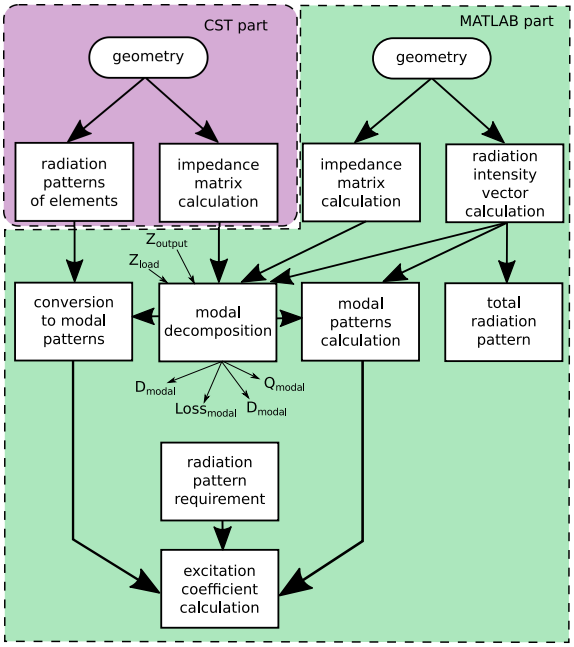

Figure C.1: A schematic diagram of the antenna array application

```
f            = 1e9;       % frequency [Hz]
lam          = 3e8/f;     % wavelength [m]
N            = 3;         % number of dipoles
L            = 0.5*lam;   % dipole length [-]
a            = 0.001*lam; % dipole radius [-]
or           = [0 1 0];   % dipole orientation
dx           = linspace(0.1*lam,1*lam,10);
                % mutual spacing between dipoles
h            = 0.2*lam;   % height of dipole
shape        = 'matrix';  % shape of the array
calcAlg      = 'mode';    % calculation mode
%--------------------------
array        = GetPosition(N,L,a,or,dx,h,shape);
          % create array
arraySweep   = Meshgrid(array,'imped',calcAlg);
          % create all combinations of properties
arrayImped   = MutualImped3Term(arraySweep);
          % impedance matrix calculation
ReZ             = real(arrayImped.Z);     % Re(Z)
ImZ             = imag(arrayImped.Z);     % Im(Z)
[Vec,Num]    = eig(ImZ,ReZ);           % naive TCM
arrayInt     = MutualRadI3Term(arrayImped);
          % radiation intensity vector
nTheta       = 180;      % number of theta points
nPhi         = 360;      % number of phi points
arrayPat = RadPat(arrayInt,'total',nT,nP,calcAlg)
          % modal patterns calculation
givenRadPat.ffTheta =sin(theta)*cos(phi)^2;
          % given radiation vector in theta
givenRadPat.ffPhi   =0;
          % given radiation vector in phi
modalCoef    = CalcModalCoef(givenRadPat,arrayPat)
          % excitation coefficient calculation
% Results:
plotPattern(arrayPat,'total','log',[-20 20],'d');
```

Figure C.2: Simple code of the MATLAB part calculation